Universidade do Minho
Escola de Ciências

Mafalda Braga Gomes

Recombinant protein-based hydrogels for biotech applications

Janeiro de 2020

Recombinant protein-based hydrogels for biotech applications

Mafalda Braga Gomes

UMINHO | 2020

UNIÃO EUROPEIA
Fundo Social Europeu

Universidade do Minho

Escola de Ciências

Mafalda Braga Gomes

Recombinant protein-based hydrogels for biotech applications

Dissertação de Mestrado

Genética Molecular

Trabalho efetuado sob a orientação do

Doutor Raul Machado e do

Doutor André da Costa

janeiro de 2020

DIREITOS DE AUTOR E CONDIÇÕES DE UTILIZAÇÃO DO TRABALHO POR TERCEIROS

Acknowledgments

First of all, I would like to thank my supervisors Raul Machado and André da Costa, for all of their support and encouragement and most importantly for the opportunity of learning and working with them. Equally important, is my thanks to Diana Gomes and Margarida Pereira, for always helping me whenever I needed. To all my lab mates, Catarina, João, Maria and Emanuel for always keeping me cheered up and with a smile on my face.

To my father, my brother and my grandmother for all of the support, encouragement and kind words and the true reason behind my strength.

Also, I would like to thank to all of my friends for never letting me give up and for always helping me to release the pressure.

Most importantly, I would like to thank my mother, for always encouraging me to do and be better, for all the kinds words and support she always gave me and without whom I would never be where I am today.

Este trabalho é financiado por fundos nacionais através da FCT – Fundação para a Ciência e a Tecnologia, I.P., no âmbito do projeto "FunBioPlas - Novel synthetic biocomposites for biomedical devices" com referência ERA-IB-2-6/0004/2014.

STATEMENT OF INTEGRITY

I hereby declare having conducted this academic work with integrity. I confirm that I have not used plagiarism or any form of undue use of information or falsification of results along the process leading to its elaboration.

I further declare that I have fully acknowledged the Code of Ethical Conduct of the University of Minho.

University of Minho: ____/____/____

Signature:_____

Abstract

Silk elastin-like protein (SELP) hydrogels are an example of protein-based materials that have gained interest in the past years for biomedical and biotechnological applications, due to their remarkable properties such as biocompatibility and biodegradability. SELPs are a class of recombinant proteins, typically composed of silk-like (GAGAGS) and elastin-like (VPGVG) blocks. In aqueous solutions, some of these polymers demonstrated the ability to self-assemble, through a temperature-mediated process, leading to the formation of a hydrogel. The mechanism behind the gelation of SELPs is thought to be driven by a combination of two factors, the crystallization of the silk-like blocks and the thermoresponsive behaviour of the elastin-like blocks, which aggregate and become insoluble after reaching a specific transition temperature (T_t). While several studies report the use of SELP-based hydrogels, the focus is usually on their applicability, lacking insights on the chemical structural and physical properties. Based on this, the main objective of this dissertation was to perform a thorough study on the effect of composition, concentration and curing temperatures on the physical-chemical properties of SELP-based hydrogels.

Three different SELP copolymers with similar molecular weights, namely SELP-59-A, SELP-520-A, and SELP-1020-A, were used, with differences in both the silk-to-elastin ratio and the length of each block. The SELPs used had their elastin block based on the pentamer VPAVG, which is known to confer an acute thermal hysteresis. The obtained results demonstrate the versatility of SELPs for the development of hydrogels, since that, by using only three polymers and by varying their concentrations and cure temperatures, an assortment of different properties was obtained. The thermo-responsive behaviour was shown to be reversible at some extent coupled with an acute hysteresis behaviour, being dependent on both polymer concentration and composition. Formation of non-flowing hydrogels was observed with a dependence on cure temperature (higher temperature resulted in higher gelation rates), polymer composition and concentration. The secondary structure of the hydrogels was found to be mainly dependent on cure temperature (increase in temperature resulted in an increase in ordered structures) and on polymer composition. The formation of a defined porous network and particles was also observed, with a dependence on both polymer composition and concentration as well as on cure temperature. The mechanical/rheological properties of SELPs were also found to be dependent on the parameters described above.

Keywords: recombinant proteins, SELPs, hydrogel, gelation.

Resumo

Hidrogéis com base em proteínas semelhantes à seda e elastina (SELPs) têm sido alvo de interesse para a área biomédica, devido às suas propriedades excecionais de biocompatibilidade e biodegradabilidade. SELPs são uma classe de proteínas recombinantes, tipicamente compostas por blocos tipo-seda (GAGAGS) e tipo-elastina (VPGVG). Em solução aquosa, alguns destes polímeros demonstraram a capacidade de se auto-organizarem ("self-assemble") e formarem hidrogéis, num processo de gelificação mediado pela temperatura. O mecanismo por detrás do processo de gelificação dos SELPs é atribuído a uma combinação de dois fatores, a cristalização dos blocos de seda e ao comportamento termo-responsivo dos blocos de elastina, que formam agregados insolúveis acima de uma determinada temperatura de transição (T_t). A grande maioria dos estudos feitos nesta área tem como principal foco a aplicabilidade destes materiais, faltando estudos relativos à caracterização estrutural e física. Assim, esta dissertação teve como principal objetivo avaliar o efeito da composição, concentração e temperatura de cura nas propriedades físico-químicas de hidrogéis de SELPs.

Nesta dissertação foram considerados três SELPs diferentes, nomeadamente SELP-59-A, SELP-520-A e SELP-1020-A, que apresentam peso molecular semelhante mas de diferente composição a nível do rácio seda-elastina e do comprimento dos blocos. No caso específico destes co-polímeros, o bloco de elastina consiste no pentâmero VPAVG, o qual é caracterizado por uma histerese térmica aguda quando em solução aquosa. Os resultados obtidos demonstram a versatilidade dos SELPs para o desenvolvimento de hidrogéis, dado que, utilizando apenas três polímeros e variando apenas concentrações e temperaturas de cura, foi possível obter uma variedade de diferentes propriedades. O comportamento termo-responsivo mostrou ser reversível e associado a um comportamento de histerese aguda, sendo dependente tanto da concentração como da composição do polímero. A formação de hidrogéis não fluidos foi observada, e mostraram dependência da temperatura de cura (temperaturas mais altas resultaram em taxas de gelificação mais altas) e da composição e concentração do polímero. A estrutura secundária dos hidrogéis também mostrou ser influenciada principalmente pela temperatura de cura (aumento da temperatura resultou num aumento de estruturas ordenadas) e pela composição do polímero. Foi observada a formação de uma rede porosa definida e de partículas, que dependendeu tanto da composição e concentração do polímero como da temperatura de cura. As propriedades reológicas dos SELPs também demonstraram serem influenciadas pelos parâmetros descritos acima.

Palavras-chave: SELPs, proteínas recombinantes, hidrogéis, gelificação

Table of contents

Abbreviations and acronyms

Amp – Ampicillin

ATR-FT-IR – Attenuated total reflection – Fourier transform infrared spectroscopy

CGC – Critical gelation concentration

D_h – Hydrodynamic diameter

DLS – Dynamic Light Scattering

DMA – Dynamic Mechanical Analysis

DNA – Deoxyribonucleic acid

DSC – Differential Scanning Calorimetry

EGDMA – Ethylene glycol dimethacrylate

ELPs – Elastin-like polymers

Lac - Lactose

LB – Lysogeny Broth

mRNA – messenger ribonucleic acid

PDI – Polydispersity Index

pHEMA – poly(2-hydroxyethyl methacrylate)

SDS-PAGE – Sodium Dodecyl Sulphate polyacrylamide gel electrophoresis

SELPs – Silk-elastin-like polymers

SEM – Scanning Electron Microscopy

TB – Terrific Broth

T_r – Resolubilisation temperature

tRNA – transfer ribonucleic acid

T_t – Transition temperature

List of figures

List of tables

1.Introduction

1. Introduction

1.1 Protein-based materials: a versatile class in materials science

Currently, polymer science has an enormous role on society's life and very few technological areas had the same level of development and impact as this field. This is caused by the availability of thousands of different monomers and the possible combinations between them, giving rise to materials that can vary in complexicity from very simple and for everyday use (e.g. textiles, packaging, etc.) to very complex (e.g. for biomedical, biotechnological, engineering or nanotechnological applications) (Lutz, 2008; Rodríguez-Cabello *et al.*, 2009). Even though polymers can come from various sources, the most used ones derive from fossil-based feedstocks, with known issues regarding sustainability and prices. With that, alternatives are needed, forced by the depletion of fossil-based feedstock reserves, combined with a need for more sustainable processes with reduction of environmental impact, putting polymer science in a similar challenge to the one faced in the energy sector in the past decades (Casal *et al.*, 2014; Rodríguez-Cabello *et al.*, 2009).

In the past century, technological development was usually accompanied by a progressive substitution of natural elements over synthetic ones. Only more recently, and by facing problems such as resource scarcicity and the need for a sustainable devlopment, scientists have regained interest in bio-based products. Sustainable development can be defined as the "development that meets the needs of the present without compromising the ability of future generations to meet their own needs" (*Source*: IISD, our common future report). With that in mind, polymer science faces the challenges to create new polymers and methodologies that need to be sustainable, biodegradable, from renewable sources, more efficient and functional than the ones we had before. And not so surprinsingly, bio-based and bio-inspired polymers could be the solution to the problems and needs presented above (Gupta & Nayak, 2015; Halley & Dorgan, 2011; Rodríguez-Cabello *et al.*, 2009).

Nature has developed, throughout evolution, structural materials that display the most diverse and complex structures while carrying out a multitude of functions. With the developments in areas of genomics, proteomics and molecular biology, scientists are now able to understand at an higher extent the mechanisms behind the assembly and function of these materials in natural environments and utilize such information for the development of new bio-based materials. Some concepts that are relatively new to material science, such as self-assembly, stimuli-responsiveness, hierarchical organization, among others, were already familiar to those who studied natural macromolecules (proteins, polysaccharides,

nucleic acids) (Rodríguez-Cabello *et al.*, 2009). One of the best examples of these polymeric macromolecules are proteins, due to their high diversity and extreme versatility. Proteins are comprised of building blocks known as amino acids and are essential macromolecules to all living-systems. They are usually composed of different combinations of the naturally occuring amino acids that can be categorized as aromatic, anionic, cationic, polar or non-polar They participate in many fundamental processes such as cell signalling, hormonal regulations, immune responses, transport, structural integrity, among others (Gupta & Nayak, 2015; Pieters *et al.*, 2016). The repetitive amino acidic blocks will mainly determine the protein's conformational changes and ultimately, it's functions (Casal *et al.*, 2014). Proteins are synthesized within the cell, where the information stored in the DNA is translated into a functional amino acidic sequence, through a multi-step process (Silva *et al.*, 2014). The biological synthesis occurs with a complete control over sequence, and this type of control is essential, as a simple genetic disorder, such as a substitution or lack of an amino acid, can cause loss of function and ,consequently, a disease. (Rodríguez-Cabello *et al.*, 2009).

Protein's structure can also be categorised into four main structural forms: primary structure (amino-acid sequence), secondary structure (conformations), tertiary structure (folding of peptide chain) and quaternary structure (association with other proteins). In the primary structure, amino-acids are linked to each other through peptide bonds, which are, in fact, amide bonds between the amine and carboxylic groups, thus forming a linear amino-acid sequence. This sequence can then self-assemble into secondary structures (α-helix, β-turns, β-sheets, among others) (Figure 1), stabilized by supramolecular interactions such as hydrogen bonds, van der Walls, π or ionic interactions between neighbouring amino acids. The tertiary structure can be defined as the protein's overall spatial conformation, that is defined by interactions between amino acid that are located apart from each other in the peptide chain. These same interactions occur due to the specific amino acid compositions, namely the R-groups, and can be stabilized by hydrogen/sulphide bonds and non-local interactions. Finally, the quaternary structure, is achieved by the non-covalent bonding of the tertiary structures, and can be divided in two, globular (ex:hemoglobin) and fibrous (elastin). Furthermore, proteins can be divided into homoproteins (comprised only of amino-acids), like keratin or albumin, into heteroproteins (amino acids plus non-protein components) like lipoproteins or glycoproteins, and also into functional proteins (ex: enzymes) or structural (ex: silk fibroin) (Bassas-Galia *et al.*, 2017; Gupta & Nayak, 2015; Pieters *et al.*, 2016; Silva *et al.*, 2014).

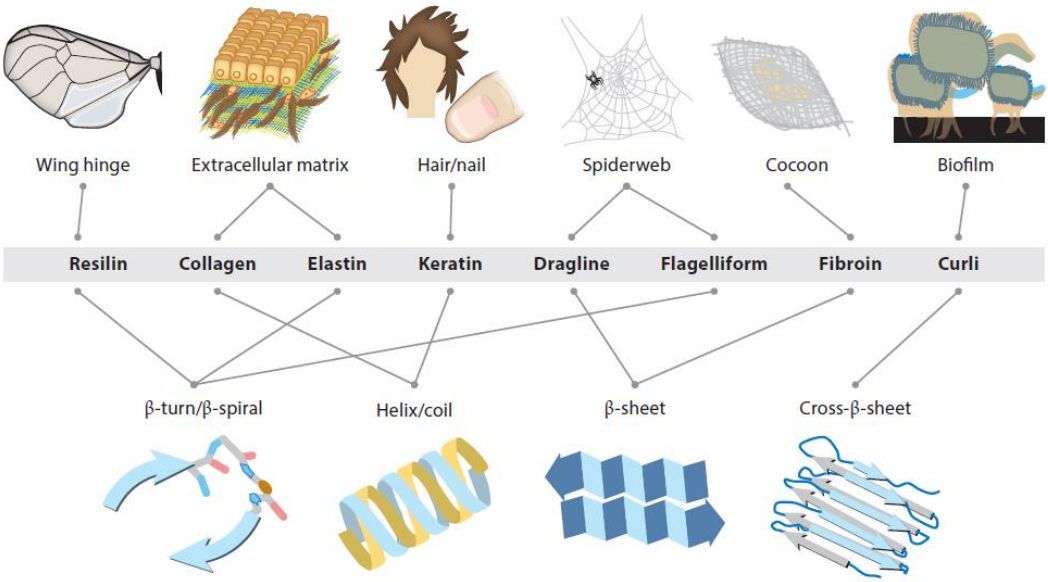

Figure 1 - Schematic representation of the relationship between natural materials, protein polymers, and the proteins' secondary structures (reproduced from Yang *et al.*, 2017).

Protein-based materials like silk, wool and leather have been used by humankind for thousands of years and are normaly associated with structural protein sequences (Table 1). All these materials were extensively exploited, due to their unique physical properties and the fact that they are biodegradable. Nowadays, several protein-based materials have been studied and developed, including films, gels, plastics, composites, etc, mainly for use in biomedical applications, such as scaffolds, drug delivery systems and biosensors (Abascal & Regan, 2018; Silva *et al.*, 2014).

By exploiting all of the characteristics presented above and by combining knowledge in the molecular biology fields and polymer science, scientist are able to create new materials with refined sequences and specific functions. Through a combination of the many naturally occurring amino acids, researchers are able to select the desired building blocks in order to achieve the material's desired properties. In the last two decades, with advances in recombinant DNA technologies, scientists were able to produce genetically engineered protein-based polymers, which are polymers derived from natural occurring proteins, produced by genetic engineering and biological synthesis (Casal *et al.*, 2014; Frandsen & Ghandehari, 2012).

Table 1 - Amino acid repeating units found in some natural structural proteins. Sequences given in single letter code with X representing any amino acid (adapted from Casal *et al.*, 2014).

Protein Family	Monomeric unit sequence
Silk fibroin	GAGAGS
Elastin	GVGVP, VPGG, APGVGV
Collagen	GAPGAPGSQGAPGLQ GAPGTPGPQGLPGSP
Keratin	AKLKLAEAKLELA
Abductin	GGFGGMGGGX
Dragline silk	GPGQQ, GPGGY, GGYGPGS
Flagelliform silk	GPGGX

1.1.1 Genetically Engineered Protein-Based Polymers

Genetically engineered protein-based polymers can be defined as macromolecules with high molecular weights, comprised of repeating units of a sole amino acid or blocks of amino acids. These polymers can have the most varied primary structures, such as those formed by: (a) polymerization of a sole amino acid (poly-L-lysine, poly-L proline); (b) polymerization of monomeric units belonging to the same protein family type (poly-GVGVP or poly-APGVG); (c) copolymerization of a block comprising, two or more monomeric units from different protein family types (poly-[(GVGVP)*n*(GAGAGS)*m*]) (Casal *et al.*, 2014).

Usually, polymeric materials obtained by chemical synthesis, tend to be more robust than protein-based materials, even though they possess a wide range of properties, compositions and architectures, they still lack the structural complexity characteristic of proteins (Knight *et al.*, 2015). And so, when developing new synthesis methods, scientist have taken an inspiration on one of the most import features of biological synthesis - the complete control over sequence, and ultimately structure and function - as well as monodispersity of produced molecules, something that is not possible using traditional polymer synthesis methods (Figure 2) (Dandu *et al.*, 2009; Knight *et al.*, 2015; Krishna & Kiick, 2010). Nowadays, most of these engineered protein polymers are obtained using standard molecular genetics tool, mainly by recombinant DNA techniques (Jang & Champion, 2016). This type of synthesis provides a number of advantages that are simply not possible using the traditional methods: allows the insertion of synthetic

genes into the genetic information of a microorganism, which then produces the genetically engineered protein; enormous degree of control and complexity; polymers are monodisperse and with a wide range of molecular weights (few hundred to 200 kDa); they can combine characteristics from both natural and synthetic materials like biocompatibility and tunability, respectively; and batch to batch consistency (Rodríguez-Cabello *et al.*, 2009; Sengupta & Heilshorm, 2010).

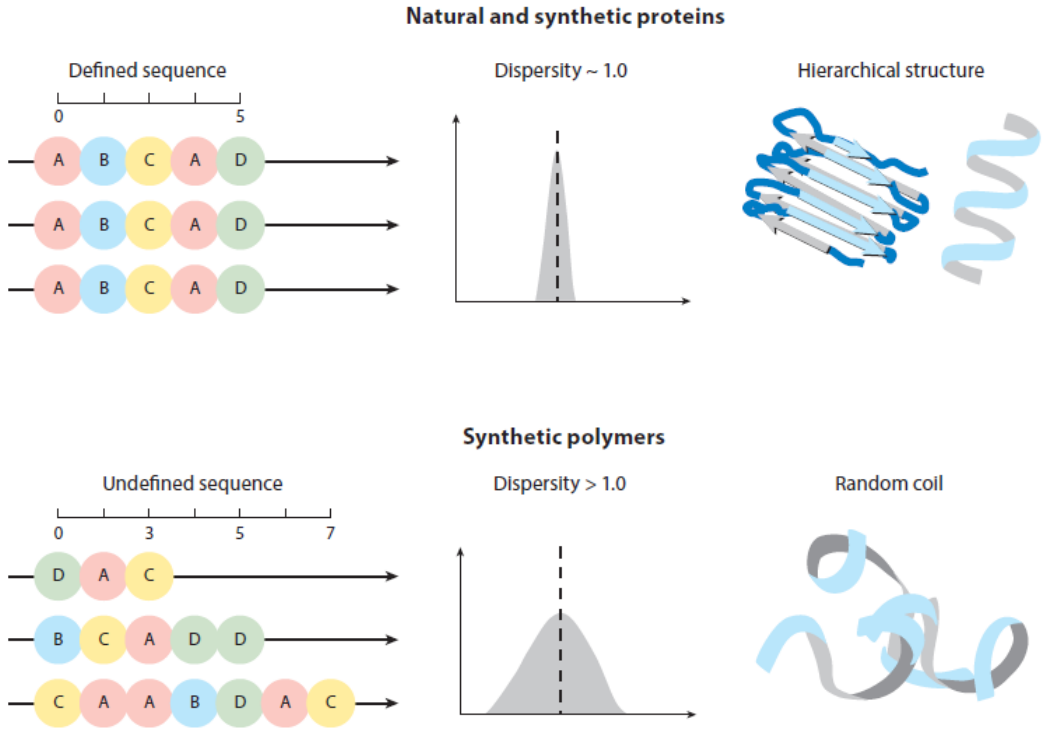

Figure 2 - Schematic representation of major differences between proteins and chemically synthesized polymers (reproduced from Yang *et al.*, 2017).

Genetically engineered protein polymers can be comprised of repeating units that derive from wild-type or engineered sequences, where each unit has a specific function, and are ultimatelly combined to create multifunctional polymers. Since these methods allow for refinement at the molecular level, after *in vitro* and *in vivo* studies, one can modify the amino acid sequence in order to obtain specific functions (Gomes *et al.*, 2012; Sengupta & Heilshorn, 2010). Generally, the biosynthesis of any artificial protein includes: (1) Construction of a synthetic gene that encodes the protein of interest in a plasmid; (2) Transfeccion of the plasmid into the selected expression system (3) Expression of the engineered protein by host; (4) Purification of the protein of interest (Mi, 2006; Sengupta & Heilshorn, 2010). Usually, for the fabrication of the synthetic DNA sequence from these recombinant protein-based polymers, a "Lego"

approach is used, where a synthetic block monomer, chemically synthesized or obtained by polymerase chain reaction, is subjected to a multimerization process (McMillan *et al.*, 1999). A careful design of the cloning strategy enable easy DNA modification, allowing for the creation of a family of genetically engineered protein family with tuneable properties. However, challenges exist in this approach of recombinant protein-based polymers design. Even though the genetic code is essentially the same throughout all organisms, the frequency of which codons are used varies from organism to organism so there's a need for optimizing the codon usage of the chosen organism in order to achieve higher yields. Codon usage also needs to be diverse in order to avoid DNA recombination and depletion of codons (Sengupta & Heilshorn, 2010). Formation of DNA structures, similarity/proximity of the DNA codons to neighbouring translational places, ribosome-binding sites, codon bias, tRNA availability and mRNA stability and structure are also thought to play important roles in the gene expression process. The choosing of the expression host is also very important, typically the preferred microorganism is *Escherichia coli*, mainly due to the rapid and relatively inexpensive growth and because it enables genetic modification to improve protein expression, even though, protein overexpression can lead, from now and then, to the formation of aggregates known as inclusion bodies (Sengupta & Heilshorn, 2010) . Furthermore, *E. coli* is a prokaryote and its simple translational mechanisms make this organism not capable of most of the posttranslational modifications and so, for this purpose, yeasts (eukaryote) can be used due to the low costs of production and rapid growth, when compared to more complex, higher organisms (Sengupta & Heilshorn, 2010; Sivashanmugam *et al.*, 2009). Likewise, production of genetically engineered proteins has been described in yeast (Soni, 2017; Yang & Zhang, 2018), filamentous fungi (Madhavan *et al.*, 2017), plants (Reuter *et al.*, 2014), insects (Cox, 2012) and mammalian cells (Hacker & Balasubramanian, 2016), even though protein expression in these systems tend to be more complex and expensive (Kim, 2013). Usually, the more complex the expression system, the more complex the growth and media conditions. Cell transfection process is typically less effective in these complex systems and protein expression is usually a slower process than in simpler organisms (Sengupta & Heilshorn, 2010). Thus, when it comes to choosing the best expression system, several points need to be taken in consideration.

Nowadays, several genetically engineered protein polymers have been synthesized and studied, like collagens (Yang *et al.*, 2017), resilin (Su *et al.*, 2014), silk (Numata *et al.*, 2009), mussel adhesive protein (Castillo *et al.*, 2017), among others. In this family, most two of the must studied protein families include, silk-like and (Anderson *et al.*, 1994; Winkler *et al.*, 2000) elastin-like polymers (Luan *et al.*, 1990; Yamaoka *et al.*, 2003), as well as co-polymers of several different combinations of both families (Cappello

et al., 1990; Megeed *et al.*, 2002), mainly due to their unique properties in terms biocompatibility and biodegradability and mechanical performances (Rodríguez-Cabello *et al.*, 2009)

1.1.2 SELPs

Originally developed by Capello, Ferrari and co-workers in the late eighties and early nineties (Cappello *et al.*, 1990), silk-elastin-like proteins (SELPs) are a versatile class of genetically engineered biopolymers that has gained attention throughout the years. They are composed of repetitive amino acid blocks, normally inspired in both natural occurring silk fibroin (GAGAGS) from *Bombyx mori* (silkworm) and mammalian elastin (VPGVG) (Cappello *et al.*, 1990, 1998; Urry *et al.*, 1992). Regarding the silk-like units, they tend to self-assemble into insoluble, tightly packed β-sheets, stabilized by hydrogen bonding (Anderson *et al.*, 1994). This conformational change is possible due to serine residues that enable the physical cross-link between adjacent polymer molecules, imparting mechanical, chemical and thermal stability of the system (Megeed *et al.*, 2002). The periodic inclusion of elastomeric sequences decreases the overall crystallinity of the system, increases flexibility and provide higher aqueous solubility, since the elastin blocks are highly hydrated below a certain temperature (Cappello *et al.*, 1990). Elastin also provides a stimuli responsiveness to the co-polymer, since they undergo a reversible structural transition when exposed to certain stimuli (Nagarsekar *et al.*, 2003). The elastin units have been reported to form either β-turns or an amorphous structure with no defined conformation, but accepted to have a highly flexible conformation (Casal *et al.*, 2014; Rodríguez-Cabello *et al.*, 1999).

Typically, SELPs are represented by the nomenclature [(S)*x*(E)*y*]*n*, where S stands for the silk-like unit and E for the elastin-like unit, *x* and *y* for the number of block, repeats of silk and elastin-like units, respectively and *n* is the number of repetitions for the overall block (Cappello *et al.*, 1998). Another nomenclature used for SELPs, and the one utilized in this work, is the generic name SELP followed by a numeric refrence *xy* that stands for the number of repeats of the silk-like (*x*) and elastin-like (*y*) units. In copolymers, where an aminoacid substituition has been performed on the elastin block, the corresponding aminoacid letter will be added to the formulation (Cappello *et al.*, 1998) It is very important to note that the physiochemical properties of these materials are highly dependent on length, sequence and number of repeats of the blocks and that by changing these same aspects, the material properties can be tuneable. As example, depending on the composition, some SELPs in aqueous solutions are liquid at room temperature but self-assemble irreversibly above a certain temperature depending on the number

of silk-like blocks (Cappello *et al.*, 1990); another example is the simple substitution of the guest residue in the elastin block, giving rise to polymer sensitivity to pH and ionic strength of the solution(Nagarsekar *et al.*, 2003).

The first SELP copolymers were designed to have different silk-to-elastin ratio, with the following compositions, $(S_9E_4)_{14}$ and $(S_8E_8)_{12}$, designated as SELP-94 and SELP-88, respectively (Cappello *et al.*, 1990). In this work, the authors assessed the degree of crystallinity of the produced SELP lyophilized powders. As it is known the influence of the silk-like blocks in the overall crystallinity of the polymer, one could theorize that between, SELP-94 and SELP-88 , SELP-94 would present a higher degree of crystallinity. Using X-Ray diffraction and FTIR spectroscopy, the degree of crystallinity and β-sheets content of the produced polymers were determined concluding that, in fact, SELP-94 effectively showed higher degree of crystallization with an also higher content of β-sheets, when compared to SELP-88. The study also demonstrated that the polymers were able to form a gel in aqueous solutions, thought it took a higher amount of time for SELP-88 to gelate when compared to SELP-94 (difference in days). This work represented the beginning of SELPs criation and characterization and since then, several new SELPs have been produced and extensively characterized (Cappello *et al*, 1990; Roberts *et al.,* 2018).;

SELPs are usually produced using recombinant DNA technology and with *E. coli* as the prefered host (Hart & Gehrke, 2006). Average volumetric productivities varie from protein to protein but values of 12.8 g/L have been described in literature (Barroca *et al.*, 2016). Depending on their aqueous solubilities, SELPs can be purified using different methods. For water soluble polymers, purification can be achieved using non-chromatographic methods such as salting out (Collins *et al.*, 2013; Machado, *et al.*, 2013b) or inverse temperature transition cycling (Huang *et al.*, 2016; Xia *et al.*, 2011). In the case of chromatographic purifications, affinity chromatography is the preferred method (Dandu *et al.*, 2009; Nagarsekar *et al.*, 2002). While affinity chromatography is the preferred method for SELPs purification as it allows very pure polymers fractions, is a very expensive and very laborious technique (Casal *et al.*, 2014; Haider *et al.*, 2005; Nagarsekar *et al.*, 2002). For copolymers with higher silk contents or less interrupting elastin-like blocks, dissolving the pellet with Lithium Bromide, followed by dialysis, can be the successful method for polymer purification (Cappello *et al.*, 1990).

Since SELPs are known for their biocompatibility, biodegradability and versatility, it's not very surprising that the majority of SELP applications are towards the health sciences (Cappello *et al.*, 1998; Huang *et al.*, 2015). Nowaday, SELPs have been processed into fibers (Roberts *et al.*, 2018), films (Chen *et al.*, 2017), gels (Jensen *et al.*, 2017), nanoparticles (Xia *et al.*, 2011) or 3D scaffolds (Qiu *et al.*, 2010) and have been used for the most varied biomedical and biotechnological purposes. SELPs have been

devoleped to be used as cancer therapy systems (Greish *et al.*, 2009; Gustafson & Ghandehari, 2010; Gustafson *et al.*, 2009, 2010), wound dressings (Ozaki *et al.*, 2014), scaffolds for cell growth and adhesion (Qiu *et al.*, 2010) and tissue engineering (Haider *et al.*, 2008).

In the SELPs used in the work described in this dissertation, the traditional mamallian elastin sequence VPGVG was altered to VPAVG by substitution of the central glycine (G) by an L-alanine (A) (Machado, *et al.*, 2013a). This simple amino acid substitution has been firstly reported in elastin-like polymers (ELPs) by Dan Urry in the early nineties (Urry *et al.*, 1992). These polymers exhibited unique properties among elastin-like polymers such as a Young's modulus two orders of magnitude higher than that for poly(VPGVG) (Luan & Urry, 1999) thermoplastic characteristics (Nagapudi *et al.*, 2005) and the inverse temperature transition was characterized by an acute hysteresis behaviour (Reguera *et al.*, 2003). The inverse temperature transition of these polymers (and all elastin-like polymers) is due to their capability of hydrophobically driven self-assembly into higher-ordered structures above a determined temperature known as transition temperatute (T_t) (Urry *et al.*, 1992; Xia *et al.*, 2011). The hysteresis behaviour is due to two facts: presence of a methyl group in the Ala residue and a more stable folding state when compared to VPGVG (Kim & Conticello, 2007; Nagapudi *et al.*, 2005).

Usually, above the transition temperature (T_t), elastin-like polymers have been reported to adopt an ordered structure, repeated type II β-turns are formed within the chain and are stabilized by hydrogen bonds. The pair Pro-Gly in VPGVG is involved in the formation of these same β-turns, and even though the substitution of the glycine by an alanine does not prevent the formation of β-turns, it changes the turns from type II to type I β-turns, changing the mechanical response from elastic to plastic (Nagapudi *et al.*, 2005; Reguera *et al.*, 2003). Above the T_t, VPAVG contains less water bound, leading to a more compact and rigid structure, due to decrease in the plasticizing effect of water, this also prevents coacervation of the polymers and causes the formation of a stable particle suspension. The redissolution and unfolding of this polymer is then prevented by the lack of water between molecules and the strongly bound amide groups, that can only be destroyed after strong undercoolings (Herrero-Vanrell *et al.*, 2005; Machado *et al.*, 2009). The substituition of VPGVG for VPAVG in ELPs has also been reported to increase the T_t in water, from around 25-27 °C to around 30 °C (Machado *et al.*, 2009).

With all this in mind, one can only expect that SELP copolymers synthesized with this pentapeptide would present the same characteristics. An increase in the number/length of elastin-like blocks should render the copolymer a higher T_t in water and also lead to a thermoplastic behaviour. The overall copolymers should still present a thermoplastic behaviour and an inverse temperature transition

characterized by an acutte hysteresis behaviour. Such copolymeres are worthy of a thorough study in terms of the physiochemical properties, thus broadening it's potential applications.

1.1.3 SELP-based Hydrogels

Hydrogels are three-dimensional, cross-linked, hydrophilic polymeric networks, that are capable of absorbing large amounts of water or aqueous fluids without compromising their structural integrity (Peppas *et al.*, 2000). The first scientific report of the term hydrogel dates back to the late nineteenth century, where it was used to describe a colloidal suspension made with inorganic salts (Bemmelen, 1894). Even though the term hydrogel was used, the material described was not a hydrogel as we describe it today, but a colloidal suspension (Yahia, 2015). Only 30 years later the first synthetic hydrogel, named poly(2-hydroxyethyl methacrylate) (pHEMA), was described by Nemours in 1936 (Nemours, 1936). Fastforwarding 30 years in time again, in the sixties, the first hydrogel for application in the biomedical field is developed (Wichterle & Lím, 1960). Wichterle and Lim (1960) polymerized and cross-linked pHEMA) into a soft gel with promising applicability as contact lenses (Wichterle & Lím, 1960). The great water absorption capability of the hydrogel, known as swelling behaviour, render the hydrogel a soft and rubbery character, making them very useful for biomedical applications (reviewed in Chai *et al.*, 2017; Feksa *et al.*, 2018; Hoffman, 2012). Research throughout the years demonstrated that hydrogels could be used not only in the biomedical field but also in areas like agriculture (Guilherme *et al.*, 2015), water treatment (Hao *et al.*, 2018), tissue engineering (Jeon *et al.*, 2017), pharmaceutics (Badruddoza *et al.*, 2016), plastic surgery (Nuutila *et al.*, 2018), among others.

During the last few decades, interest in hydrogels was regained, and there was an increase in the number of publications on this subject since mid-nineties (Yahia, 2015). Hydrogels can be classified based on different parameters such as origin (natural, synthetic, hybrid), composition (homopolymers, copolymers, multipolyme, interpenetrating network), overall charge (neutral, anionic or cationic), pore size (non-porous, microporous and superporous), physical structure (amorphous, semi-crystalline) and appearance (matrix, film or microsphere). Furthermore, hydrogels can be divided into two very different categories based on the nature of the crosslinks: chemical and physical hydrogels. In "chemical" or "permanent" hydrogels, they are bound together by covalent linkages (Figure 3) (Ahmed, 2015; Peppas *et al.*, 2000; Thakur *et al.*, 2018; Zhu & Marchant, 2011).

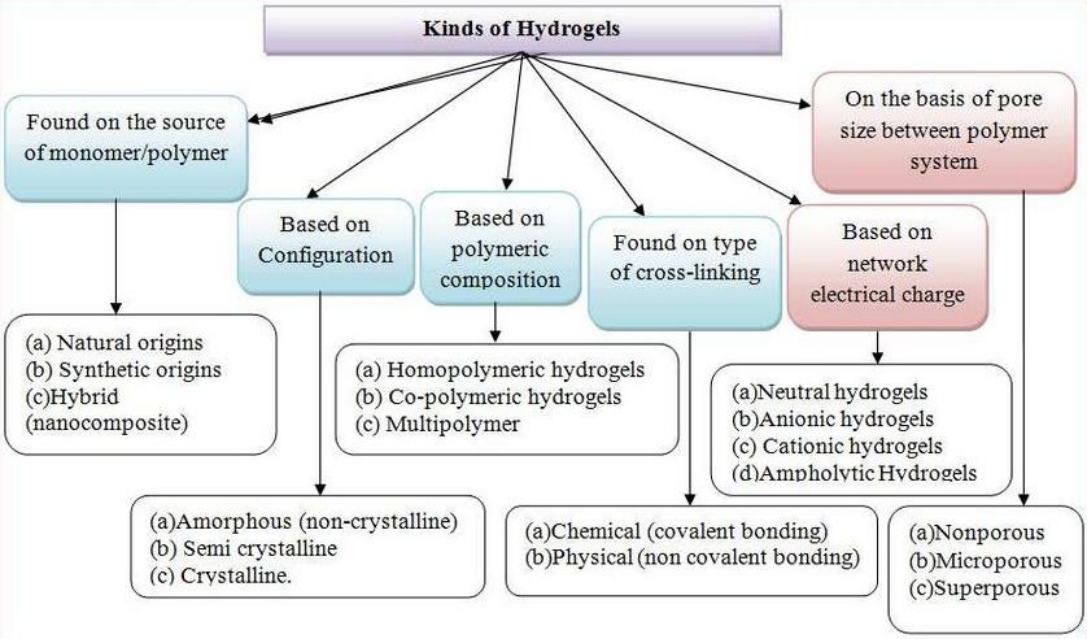

Figure 3 - Classification of hydrogels (reproduced from (Devi & Gaba, 2019).

The synthetic hydrogels mentioned before were based on the copolymerization of HEMA with the crosslinker (EGDMA) (Wichterle & Lím, 1960) can be designated as chemical gels. This type of gels can also be synthesized by either the conversion of hydrophobic to hydrophilic polymers plus crosslinking to form a network or by crosslinking water-soluble polymers. In the crosslinked state, the equillibrium sweling of these hydrogels is strongly dependent on the crosslink density. Chemical hydrogels are considered not homogenous, since they contain regions of low water swelling and high crosslink density, called “clusters” (Hoffman, 2012). Physically cross-linked hydrogels typically result from the self-assembly of the molecules and demonstrate no significant volume changes during the sol-to-gel transition. In this type of hydrogels, the network is tipically held together by physical interactions such as molecular entaglements, van der Waals, hydrogen bonding, hydrophobic, ionic, electrostatic and/or π-stacking The physical interactions decribed before are reversible and they also lead to a stimulli responsivness of hydrogels to factors like temperature or stress, among others (Altunbas & Pochan, 2012; Hoffman, 2012). Like the chemical gels, physically crosslinked hydrohgels are not homogenous, due to the existence of clusters of either molecular entaglements or ionically- or hydrophobically-driven domains (Hoffman, 2012). Even though physically cross-link leads to formation of weaker hydrogels, it does not depend on the addition of organic solvents or crosslinking agents, and this can pose as an advantage in some applications. For example, components can be mixed with the aqueous solution, which can also be used as an injectable material, being very promising especially for biomedical applications (Jonker *et al.*, 2012; Kapoor & Kundu, 2016; Van Vlierberghe *et al.*, 2011).

The traditional methods used to obtain synthetic polymeric hydrogels offer limited control over the structure, and hydrogels assembly typically exhibits poor or slow response to external stimuli. The majority of these stimuli responsive materials are derived from a small range of synthetic polymers, mostly from (meth)acrylate derivatives and their copolymers (Kopecek, 2007; Kopecek & Yang, 2007). However, due to a requirement of higher versatility than the one offered by synthetic polymers, scientist started to develop nature-inspired materials that are tuneable and responsive to multiple stimuli (Yeo *et al.*, 2018). Nowadays several bio-inspired, especially protein/peptide -based hydrogels due to the self-assembly or aggregation capabilities, have been designed, synthesized and characterized (reviewed by Jonker *et al.*, 2012). Hydrogels synthesized using these peptide/protein segments provide for biocompatibility and biodegradability and can show a temperature induced phase transition and sensitivity to the presence of biologically active molecules. The fact that these gels are typically soft and rubbery, resembling living tissues, leads to a variety of applications, especially in the biomedical area. Numerous polypeptide-based responsive hydrogels have been manufactured from block copolypeptides (Nowak *et al.*, 2002), recombinant segments of natural structural polymers (for example, silk fibroin (Wu *et al.*, 2016), elastin-like (Wang *et al.*, 2018) and silk-elastin-like recombinamers (Huang *et al.*, 2016) or recombinant triblock copolymers of a polypeptide sequence flanked by two coiled coils (Xu *et al.*, 2005). More specifically, SELP hydrogels have properties that make them promising for use in the biomedical field. SELP solutions were found to be soluble at room temperature and can form gels when temperature is elevated (Cappello *et al.*, 1990). Depending on the sequence, some of these copolymers were found to have an reversible transition in structure, around a defined transition temperature (T_t) (Huang *et al.*, 2016; Xia *et al.*, 2011) whereas others are able to undergo an irreversible sol-to-gel transition (Cappello *et al.*, 1990). Stimuli responsiveness of the copolymer can also be altered: by changing the guest residue in the elastin sequence for instance, enables polymer responsiveness to alterations of pH, phosphorylation or ionic strengths (Haider *et al.*, 2005; Megeed *et al.*, 2002; Wang *et al.*, 2014). Gel formation occurs through crystallization of the silk-like domains, where the molecules form tightly packed β-sheets stabilized by hydrogen bonding (Cappello *et al.*, 1998). This hypothesis was proved by the addition of urea to the gel forming solution, disrupting any forming hydrogen bonding, resulting in the absence of gel formation. On the other hand, addition of precrystallized SELP to the solution lead to an increase in the gelation rate (Cappello *et al.*, 1998). It was also proved, using UV-vis spectophotometry, that some SELPs in aqueous solutions present a two-step self assembly process (Xia *et al.*, 2011). The first step is characterized by the formation of micellar-like particles, with a core composed of hydrophobic silk-like blocks and a hydrated corona of elastin-like blocks. The second step describes the the formation of large coacervates,

driven by particle-particle interactions (Xia *et al.*, 2011).Other factors like concentration, temperature and cure time also affect the gelation process and can be explored for the production of different type of hydrogels (Casal *et al.*, 2013; Jonker *et al.*, 2012; Yeo *et al.*, 2018).

SELP materials proved to be biocompatible and biodegradable (Cappello *et al.*, 1998; Qiu *et al.*, 2010), and when injected in guinea pigs, SELP solutions formed stable hydrogels with no visible migration from injection site and without triggering immune responses (Cappello *et al.*, 1998). The fact that the gelation process occurs without the need for chemical agents, allows entrapment of compounds within the matrix without loss of function or chemical changes. SELP hydrogels present a Fickian type of diffusion (Cappello *et al.*, 1998; Dinerman *et al.*, 2002), where the release rate is dependent on sequence, concentration, cure time and molecular weight of the loaded compound. In previous studies, where the release rate of several compounds with various molecular weights in SELP hydrogels was determined, it was demonstrated that that the release rate varied from few days, for low molecular weights (< 10 kDa), to several weeks, for high molecular weight compounds (>40 kDa) (Cappello *et al.*, 1998). Increasing concentration or cure time leads to increased polymer-polymer interactions and allow for the silk units to align and form more and / or stronger physical contacts, leading to the formation of a network with reduced mean pore size and denser network, thus decreasing the compound release rate (Casal *et al.*, 2014; Dandu *et al.*, 2009; Kapoor & Kundu, 2016; Megeed *et al.*, 2002).

The literature avaliable on this theme already provides for a huge insight on some of the properties of SELP hydrogels. Even though there is many research avaliable regarding stimulli-responsive SELP hydrogels and their properties, few work has been done in copolymers where the sequence VPAVG is used and none in the hydrogel area. The remarkable properties of this pentapeptide and its influence on the physiochemical properties of the hydrogel should be a target of study. The effect of temperature and polymer concentration should also be included in the study.

1.1.4 Mechanical/rheological properties of SELP hydrogels

The mechanical properties of hydrogels are greatly influenced by the density of the chain network, which is in turn, a function of polymer concentration and structure, as well as curing conditions. In the gelation process of SELP solutions, the formation of hydrogen bonds between the silk-like units is known to be the force behind network formation (Cappello *et al.*, 1998). Higher polymer concentrations will lead do denser networks and tighter pores, likely due to a greater number of molecules available to establish

physical contacts, thus decreasing network spacing (Cresce *et al.*, 2008). The effect of concentration and molecular structure in the viscoelastic behaviour of different SELPS was studied with SELP-47K and SELP-415K hydrogels (similar molecular weights, but different S:E ratio, 1:2 and 1:4, respectively), with the same curing conditions (Cresce *et al.*, 2008). The storage and loss moduli of 4 wt% and 12 wt% SELP-47K hydrogels were analysed using Dynamic Mechanical Analysis (DMA). It was shown that the storage modulus was directly related to concentration: 4 wt% SELP-47K hydrogels presented a storage modulus of 75.4 kPa while 12 wt% SELP-47K gels had a storage modulus of 1600 kPa. Visually, the 4 wt% hydrogels were translucent, soft and easily deformed whereas 12 wt% hydrogels were opaque and firm. When comparing hydrogels with the same concentration but different SELP sequence, the authors observed that the storage modulus of 12 wt% SELP-415K was also significantly lower (70kPa) when compared to 12 wt% SELP-47K (1600 kPa), although SELP-415K hydrogels were more flexible than SELP-47K ones (Cresce *et al.*, 2008). In a different study, the complex shear modulus (G*) in function of time (120 min) was analysed for 12 wt% SELP-47K and SELP-415K-8mer polymer solutions. SELP-47K showed a greater G* value at the end of the analysis, $1.33x10^{6}$ GPa, compared to 3.37×10^{5} GPa for SELP-415K-8mer. SELP-415K also displayed higher gelation rate (120 min) when compared to SELP-47K (10 min). These differences can be due to differences in polymers' sequence, where the increased length of elastin-like blocks of SELP-415K-8mer relatively to SELP-47K reduces the number of crosslinking forming units, thus increasing gelation time and elasticity of the gel (Haider *et al.*, 2005). Dandu and colleagues analysed the storage modulus of 12 wt% hydrogels of SELP-47K, SELP815K and SELP-415K as a function of compression. SELP-415K hydrogels remained intact up to a strain of failure of 2%, while SELP-47K and SELP-815K failed with a strain to failure between 1.7% and 1.8%. With a strain to failure of 1.5% the storage modulus was 0.52 MPa, 1.98MPa and 5.09 MPa for SELP-815K, SELP-415K and SELP-47K, respectively (Dandu *et al.*, 2009). The high storage modulus value presented by SELP-47K was attributed to the fact that this copolymer presents shorter interrupting elastin units, leading to a higher frequency of crystalline crosslinks, when compared to SELP-815K and SELP-415K hydrogels. The later copolymers are more flexible and less resistant to deformation, due to the separation of the silk units by larger elastin units, which in turn influences the rate and extent of crosslink formation needed to stabilize the polymer network (Dandu *et al.*, 2009).

Polymer composition and concentration have also been studied in relation to hydrogel formation in SELP-47K and 415K-8mer polymer solutions (Cappello *et al.*, 1998). SELP-47K formed physically robust gels, after only 4 h of cure time, with concentrations as low as 6 wt%, while 415K-8mer was only able to form physically robust gels at higher concentrations, 12 wt%, even when the cure time was extended to

24 h and 48 h. These differences might be due to an insufficient number of silk-like units for polymer cross-linking and gel formation at lower concentrations for the case of SELP-415K-8mer (Haider *et al.*, 2005). Viscosity as a function of time and temperature was also studied. Viscosity of SELP-47K and SELP-816 solutions at 20% (w/w) was monitored as a function of time at defined temperatures (4 °C, 23 °C and 37 °C). In all temperatures, SELP-816 gelled faster than SELP-47K. Even though both polymers have the same silk to elastin ratio (1:2), SELP-816 has more silk-like blocks per repeat, thus decreasing gelling rates (Cappello *et al.*, 1998).

In conclusion, increasing the number of silk-like blocks in the polymer, will increase the number of molecules able to establish physical contact, and variations in the length of the elastin-like blocks will result in a bigger spacing between the silk-like blocks for contact. It can be said that the silk-like blocks provide mechanical stiffness and structural rigidity and elastin-like blocks determine the spacing between the junction areas of the polymeric network, and so, with larger interrupting elastin-like blocks, both the gelation rates and critical gelation concentration increase (Casal *et al.*, 2014).-

Keeping in mind all of what was described previously in this introduction, one can theorize some of the properties presented by VPAVG-based SELP hydrogels. Since this amino acid substituition has been reported to change the mechanical behaviour of the material from elastic to plastic, using these SELP copolymers, should render the fabricated hydrogels with more stiffness and resistance that the presented by previsouly synthesized SELP hydrogels. The newly fabricated material should also present thermal transition properties, including the hysteresis behaviour. Since this substituition brings new features, one should also study its effect regarding the pysiochemical properties, being that the length and number of the elastin-like blocks should be responsible for the differences in terms of transition temperatures and mechanical response. On the other hand, we cannot forget the role of the silk-like blocks in the hydrogel characteristics, since the cristalization of these blocks is the main force behind gelation. The number/length of these blocks should then affect some aspects, like the secondary structures formed during gelation, that will ultimately determine the protein tertiary structure. In conclusion, copolymers with more elastin-like blocks, coupled with more silk-like units should present higher temperature transitions and better mechanical peformance (i.e. more stiff and resistant to deformation). SELPs with more silk-like units wil tend to gel at a higher rate and at lower temperatures, and also present a denser and tighter polymer network.

1.2. Objectives and Tasks

The SELP copolymers used in this study differ among themselves in only in terms of composition, since they were design to present the same molecular weight. We will use three different formulations, namely SELP-59-A, SELP-520-A and SELP-1020-A, the main differences are in the silk-to-elastin ratio (1:2 and 1:4) and in the lenghth of the silk and elastin-like blocks. These small differences should render the obtained hydrogels different properties when compared to one another.

The main goals of this dissertation can be divided into four categories: a) production and purification of different SELP copolymers; b) characterization of the gelling process for each SELP and c) evaluation of the hydrogels' viscoelastic and mechanical properties; d) study of the effect of the VPAVG sequence on the physiochemical characteristics of the hydrogels. In order to achieve the later objectives, a work plan was designed:

1. Heterologous expression on *Escherichia coli* and purification of SELP copolymers;
2. Determination of the most adequate parameters for the gelling process;
3. Characterization of the gelling process for each SELP;
4. Characterization of hydrogels' physico-chemical properties.

2. Materials and methods

2. Materials and methods

2.1 Biological material and culture media

Escherichia coli strain BL21(DE3) was used for all proteins' expression. Bacterial cells in this dissertation were grown in Lysogeny Broth (LB) or Terrific Broth (TB), either liquid or solid (supplemented with 2% agar). All media were supplemented with ampicillin (100 μg/mL), as the selective marker for plasmid-containing cells. For the recombinant protein production, media was supplemented with lactose (0.2% (w/v)) as inducer (auto-induction media). The strain genotype and media recipes are depicted in Annex I a).

2.2 Heterologous protein expression and purification

2.2.1 Genetic material

In this study, the plasmid pCM13 containing the genes for the three different SELPs was used as expression vector. The pCM13 is a pET-system (Novagen) based plasmid that was constructed previously in our lab (Machado *et al.*, 2013b). The expression plasmids pCM13::SELP-59-A, pCM13::SELP-520-A and pCM13::SELP-1020-A were constructed previously (Machado *et al.*, 2013b) and provided for the realization of this study. All of the copolymers were designed to have similar molecular weight (around 55 kDa), but different silk to elastin ratio or different number of silk-like or elastin-like blocks (Figure 4).

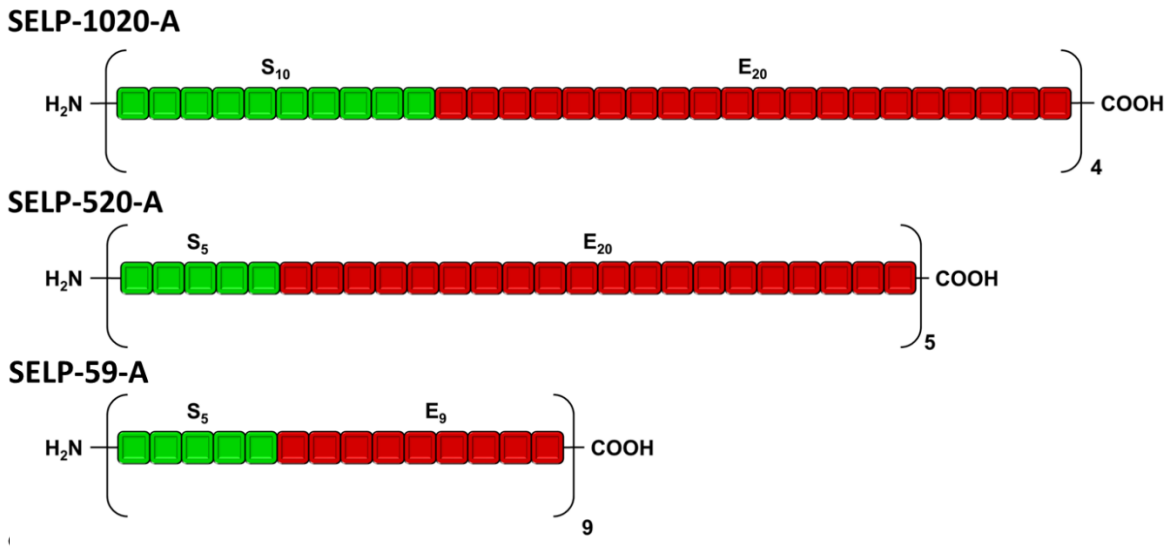

Figure 4 - Schematic representation of the SELP constructs used in this work, where Sx represents the number of silk-like blocks and Ey the number of elastin-like blocks (adapted from Machado *et al.*, 2013b).

2.2.2 Recombinant protein production and purification

2.2.2.1 *E. coli* transformation

E. coli strain BI21(DE3) was transformed with plasmid DNA, using a standard (thermal shock) transformation protocol (Sambrook & Russel, 2006). 200 µL of competent cells were thawed on ice and 0.5 to 5 µL (depending on the concentration) of plasmid DNA was added. The cells were kept in an ice bath for 30 min and subjected to a heat shock at 42°C for 1 min, followed for a new ice incubation for 10 min. Then, 800 µL of LB media was added and allowed to incubate at 37 °C with agitation (200 rpm) during 60 min. The cells were collected by centrifugation (13900 g, 10 min); 900 µL of supernatant was discarded and cells were resuspended in the remaining volume. 100 µL of sample were spread on a LB plate, supplemented with ampicillin (100 µg/mL), and incubated at 37 °C overnight.

2.2.2.2 Production screening

For analysis of the protein production levels of selected transformants, 7 colonies from each transformed construction were chosen and inoculated into 10 mL of fresh LB media, supplemented with ampicillin (100 µg/mL) and lactose (0.2% (w/v)), and grown at 37 °C, for 22 h, 200 rpm. Analysis of the

protein production levels was evaluated using Sodium Dodecyl Sulphate Polyacrylamide Gel Electrophoresis (SDS -PAGE). 1 mL of each culture was collected and centrifuged at 1900 g (Legend Micro 17 Centrifuge - Sorvall) for 10 min. The pellet was resuspended in 100 µL of TE buffer (Annex I b) and 25 µL of loading buffer (Annex I b) was added. To be able to compare production levels from different colonies, we normalized all samples to the same optical density (O.D. = 0.1 at 600 nm) using the following formula:

$$OD_i * V_i = OD_f * V_f$$

, where the OD_i is the OD_{600} of the cell culture and the OD_f is 0.1 final optical densities of the samples, and V_i is the initial sample volume (125 µL) and V_f is the final sample volume, that is to be loaded into 10% polyacrylamide gels (Annex I – Table 13), using 3.5 µL of molecular marker (NZYColour Protein Marker II – NZYTech or GRS Protein Ladder Multicolour - GRiSP) as size standard. Each gel was run at 15 mA and stained with copper chloride (3 M). The best producing colonies were chosen using a visual analysis of the obtained gels and preserved at – 80 °C using glycerol stocks for future use.

2.2.2.3 Protein production

The best producing colonies were then allowed to grow in TBlac + amp media, with a media to air ratio of 1:4 (250 mL of media in 1L flask), at 37 °C, during 22 h and 200 rpm. After the predefined elapsed fermentation time, the OD_{600nm} was measured for growth monitorization and the cells collected by centrifugation at 7585 g (Sigma 4-16KS), 4°C, 10 min, and stored -20 °C until purification.

2.2.2.4 Protein Purification

Collected cells were resuspended in TE buffer and lysed by ultrasonic disruption (sonication) using a Vibra cell™ 75043 (Bioblock Scientific, 750W max power) sonicator with a solid probe of 25 mm diameter. Ultrasonic treatment was applied with an amplitude of 60% for 3 s, followed by a 9 s pulse-off delay with a total sonication time of 10 min. Samples were kept on ice throughout the process. Following disruption, the samples were subjected to an acidification process, using concentrated Hydrochloric acid (HCl) (37%(v/v)) (Annex I b) to a pH value of 3,5 and incubated for 30 min, at 4 °C. After acidification, precipitated proteins that were not of interest were removed by centrifugation at 10695 g for 20 min, at

4°C. The SELP copolymers that remained in the collected supernatant were then subjected to a salting-out process, utilizing a % of ammonium sulphate saturation of 30% (Sigma- Aldrich Lot # SZBD1160V) at 4 °C during 30 min. Calculation of the % of saturation was performed using the online calculator provide by EncoBio (https://www.encorbio.com/protocols/AM-SO4.htm).After precipitation, samples were centrifuged at 10 695 g (Sigma 4-16KS) for 20 min, at 4°C and the pellet resuspended in ultrapure water overnight, at 4 °C. Dialysis against water was performed to remove the remaining salts, for 3 days at 4 °C with 12-14 KDa dialysis membranes from Medicell Membranes, Ltd.The protein solution was then filtered through a PES 0.45 µm Minisart Syringe Filter (Sartorius) and freeze-dried (Christ Alpha 2-4 LDplus from Bioblock Scientific). Samples were stored, lyophilized, at room temperature until further use. The purification process was monitored using SDS-PAGE (for polyacrylamide gel recipe see Annex II – Table 15) throughout all the steps.

2.2.2.4.1 Optimization of the purification process

All SELP constructions had their purification process optimized in terms of salting out parameters, namely the % of ammonium sulphate saturation. Small production batches were used to test 15%, 20%, 25%, 30% and 35% of ammonium sulphate saturation. The results were then analysed by SDS-PAGE.

2.3 Characterization of the physio-chemical properties of the gelation process

2.3.1 Thermal characterization by Differential Scanning Calorimetry (DSC)

DSC experiments were carried out on a differential scanning calorimeter (DSC821 - Mettler Toledo) to detect exothermic and endothermic reactions occurring in SELP solutions. Analyses were carried out in aqueous protein polymer sample solutions in different concentrations (5%, 10%, 15% and 20% (w/v)). In each DSC run, 25 µL of sample solution were loaded into a 40 µL aluminium crucible, hermetically sealed and placed on the calorimeter. The samples were then subjected to 4 heating/cooling cycles, with three different stages, with liquid nitrogen acting as the cooler. The samples were firstly subjected an isothermal step, stabilization period of 5 min. at 4°C, followed by a heating stage from 4°C to 70 °C and a cooling stage, from 70 °C to 4 °C, both at a heating/cooling rate of 1°C/min. The heating and cooling

stage were repeated 3 times without isothermal steps in-between. The peaks onset temperature and enthalpy (ΔH) values were calculated using the STARe software (Mettler Toledo).

2.3.2 Turbidimetry assays using UV-Vis Spectrophotometry

Turbidimetry assays were performed to monitor the gelation process and the presence of an inverse temperature phase transition, based on protocols previously described (Isaacson *et al.*, 2017; Xia *et al.,* 2011)]. Monitorization of absorbance changes in function of temperature and time was carried out using aqueous protein solutions, of 2.5% (w/v) at 300 nm on an UV-Visible Spectrophotometer(UV-1700 PharmaSpec - Shimadzu), connected to a temperature controlled cell holder (TCC-240A - Shimadzu). Two different assays were performed, at constant and variable temperature. For the constant temperature assays, absorbance readings were taken each 4 seconds, for 2 h, at the following temperatures: 37 °C, 50 °C and 65 °C, with no equilibration time. For the variable temperature assays, protein polymer samples were heated from 20 °C to 70°C and back to 20°C at a manual rate of 1 °C/min. In this assay absorbance readings were taken after an equilibration period of 30 s.

2.3.3 Molecular size distribution profiles by Dynamic Light Scattering (DLS)

Dynamic Light Scattering (DLS) characterization was performed using a Zetasizer Nano equipment (Malvern). Measurements were performed with aqueous protein solutions (0.5% (w/v)), into disposable 4-clear sides plastic cuvettes and with no stabilization period. Four different temperatures were tested: 25 °C, 37 °C, 50 °C and 65 °C. 6 individual runs were done for each temperature, with 20 measurements each. Analysis of results was performed using Zetasizer software v 7.13 from Malvern.

2.3.4 Monitorization of the gelation process

For the monitorization of the gelation process we tested the three SELPs at four different concentrations: 2.5 %, 5%, 10% and 15% (w/v) and two different temperatures: 65 °C and 37°C. We used 400 – 500 µL of an aqueous SELP solution, loaded into 1 mL clear glass vials and incubated for 2 h at the desired temperature. The curing process was accompanied by taking photos of the vials every 15 seconds

using a time-lapse procedure. After the cure time, all shells were immediately immersed in liquid nitrogen and stored at -80°C until lyophilization.

2.3.5 Morphological evaluation using Scanning Electron Microscopy (SEM)

We used Scanning Electron Microscopy (SEM; Leica Cambridge) to perform morphological evaluation of the dried samples obtained in the previous step. Prior to evaluation samples were coated with a thin gold/palladium layer using a sputter coater (Polaron model SC502), and ImageJ software (Schneider *et al.*, 2012) to determine mean pore size. Both the top and lateral sides were used.

2.3.6 Mechanical characterization

For the studies of the viscoelastic properties, we used aqueous polymer solutions at four different concentrations: 2.5%, 5%, 10% and 15% (w/v).The assays were performed in a Ares G2 rheometer and monitorization of changes in tan δ values and storage (G') and loss (G'') moduli was done using TRIOS software v 4.1.1.3307 (TA instruments). The studies were done using plate-plate geometry, in a 25 mm stain-less steel parallel plate (gap of 1000 µm). The samples were subjected to a heating ramp from 4°C to 65 °C, at a rate of 1 °C/min., at a constant strain (1%) and frequency (1 Hz or 6.28 rad/s). Before the measurements took place, samples were stabilized at the initial temperature during 1 min.

2.3.7 Attenuated Total Reflection (ATR) FT-IR

Secondary structure of the lyophilized aerogels was analysed using a FT-IR Spectrometer Spectrum Two coupled with Perkin Elmer UATR Two accessory and data was analysed using Spectrum IR software (Perkin Elmer). Spectra from 4000 cm^{-1} to 400 cm^{-1} was acquired at room temperature, for each measurement 64 scans were taken with a resolution of 4 cm^{-1} and using a diamande crystal.

3.Results and Discussion

3. Results and Discussion

3.1. Protein production and purification

3.1.1. Production screenings

The pET-based plasmids containing DNA sequences coding for the SELPs utilized in this work were transformed into Escherichia coli strain BL21(DE3) for protein production. Analysis of protein production levels of the selected transformants was performed using SDS-PAGE. For each SELP construct 7 different colonies were analysed, all normalized to same optical density ($O.D._{600}$= 0.1). The best producing colonies were chosen based on a visual analysis of the obtained gels (Figure 5). It was observed that all chosen transformants were able to produce their respective SELP copolymer. The bands that correspond to the SELP constructs have a molecular weight of around 55 kDa, even though in Figure 5, the proteins appear at a higher molecular weight. This phenomenon is not entirely uncommon and it is known as "gel shifting" (Rath *et al.*, 2009). The direct cause for this behaviour is yet unknown but some theories have been proposed regarding SDS binding (Rath *et al.*, 2009), the hydrophobicity of the molecules (Shirai *et al.*, 2008) and also post-translational modifications (Wold, 1981). In figure 5 c), in lane 7, it was observed a band with lower molecular weight. We believe this band corresponds to a truncated isoform of SELP-1020-A copolymer due to the high number of repetitions of the same amino acid residues. For both SELP-59-A and SELP-1020-A, colony 6 was chosen as the best producers whereas for SELP-520-A, colony 4 was considered the best producer.

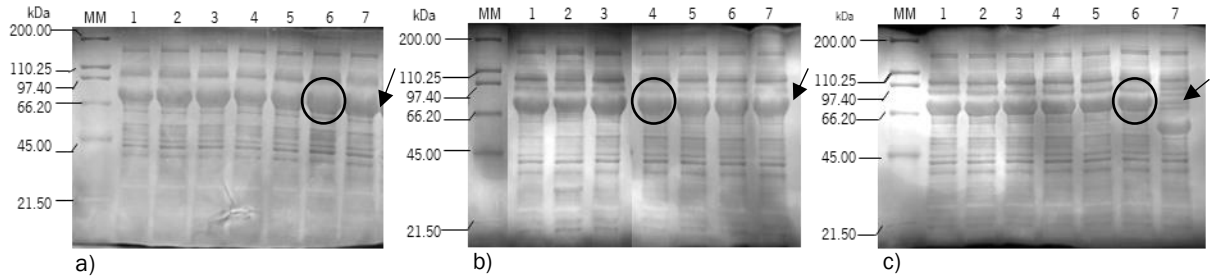

Figure 5 - SDS-PAGE of the production screening from different *E. coli* transformants producing different SELPs: a) SELP-59-A; b) SELP-520-A; c) SELP-1020-A. Lanes 1 to 7 represent different colonies used in the production screenings; MM – Molecular Marker (GRS Protein Ladder Multicolour – GRiSP). The arrow points to the protein of interest and the chosen colonies for subsequent production are indicated with a circle.

3.1.2. Optimization of purification protocol

Affinity chromatography is usually the preferred method for purification of recombinant proteins, and even though it allows for very pure protein fractions, is a very laborious and expensive technique and difficult to scale-up. On the other hand, non-chromatographic, are much less expensive and more straightforward and should be considered as on option for SELP purification. In the present dissertation a non-chromatographic method, based on the use of an acidic pH coupled with ammonium sulphate precipitation, was chosen (Machado, *et al.*, 2013a). Due to the known chemical stability of these proteins, the low pH is expected to precipitate the endogenous *E. coli* proteins, while the proteins of interest remain in solution (Machado, *et al.*, 2013a). The ammonium sulphate precipitation takes advantage of the hydrophobic nature of these proteins, causing their precipitation in solution and leaving possible contaminants soluble (Lyons *et* al., 2007; Machado, *et al.*, 2013a). The ammonium sulphate concentration required to precipitate has been shown to be dependent on protein size, in spider silk proteins, where lower % of saturation caused larger proteins to precipitate, and smaller proteins required higher % to achieve the same response (Scheller & Conrad, 2001). With that in mind, several % of saturation of ammonium sulphate were tested in this dissertation. To assess the optimal % of ammonium sulphate to cause the complete precipitation of the SELP proteins, five different final concentrations were chosen, 15, 20, 25, 30 and 35% saturation. All SELP copolymers precipitated from the acidic solutions at relatively low % of saturation. A concentration of ammonium sulphate of 15% was enough to precipitate SELP-59-A from solution, while for SELP-520-A and SELP-1020-A a concentration of 20% saturation was required (Figure 6). Precipitation of SELP proteins using this method had already been described by Machado and co-workers (2013a). In this study, a low concentration of ammonium sulphate (20% saturation) were sufficient to cause the precipitation of the SELPs studied and this fact was attributed to the hydrophobic nature of the copolymers (Machado, *et al.*, 2013a). Even though a saturation of 20% of ammonium sulphate would be sufficient to precipitate our copolymers, the concentration of 25% saturation was chosen to ensure that protein precipitation is as efficient as possible All possible remaining contaminants are further removed when the precipitate, obtained after centrifugation of the solution with ammonium sulphate, is later resolubilised in deionized water, while the contaminants remain insoluble. The obtained solution in later subjected to centrifugation and filtration in order to remove the remaining contaminants (Figure 7).

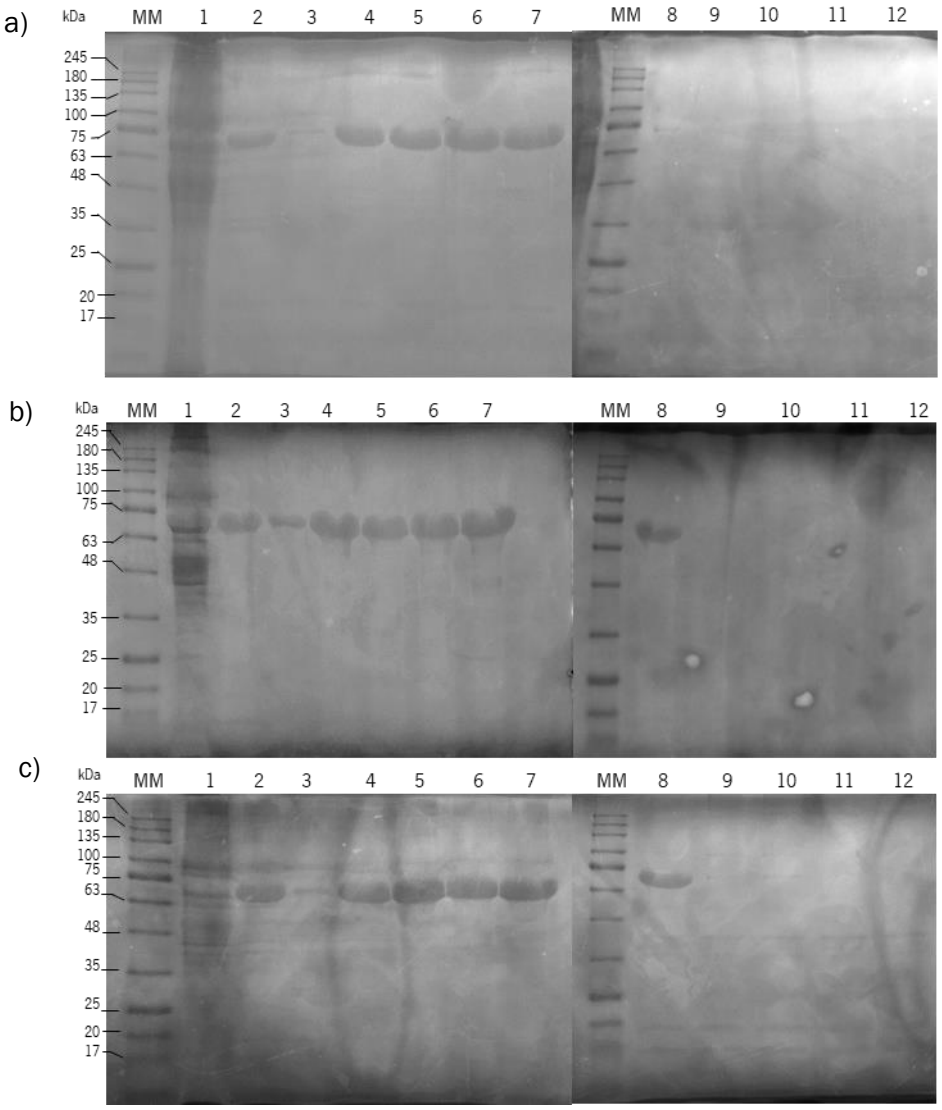

Figure 6 - SDS-PAGE representing the purification of the recombinant SELPs: a) SELP-59-A ;b) SELP-520-A; c) SELP-1020-A; lane 1 - crude cell extract; lane 2 – supernatant of the pre-acidification step; lanes 3 to 7 – pellet obtained after ammonium sulphate precipitation at increasing % saturation (15%, 20%, 25%, 30%, 35%); lanes 8 to 12 – supernatant obtained after ammonium sulphate precipitation at increasing % saturation (15%, 20%, 25%, 30%, 35%). MM – Molecular Marker (NZYColour Protein Marker II)

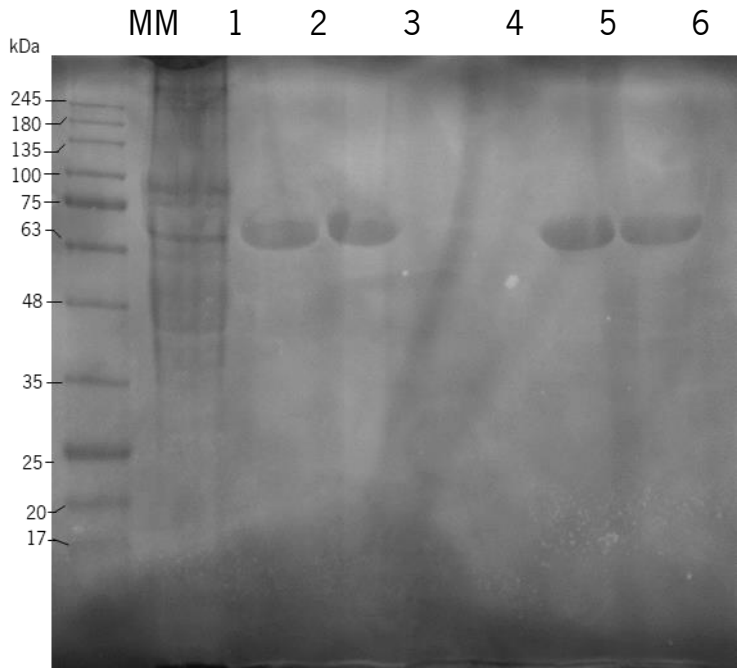

Figure 7 - SDS-PAGE representing the optimized purification protocol (acidification coupled with ammonium sulphate precipitation) for SELP-1020-A; lane 1 – crude cell extract; 2 – supernatant of the pre-acidification step; 3 – pellet obtained after ammonium sulphate precipitation at 25% saturation 4 – supernatant after ammonium sulphate precipitation at 25% saturation; 5 – sample before dialysis (same as lane 3); 6 – supernatant after dialysis. MM -Molecular Marker (NZYColour Protein Marker II).

3.2. Characterization of the physical-chemical properties of the gelling process

3.2.1. Thermal transition properties

Differential scanning calorimetry assays were performed on SELP aqueous solution, to observe their thermal transition properties. We evaluated the presence/absence of peaks relative to the baseline curve, the type of occurring reaction (endothermic/exothermic), their respective enthalpy values and temperatures. These parameters were analysed in function of the number of heating/cooling cycles for each concentration, between different concentrations for the same heating/cooling cycle and of course, in function of polymer composition. All SELP solutions underwent a transition involving energy (exothermal and endothermal peaks were observed, Tables 2, 3 and 4, Annex II - Figures 19, 20 and 21). The endothermic peak is thought to represent a crystallization event, that occurs at a defined temperature, further on referred as transition temperature (T_t), whereas the exothermic peaks are thought to represent the chain unfolding that ultimately leads to dissolution, also occurring at a defined temperature, designated resolubilisation temperature (T_r). Both T_t and T_r were calculated based on the onset of the endothermal and exothermal peaks, respectively (Cappello *et al.*, 1998; Machado *et al.*, 2009; Xia *et al.*, 2011). Interestingly, in some SELP solutions this transition was fully reversible and coupled with hysteresis behaviour

(Tables 2, 3 and 4). The reversibility of the process was expected since it had already been observed in SELP solutions (Xia *et al.*, 2011). The hysteresis behaviour presented is thought to be due to the VPAVG sequence present in the used SELPs, even though this type of behaviour hasn't been reported in SELPs, it has been observed in previous DSC experiments of poly(VPAVG) homopolymers (Machado *et al.*, 2009; Reguera *et al.*, 2003). The hysteresis behaviour is typically characterized by differences in the determined transition and dissolution temperatures, meaning that the polymers assembles at a T_t and only re-dissolves after strong undercoolings are applied (Machado *et al.*, 2009; Reguera *et al.*, 2003). All SELP solutions tested presented the behaviour described, (although for SELP-59-A this was only observed in higher concentration solutions (20% (w/v). (For graphics of the DSC runs and respective tables containing reaction peak, onset and endset temperatures, as well as respective enthalpy values (ΔH), see Annex II – Figures 19-21 and Tables 16–19, respectively.)

From all SELP copolymers, at all concentrations and heating cycles, only one endothermic peak was observed, even though differences were found in the corresponding T_t in function of polymer concentration (Annex II Figures 19, 20 and 21). The SELP solutions presented a slight decrease in the T_t when the concentration was increased from 15% to 20% (w/v), while with less impact on SELP-59-A solutions. SELP-59-A presented the highest Tt of around 60 °C at 5% (w/v), decreasing only when the concentration increased to 20% (w/v) to 59 °C. For 5%, 10% and 15% (w/v) SELP-520-A and SELP-1020-A copolymer solutions, the mean transition temperatures were determined to be 40 °C and 44 °C, respectively. When the concentration was increased to 20% (w/v), a decrease in the T_t was observed to 39 °C for SELP-520-A and 38 °C for SELP-1020-A. The concentration effect on the decrease of the transition temperature seems to be related to the length of the elastin-like blocks, since SELPs with longer elastin blocks, namely SELP-520-A and -1020-A, presented the most pronounced changes. The enthalpy values determined for each peak were also found to be influenced by concentration but showed little or no difference between cycles. The polymer with lower S:E ratio (1:4; SELP-520-A) presented the lowest T_t, followed by SELP-1020-A and lastly SELP-59-A. Even though SELP-1020-A and SELP-59-A have the same S:E ratio (1:2), in SELP-1020-A, elastin-like blocks are longer than in SELP-59-A, thus increasing the temperature needed to induce crosslink formation. The increase in enthalpy values as the concentration increases can be explained by an increasing number of crosslinking forming units, thus increasing enthalpy values (Ahad, 1974).

In the cooling cycles, the three polymers displayed very different behaviours. For SELP-59-A, only after increasing the concentration to 20% (w/v) was possible to observe one exothermic peak between 25-27 °C, with little to no variation in enthalpy values from cycle to cycle. SELP-520-A also presented only

one exothermal transition between 37 ° C and 38 °C, at all concentrations and cooling cycles. Interestingly, in SELP-1020-A two exothermic peaks were observed in the polymer solutions with 5%, 10% and 15% (w/v): a smaller peak at 15-20 °C and a bigger peak around 40 °C. However, in the concentration of 20% (w/v) only one peak was observed, at an intermediate temperature of 35 °C, but with higher values of enthalpy (Table 3). One obvious hypothesis is that the sole peak presented at this concentration is no more than the fusion of the two peaks found in the lower concentrations, since the peak is much wider. The two exothermic peaks found in the cooling stage may be explained with the individual unfolding of both elastin and the silk-like blocks, since SELP-1020-A presents the longest blocks, when comparing to SELP-59-A and SELP-520-A, allowing for their behaviour to be seen separately. When comparing different concentrations of the same polymer and the same cycle, it was observed that the enthalpy values for all SELPs increased as the concentration was increased, even though no significant differences were observed between the concentrations 15% and 20% (w/v). The detection of exothermal reactions, and the fact that enthalpy values are very similar between endothermal and exothermal peaks throughout the heating and cooling cycles, would mean that the polymers' transitions are fully reversible.

Similar results were obtained by Xia and co-workers (2011), where three different SELP analogues were analysed. Only one exothermal peak was observed for SELP-18-Y and SELP-28-Y at 27 °C and 33 °C respectively, but there was an absence of a peak for SELP-48-Y. The absence of a peak for the later SELP was explained as an indicative that crystallization had already occurred before the analysis was performed. A more recent study regarding the same SELP analogues, but at higher concentrations, presented very similar results. SELP-18-Y and SELP-28-Y exhibited transition temperatures at 21 °C and 25 °C, respectively, whereas for SELP-48-Y, no thermoresponse was observed (Huang *et al.*, 2016). In another study regarding SELPs, the same phenomenon was detected (Cappello *et* al., 1998). Crystallization through β-sheet formation is thought to be the process responsible for the gelation of SELPs, due to previous studies where additives, which were known to disrupt and prevent hydrogen bonding or to induce crystal formation, were added to the solution (Cappello *et al.*, 1998; Megeed *et al.*, 2002). Addition of pre-gelled SELP to the solution effectively accelerated the gelation process and the addition of urea (a known denaturing agent) practically eliminated gelation, when compared to control solutions (Cappello *et al.*, 1998; Megeed *et al.*, 2002).

With the present study, we determined one thermal transition temperature and one dissolution temperature for each SELP copolymer. We also observed that polymer concentration plays a role on the amount of energy involved in these same transitions, meaning that higher concentrations lead to an increase in the released/absorbed energy due to a higher number of molecules present in solution. As it

was expected, all SELP copolymers tested presented a reversible thermal transition coupled with an acute hysteresis behaviour, probably due to the presence of the VPAVG sequence (Annex II Figures 19, 20 and 21).

Table 2 - SELP-59-A peak temperatures (ºC) and enthalpy values (ΔH) in function of concentration (w/v) and number of cycles.

		Heating run				Cooling run			
		Cycle 1	**Cycle 2**	**Cycle 3**	**Cycle 4**	**Cycle 1**	**Cycle 2**	**Cycle 3**	**Cycle 4**
5%	Integral (mJ)	-1.8	-1,5	-1,1	-1,0	-	-	-	-
	Onset (°C)	60	61	60	60	-	-	-	-
10%	Integral (mJ)	-0.9	-2,9	-3,0	-2,3	-	-	-	-
	Onset (°C)	61	60	60	60	-	-	-	-
15%	Integral (mJ)	-0.4	-2,4	-2,2	-2,1	-	-	-	-
	Onset (°C)	64	60	60	60	-	-	-	-
20%	Integral (mJ)	-2.4	-2.3	-3,2	-3,6	0,8	0,8	0,7	0,7
	Onset (°C)	59	59	59	59	30	30	30	30

Table 3 - SELP-520-A peak temperatures (ºC) and enthalpy values (ΔH) in function of concentration (w/v) and number of cycles.

		Heating run				Cooling run			
	Cycle	**1**	**2**	**3**	**4**	**1**	**2**	**3**	**4**
5 %	Integral (mJ)	-8.5	-8.9	-8.7	-8.7	10.8	9.7	10.3	11.7
	Onset (°C)	41	41	41	41	37	36	35	37
10 %	Integral (mJ)	-19.1	-18.0	-19.7	-18.5	24.3	25.9	25.3	24.8
	Onset (°C)	40	40	40	40	36	36	36	36
15 %	Integral (mJ)	-25.9	-25.0	-25.1	-25.0	36.5	36.2	38.4	36.3
	Onset (°C)	40	40	40	40	35	35	36	36
20 %	Integral (mJ)	-26.1	-26.8	-25.9	-26.1	32.5	37.4	36.6	35.8
	Onset (°C)	38	38	38	38	36	36	36	36

Table 4 - SELP-1020-A peak temperatures (ºC) and enthalpy values (ΔH) in function of concentration (w/v) and number of cycles.

		Heating run				Cooling run							
	Cycle	**1**	**2**	**3**	**4**	**1**		**2**		**3**		**4**	
5 %	Integral (mJ)	-5.2	-3.8	-4.0	-5.0	2.1	1.3	3.0	2.4	2.9	1.7	2.9	-
	Onset (°C)	45	45	45	44	21	40	19	40	14	40	14	-
10 %	Integral (mJ)	-6.9	-5.4	-5.3	-5.7	3.0	2.6	3.3	3.4	4.0	1.9	4.8	2.2
	Onset (°C)	43	43	43	43	22	38	20	41	20	39	19	37
15 %	Integral (mJ)	-8.5	-7.2	-6.1	-5.7	3.8	5.9	5.2	4.0	4.7	4.3	5.1	3.1
	Onset (°C)	42	43	43	43	15	39	14	39	13	39	13	40
20 %	Integral (mJ)	-45.6	-44.7	-44.5	-44.9	58.8		63.5		64.0		63.2	
	Onset (°C)	35	35	35	35	27		28		27		28	

The thermal transition properties were confirmed by UV-Vis Spectrophotometry, on polymer aqueous solutions of 2.5% (w/v). The concentration used in this assay was inferior to the ones used in the DSC studies due to higher sensitivity of the spectrophotometry device when compared to DSC sensitivity, so some differences in the obtained results would be expected. Higher concentration solutions resulted in saturation of the absorbance readings and hindered the recognition of the solution thermal events. We analysed changes in $O.D._{300\ nm}$ in two different modes: function of time and temperature. For the temperature assay, absorbance changes were monitored as function of a temperature ramp and measurements were taken at each degree increment, heated from 20 °C to 70 °C and cooled back to 20°C (Figure 8).

In SELP-1020-A solutions, it was observed a two-step thermal transition (42 °C and 53 °C), as well as in SELP-59-A solutions (53 °C and 61 °C) in a lower extent. This behaviour was not found in the DSC experiments. For SELP-520-A only one thermal transition temperature was exhibited (~ 41 °C). As expected from the DSC results, the transitions detected are fully reversible for SELP-520-A and SELP-1020-A copolymers, a process not observed for SELP-59-A solution in the temperature range tested. There are some small changes in the determined temperatures in DSC and spectrophotometry, probably due to differences in the concentrations tested and equipment sensitivity and delay. The two-step thermal transition observed in SELP-59-A and SELP-1020-A, was probably due to higher S:E ratio (1:2) of these polymers, allowing for the observation of the individual transition of the elastin-like blocks, at lower temperatures, and the silk-like blocks, at higher temperatures. This is consistent with previous findings, as it is known that elastin-like peptides might have their thermal transition properties altered upon fusion with other amino acidic sequences (Trabbic-Carlson *et al.*, 2004). Soluble ELPs were demonstrated to

have a thermal transition in the temperature range of 30-50 °C (Megeed *et al.*, 2004) and silk fibroin films containg water (acting like a plasticizer (Hu *et al.*, 2007)) were found to have a lower glass transition (~80 °C) than in pure dry silk fibroin films (178 °C) (McGill *et al.*, 2019). It was then expected for some copolymers to exibit the combined thermal transition properties of SF in water and soluble ELPs. In the case of SELP-520-A, only one thermal transition was observed probably due to smaller S:E ratio (1:4), leading to the observation of only the transition regarding the elastin-like blocks, masking the contribution of silk-like blocks on thermal transition properties.

In the cooling run, absorbance values were stable until temperature was cooled down to 38 °C and 31 °C, for SELP-1020-A and SELP-520-A, respectively. In the case of SELP-59-A it was observed a slight decrease in the $O.D._{300nm}$ values as temperature was decreased but with no measurable peak as observed for the other two copolymers, suggesting that a higher range of temperatures is needed to observe measurable peaks. The rapid decrease in the absorbance values was attributed to the resolubilisation of the copolymers due to decrease in network stability (Xia *et al.*, 2011) The obtained results were not as expected, since it was theorized that higher silk-to-elastin ratio would lead to lower reversibility of the thermal transitions, probably due to irreversible crosslinks formed between the silk-like blocks (Xia *et al.*, 2011). By this theory, SELP-520-A should present reversibility at higher temperatures (S:E ratio of 1:4), followed by SELP-1020-A (1:2) and finally SELP-59-A (1:2). Even though SELP-59-A and SELP-1020-A present the same silk-to elastin ratio, the later has longer interrupting elastin units between the crosslink forming silk-units, which should lead to a decreased network stability at lower temperatures. We believe that SELP-520-A adopts a different conformation than the ones possibly adopted by the other co-polymers. This polymer could have the ability to self-assemble into micelle-like nanoparticles upon heating, since it was previously demonstrated that in low silk-to-elastin ratios, some SELP copolymers showed the ability to self-assemble into micellar-like nanoparticles, spontaneously or heat induced, due to high differences in the blocks solubility (Xia *et al.*, 2011). In the particle-like state, chains would be closer together allowing a higher/stronger degree of crosslink and therefore, increasing stability at lower temperatures. The higher stability of SELP-59-A at low temperatures, when compared to the other two analogues, can be attributed to a high silk-to-elastin ratio, coupled with small interrupting elastin units. It is known that the elastin-like blocks are responsible for the thermoreversibility of this process (Cappello *et al.*, 1998), so it is feasible that the copolymer which presents less elastin-units also presents decreased thermoreversibility.

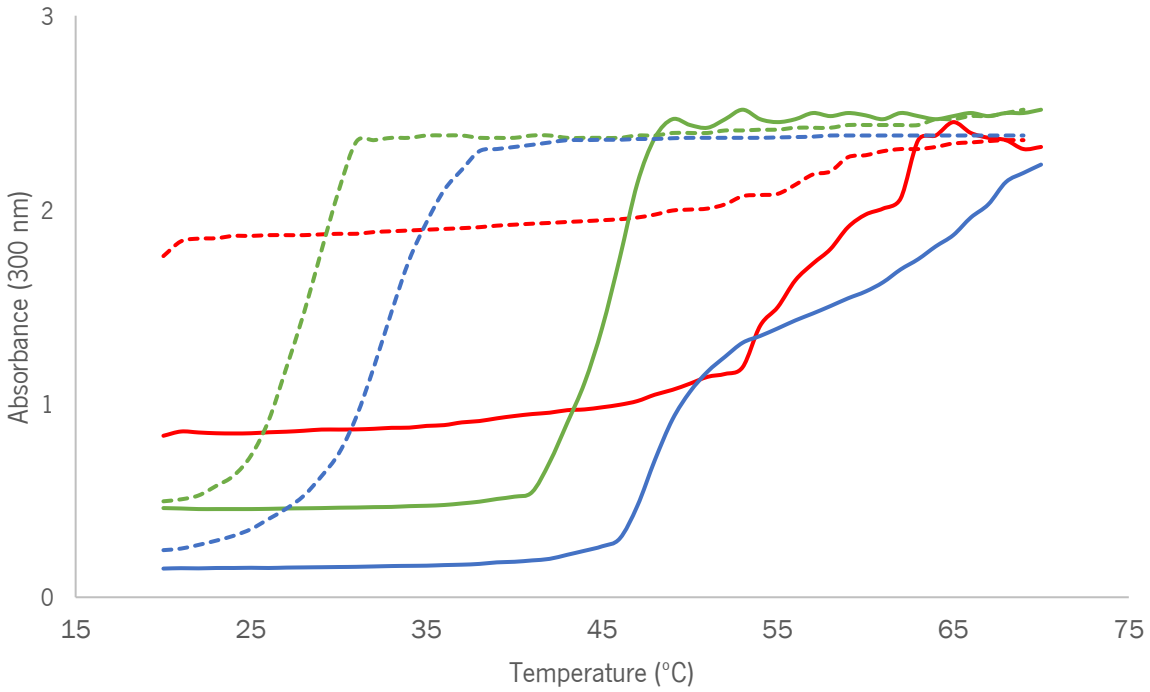

Figure 8 - Turbidimetry profiles of SELP-59-A (red), SELP-520-A (green) and SELP-1020-A (blue) in water. The absorbance of the solutions was measured at 300 nm during heating from 20 °C to 70 °C (solid line) and cooling back to 20 °C (dashed lines).

Thermal transition properties of some SELP copolymers have already been studied by some authors (Isaacson *et al.*, 2018; Nagarsekar *et al.*, 2002; Xia *et al.*, 2011). From the three copolymers studied by Xia and co-workers (2011), two demonstarted a two-step thermal transition, SELP-18-Y and SELP-28-Y: the first one starting at temperatures below 40 °C and the second at temperatures below 60 °C. The explanation given by the authors states that the first transition is caused by the self-assembly of free chains into small micellar-like particles and the second transition was caused by particle-particle interactions leading to formation of larger coacervates. We believe that this explanation cannot be completely applied to our study, since the concentrations used were significantly higher than the ones tested by Xia *et al.*, meaning that the SELP molecules could be forming different stuctures in function of the polymer concentration. Interestingly, in the previous study, another SELP studied, SELP-48-Y did not show any obvious thermal transitions and so it was assumed that the high ratio of silk to elastin-like blocks would mask the role of elastin blocks in the polymers (Xia *et al.*, 2011). In another study using different SELP nanogels, performed by Isaacson *et al.* (2018), the thermal transitions of SELP-415-K, SELP-47-K and SELP-815-K nanogels were assessed. Once again, it was observed a two-step thermal transition for SELP-415-K and for SELP-47-K whereas for SELP-815-K only one thermal transition was depicted. The

authors claimed that the fact for the appearance of only one thermal event was probably due to a gelation event already occuring prior to the experiment (Isaacson *et al.*, 2018).

Reversibility of the self-assembly process in SELPs was described by Nagarsekar and co-workers (2002), where 5% (w/v) SELP copolymer, containing one repeat of silk-like units and eight repeats of elastin-like units, was heated from 20 °C to 100 °C and cooled back to 20 °C, where the superimpositions of the heating and cooling curves would suggest reversibility of the process. The authors stated that, when the polymer is in a soluble state, polymer chains are surrounded by water in a hydrophobic hydratation state and, as temperature increses, this water will become less ordered and the polymer will self-assemble thorugh hydrophobic self-assembly. The reversibility of the self-assembly process was thought to be due to a reorganization of the waters of the hydrophobic hydration, hydrating the polymers chains, causing ressolubilization.

The results obtained in our study are consistent with previous findings. We have demonstrated a two-step self assembly process for SELP-520-A and SELP-1020-A, with higher silk-to-elastin ratios, and one thermal transition for SELP-59-A. We have also demonstrated that these transitions are fully reversible and coupled with a hysteresis behaviour. Polymer concentration was shown to have an effect on the T_t, where an increase in concentration lead to a decrease in the transition temperatures, even though was considered non significat. The enthalpy values associated with the thermal transitions were also found to be affected by concentration, these differences were found to be highly significant, since an increase in polymer concentration lead to a pronouced increase in the amount of energy involved in this process. The fact that the enthaply values showed no dependence on the number of heating and cooling cycles also point to the fact that the SELP self-assembly is fully reversible, meaning that can be heated and cooled repetidely without modification of their thermal transition properties. The differences found between the determined T_t and T_r, are indicative of a hysteresis behaviour, and this feature was atributed to the presence of the sequence VPAVG in the SELPs used. This particular characteristic means that after the solutions are heated above their transition temperatures, ressolubilisation only occurs after strong undercooling are applied, far beneath the T_t.

For the time-based assays (Figure 9), each polymer was monitored for absorbance changes during two hours at three pre-defined temperatures below and above their respective T_t, that were chosen accordingly to the DSC and temperature-based turbidimetry results, namely 37 °C, 50 °C and 65 °C. For SELP-59-A no differences were observed between 37 °C and 50 °C, since there was no significant difference in the absorbance values as time went by. When the temperature was raised to 65 °C (above the calculated T_t), we observed a very rapid increase in the absorbance value, that started to diminish as time

went by. This reduction in absorbance values was caused by the formation of aggregates that precipitated and avoided the spectrophotometer light path (Annex II, Figure 22). A similar phenomenon was observed in previous studies (Isaacson *et al.*, 2018). In this same study, SELP solutions that had been heated above their precipitation temperature T_p, demonstrated a decline in thermal reversibility, when compared to solutions only heated to temperatures below the T_t. This might explain why no reversibility was observed for SELP-59-A in the previous spectrophotometry assays, indicating that the second temperature transition is either very close to the precipitation temperature or was mistakenly labelled as a T_t. For confirmation of this assumptions, further studies are needed. For SELP-520-A solutions, 37 °C were not enough to cause any absorbance change, but when the temperature is raised to both 50 °C and 65 °C we could observe a rapid increase in the absorbance values, followed by a stabilization at 50 °C or a small increase after 1 h, at 65 °C. The $O.D._{300nm}$ profiles are similar at 50 °C and at 65 °C because this SELP only display one thermal event upon heating (~44 °C). To notice that a saturation of the absorbance values was rapidly found at 50 °C and 65 °C, that was not found in the 37 °C. SELP-1020-A also revealed no changes at 37 °C but a rapid increase in the absorbance values after the temperature is raised to 50 °C and further to 65 °C. After increase, the absorbance values stabilize throughout the experiment, even though $O.D._{300nm}$ values were greater at 65 °C than at 50 °C. The differences in absorbance values are related to the different thermal events occurring. At 50 °C only one thermal event was covered but at 65 °C, both events found in the DSC and temperature-based turbidity experiments are covered. The profiles obtained by UV-Vis spectrophotometry were as expected, since we only observed changes in absorbance in SELP solutions that had been heated above their T_t. In the overall, SELP-520-A showed the highest absorbance values at 65 °C and 50 °C and SELP-59-A had highest absorbance at 37 °C. The fact that SELP-59-A presented higher $O.D._{300nm}$ values below the transition temperature, could be due to the fact that gelation had already occurred before the experiment, and show that the gelation process, at least for this SELP, is not entirely dependent on temperature induction (Isaacson *et al.*, 2018; Xia *et al.*, 2011)

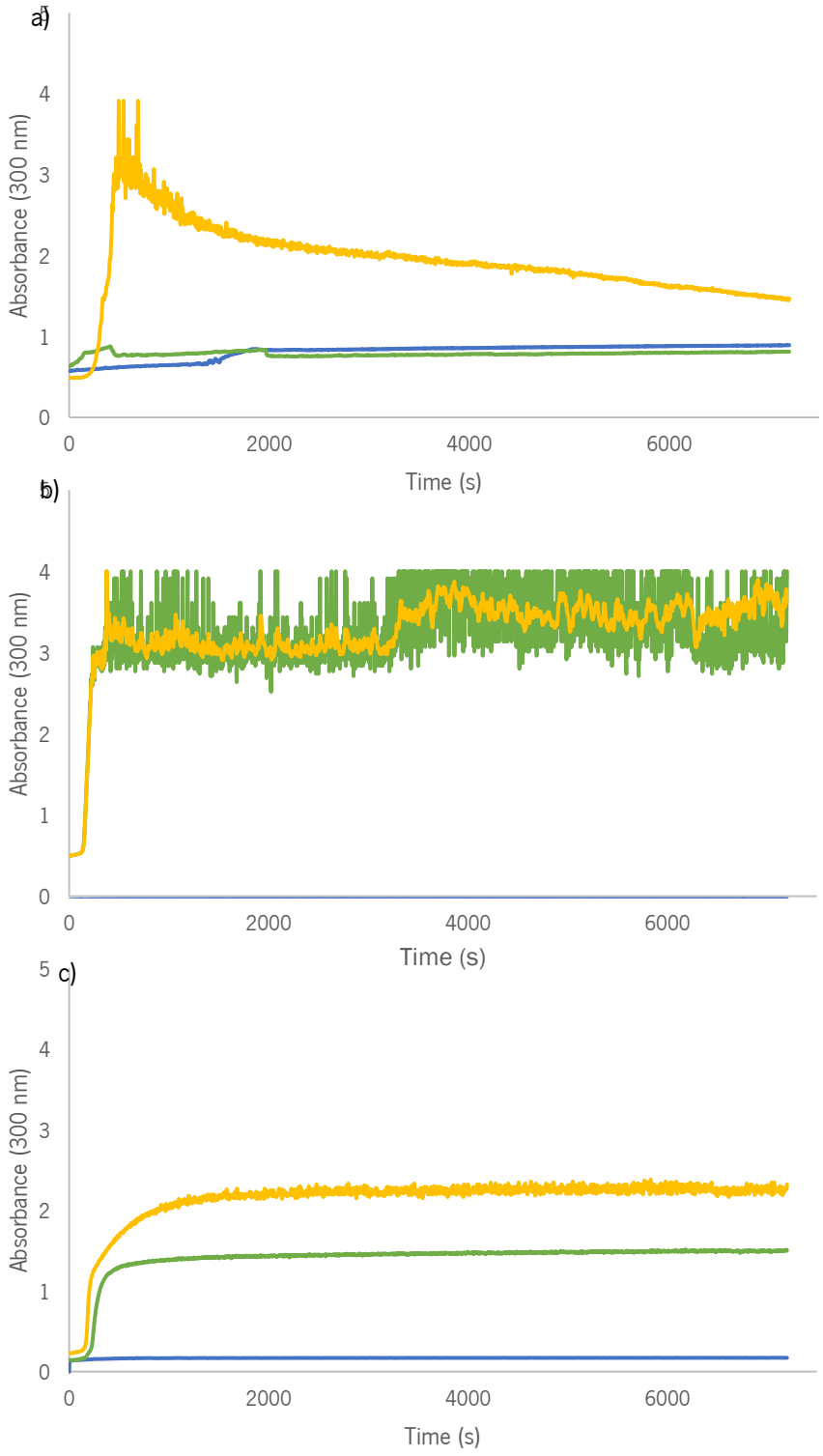

Figure 9 - Turbidimetry (absorbance measured at 300 nm) profiles for: (a) SELP-59-A, (b) SELP-520-A and (c) SELP-1020-A solutions cured at different temperatures over a period of 2 h (7200 s). Blue – 37 °C; Green – 50 °C; Red – 65 °C.

3.2.2. Molecular size distribution profiles as a function of polymer concentration, time and temperature.

Dynamic Light Scattering assays were performed to determine molecule size distribution profiles, for each SELP at a concentration of 0. % (w/v), the concentration used was further diminished relatively to the previous studies due to specifications/limitations of the used technique/device. Dynamic Light Scattering is a widely used technique to determine molecular sizes of water-soluble polymers, providing for a quick and straightforward approach. This technique allows for the study of different parameters, including determination of molecular sizes, the monitorization of aggregation phenomena and the influence of various factors on these parameters. One of the biggest advantages of this system is that it is non-invasive and non-destructive, plus it has a wide range of detectable sizes (from 0.001 to several microns) (Arzensek, 2010; Lorber *et al.*, 2012). Each SELP copolymer was subjected to four different temperatures, below and above the defined T_t: 37 °C, 50 °C and 65 °C (Figures 10-12 and Table 5-7). Room temperature samples (25 °C) were also used as negative controls of aggregates formation. We also evaluated size distribution profiles (% of intensity and PDI) in function of time, limiting DLS runs to 20 min with 6 different measurements for each sample/run, allowing us to see differences in time, t_1 vs. t_2 (measurement 1 (after 4 min) and measurement 6 (after 20 min)) (Annex II – Figure 23/Table 20-22).

No differences were observed between the profiles of SELP-59-A (Figure 10/Table 5) at 25 °C and 37 °C, both presented similar profiles with two peaks with a hydrodynamic diameter (D_h) of 14.51 ± 3.5 nm (25 °C) or 14.76 ± 3.7 nm (37 °C) and 116.2 ± 45.1 nm (25 °C) or 110.2 ± 43.9 nm (37 °C). A large intensity was found for the later peak corresponding to 80.6 % (25 °C) or 78.7 % (37 °C) of the population. When the temperature is raised above the first thermal event (~53 °C) the population of aggregates changes with the appearance of a third peak corresponding to particles with D_h of 3067 ± 1450 nm. When the temperature is further raised above the second thermal event (~61°C), the intensity of the scattered light of the third peak (in this temperature with a D_h of 2511 ± 1385 nm) increased accompanied by decrease of the other peaks intensity and a slight increase in the average D_h of the same peaks, when compared to the other temperatures tested. These results show that there is an increase of the number and size of the aggregates forming. On the other hand, we can say that, at this concentration, aggregate formation was observed throughout all temperatures tested, reinforcing the idea that, at least for this SELP, gelation can occur even at low temperature, i. e. beneath the designated transition temperatures.

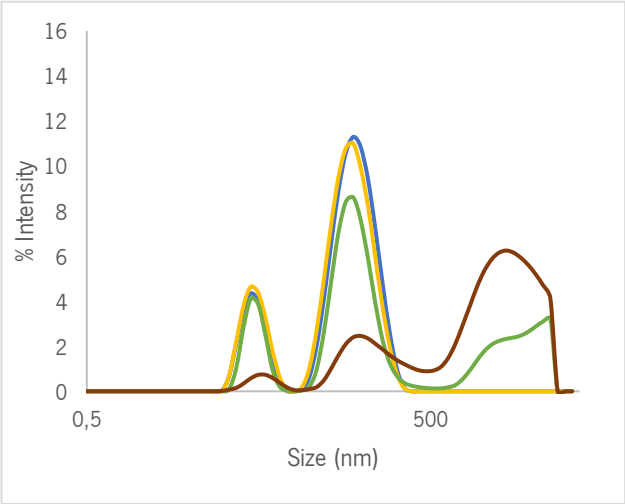

Figure 10 - Size distribution of 0.5% (w/v) SELP-59-A in water at 25 °C (blue), 37 °C (yellow), 50 °C (green) and 65 °C (brown).

Table 5 - Size distribution profiles of SELP-59-A solutions represented by the number and size of populations present, as well as their corresponding percentage of the total intensity. of the scattered light.

	Peak	Size (d.nm)	% Intensity	PDI
25 ºC	1	116.2 (± 45.1)	80.6	0.564
	2	14.5 (± 3.5)	19.4	
	3	-	-	
37 ºC	1	110.2 (± 43.9)	78.7	0.525
	2	14.8	21.3	
	3	-	-	
50 ºC	1	116.7 (± 55.5)	55.7	0.698
	2	3067 (±1450)	28.7	
	3	14.8 (±3.1)	15.5	
65 ºC	1	2511 (±1385)	72.6	0.802
	2	177.3	23.6	
	3	17.75 (± 5.5)	3.8	

SELP-520-A (Figure 11/Table 6) presented only one thermal transition around 41 °C in the previous studies. In that way it was expected that no significant changes would be found between the solutions tested at 25 °C and 37 °C (below T_t) and between solutions at 50 °C and 65 °C (above T_t). As expected, little to no difference was found when comparing the two pair of temperatures. The only major difference found regards the apparent increased homogeneity of particle size in samples tested at 65 °C relatively to the ones tested at 50 °C (Table 6). This difference may be due to a higher mobility of the polymer chains at higher temperature, making it easy for the polymers chains to find one another and form crosslinks, despite the small number of silk-like units, when compared to the other SELPs tested. The profiles at 25 °C and 37 °C, showed two peaks, the one with higher intensity with D_h of 267.6 ± 214.1 for 25 °C and 203.8 ± 105 nm for 37 °C and a peak with a smaller intensity with a D_h of 14.5 ± 3.5 at 25 °C and 15.1 ± 4.1 nm at 37 °C. When the temperature was raised to 50 °C and 65 °C we observed an increase in the hydrodynamic diameters, with a peak with higher intensity at a D_h of 385 ± 229.8 nm for 50 °C and 275.4 ± 182.5 nm for 65 °C, and the peaks with lower scattered light intensities at a D_h of 36.3 ± 16.6 nm at 50 °C and 36.4 ±16.4 nm for 60 °C. This polymer followed the tendency presented by SELP-59-A, which is the formation of ever larger coacervates as the temperature is risen above the transition temperature.

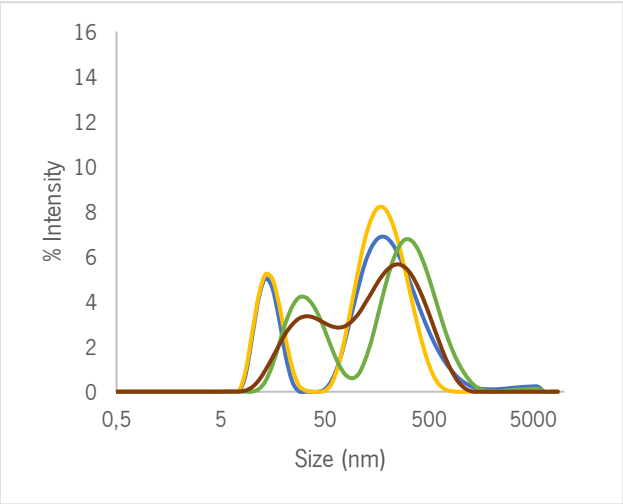

Figure 11 - Size distribution of 0.5% (w/v) SELP-520-A in water at 25 °C (blue), 37 °C (yellow), 50 °C (green) and 65 °C (brown).

Table 6 - Size distribution profiles of the SELP-520-A solutions represented by the number and size of populations present, as well as their corresponding percentage of the total intensity of the scattered light.

	Peak	Size (d.nm)	% Intensity	PDI
25 ºC	1	267.6 (± 214.1)	76.1	1.0
	2	14.5 (± 3.5)	22.5	
	3	3814 (± 1144)	14	
37 ºC	1	203.8 (± 105)	74.1	0.675
	2	15.1 (± 4.2)	25.9	
	3	-	-	
50 ºC	1	385 (± 229.8)	66.1	0.676
	2	36.3 (± 16.6)	33.3	
	3	4087 (± 1045)	0.6	
65 ºC	1	275.4 (± 182.5)	68.1	0.537
	2	36.4 (± 16.4)	31.9	
	3	-	-	

In SELP-1020-A size distribution profiles (Figure 12/Table 7), it was observed different profiles with the increasing temperature. At 25 °C and 37 °C (bellow the first thermal event, 42 °C) small changes were depicted, but in the increased temperatures a shift on the aggregates' population was observed. The peaks representing smaller D_h, would increase terms of scattered light intensity when the temperature was risen to 50 °C and then to 65 °C, meaning that with increasing temperature a structuration could be occurring. At 25 °C and 37 °C, two peaks were observed at D_h of 14.9 ± 4.9 nm and 258.3 ± 113.8 nm at 25 °C and 14.1 ± 3.9 nm and 181.1 ± 64.7 nm at 37 °C. When the temperature is further raised to 50 °C and 65 °C a third peak, with lower intensity, was observed corresponding to with a dynamic diameter of 2551 ± 1313 nm for both temperatures. We believe that the peaks corresponding to smaller hydrodynamic diameters (14-40 nm) represent small particle aggregates and that the increase in the hydrodynamic diameter could be caused by the coalescence of the small aggregates into globular-like aggregates, according to previous findings in other SELPs (Isaacson *et al.*, 2018; Xia *et al.*, 2011).

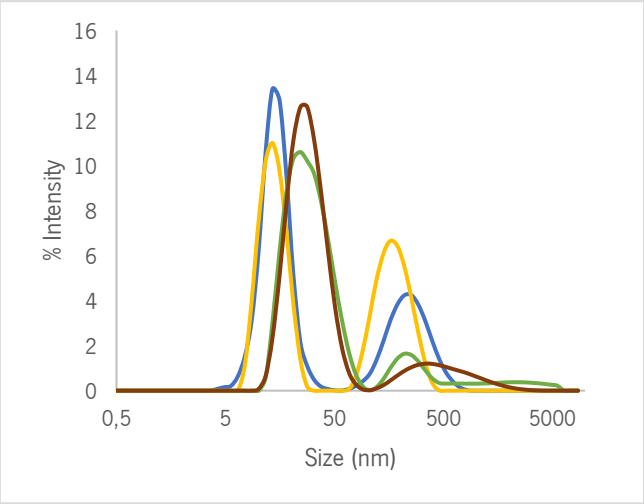

Figure 12 - Size distribution of 0.5% (w/v) SELP-1020-A in water at 25 °C (blue), 37 °C (yellow), 50 °C (green) and 65 °C (brown).

Table 7 - Size distribution profiles of the SELP-1020-A solutions represented by the number and size of populations present, as well as their corresponding percentage of the total intensity of the scattered light.

	Peak	Size (d.nm)	% Intensity	PDI
25 ºC	1	14.9 (± 4.9)	67.6	0.445
	2	258.3 (± 113.8)	32.4	
	3	-	-	
37 ºC	1	14.05 (± 3.9)	56.2	0.501
	2	181.4 (± 64.7)	43.8	
	3	-	-	
50 ºC	1	30.8 (± 13.8)	84.5	0.290
	2	258.8 (± 92.8)	97	
	3	2551 (± 1313)	4.2	
65 ºC	1	29.4 (± 11.6)	85.7	0.288
	2	585.4 (±456.3)	14.3.	
	3	-	-	

The results obtained from this assay were as expected, since all SELP copolymers only demonstrated changes in size distribution profiles when temperature was increased above their T_t, as determined by DSC and spectrophotometry studies. SELP-59-A and SELP-520-A demonstrated a tendency to form aggregates with larger hydrodynamic radius when their transition temperatures were reached, on the contrary, SELP-1020-A presented the opposite behaviour. As temperature was increased above the T_t, this polymer showed a tendency to form smaller sized aggregates, probably due to a higher degree of molecules arrangement.

The Polydispersity Index (PDI) is a dimensionless value that indicates the broadness of the size distribution and can be used to evaluate aggregation phenomenon (Worldwide, 2011). These values usually range from 0 to 1, being that a value of 1 is indicative of broad range of size distribution, and a value of zero would indicate a perfect uniform sample. Usually, a PI value < 0.1 indicates a monodisperse distribution, whereas values >0.4 indicate a broad polydispersity. Any values in between indicate that the distribution is neither extremely broad nor narrow (Nobbman, 2017) and values >0.7 indicate that the sample presents a very broad size distribution and is probably not suited for this technique (Worldwide, 2011). An increase in this value is normally attributed to particle aggregation whereas a decrease is attributed to the opposite behaviour, disaggregation or dissolution (Arzensek, 2010; Lorber *et al.*, 2012; Worldwide, 2011). The PDI values obtained ranged from 0.2 to 1, meaning that the polymers tested

presented a broad range of distribution of sizes. SELP-520-A and SELP-1020-A showed a decreased in the PI as temperature was increased, this was an indicative of particle disaggregation, meanwhile PI values of SELP-59-A solutions increased with increased temperature, meaning that this polymer has a tendency to aggregate as temperature increases. Below the first thermal transition temperature, i.e. at 25 °C and 37 °C, all SELP solutions presented a PDI > 0.4, this would mean that the solutions were polydisperse at these temperatures. When the concentration was increased to above the thermal transition temperatures, i.e., to 50 °C and 65 °C, the PI values clearly suffered a change. Polydispersity in SELP-59-A solutions increased when the temperature was increased, from around 0.5, at 25 °C and 37 °C, to 0.7 and 0.8 at 50 °C and 65 °C, respectively (Table 5). On the other hand, SELP-520-A and SELP-1020-A showed the opposite behaviour, were the polydispersity of sizes, substantially decreased when the temperature was increased. SELP-1020-A went from PI values of around 0.5 at 25 °C and 37 °C to values of 0.3, for both 50 °C and 65 °C (Table 7). In SELP-520-A, a change in the PI value was readily noticed when the temperature was increased from 25 °C to 37 °C, even though is below the transition temperature. The PI value at 25 °C was of 1, while at both 37 °C and 50 °C was of 0.7 and at 65 °C was of 0.5 (Table 6). The PI values obtained for SELP-59-A solutions at temperatures below 65 °C are substantially high, and maybe, a different technique should be applied in these samples for evaluation of their size distribution profiles. When comparing between the different polymers, above the transition temperatures, SELP-1020-A presented the lowest PI values (0.3) when compared to SELP-520-A (0.5) and SELP-59-A (0.8). Unfortunately, no studies have been made regarding neither the effect of SELP composition nor the cure temperature, so it is not possible to make comparisons between studies. These results suggest that the length of both the silk-like and the elastin-like blocks affect the polydispersity of the sample. Longer silk-like units coupled with longer elastin-like units seem to lead to a narrower polydispersity of the sample, since SELP-1020-A presented the lowest PI and SELP-59-A (which presents silk- and elastin-like blocks with half the length) the highest value, between the SELPs tested.

It was previously demonstrated that the self-assembly process of SELPs in aqueous solutions depends on both hydrogen bonding between the silk-like units and the difference in hydrophobicity of the silk and elastin-like blocks (Xia *et al.*, 2011). In this study, the authors describe and characterize the self-assembly of different SELPs- into micellar-like nanoparticles, composed of silk-like blocks in the particles core and the elastin-like blocks in the corona. Furthermore, the size could be altered by changing the silk to elastin ratio. SELP-1020-A was the polymer which presented the highest number of silk-like blocks, when compared to the other two polymers (10 blocks for 1020-A vs. 5 blocks for -59-A and 520-A). Since the silk-like blocks are more hydrophobic that the elastin units, explains the reason why this specific

polymer tended to form smaller sized aggregates when the temperature was increased. In the overall, and by comparing the size of the populations which presented the highest percentage of scattered light intensity, SELP-59-A formed aggregates with the biggest hydrodynamic diameters (2000-3000 nm), followed by SELP-520-A (200-400 nm) and finally SELP-1020-A (15-30 nm), these . This was as expected, since it was previously demonstrated that fewer silk units would lead to the formation of smaller sized aggregates. (Xia *et* al., 2011). Even though SELP-520-A and SELP-59-A have the same number of silk-units, in SELP-59-A, the elastin-like unit is decreased to half, this would mean that there are less interrupting elastin units between the silk units, leading to an easier formation of crosslinks between the silk units of different polymers, and, consequently, to the formation of larger aggregates.

Few studies have been done regarding the formation of self-assembled SELP micelle-like particles and changes in particle sizes in function of temperature. Xia and co-workers (2011), studied particle formation of three different SELP analogues (with varied silk-to-elastin ratio), namely SELP-18-Y, SELP-28-Y and SELP-48-Y. They observed that, as the silk-to-elastin ratio was increased, the average hydrodynamic radius of the particles increased, as did the homogeneity of the solution. They also observed a hight intensity of scattered light at 4.5 nm, for SELP-18-Y, that was thought to represent free chains in solution. This theory was backed up when the silk-to-elastin ratio was increased from 1:8 to 1:4 lead to a decrease in the scattered light intensity of this smaller sized peak, to give rise to a peak at an D_h of 38 nm, suggesting the assembly of the free chains into particles. This was also observed when the S:E ratio was further increased to 1:2, with only one sharp peak observed at and D_h of 68 nm, suggesting the formation of uniform particles for this copolymer. These authors also proposed a model for SELP self-assembly that was based on differences in solubility of the individual blocks. They proposed that SELPs would self-assemble through phase separation, were they formed micellar-like particles composed of a core of silk-like blocks (less soluble) and a hydrated corona of more soluble elastin blocks. It is noteworthy that the concentrations tested in our study are far more superior than the ones chosen by Xia and co-workers (2011), and polymer concentration might play a role in this self-assembly process, since the sizes we obtained are far more superior than the ones obtained by that study.

When analysing time effect on size distribution (see Annex II for Figure 23 and Tables 20-22), we observed that at 25 °C and 37 °C no significant changes were observed between measurement 1 and 6 for SELP-59-A, but when the temperature is raised to 50 °C and 65 °C, three peaks are visible. As time goes by there is a tendency to the formation of higher aggregates, in detriment of aggregates with intermediate and smaller sizes. Curiously, SELP-1020-A exhibited the opposite behaviour, where at all temperatures tested only two peaks were visible, one corresponding to smaller sized particles and the other

corresponding to intermediate sized molecules. We verified that as time went by there was an increase in the intensity of the peak corresponding to the smaller sized particles, suggesting a tendency to structuration of particles with temperature and time. Temperature increase had an interesting effect on the distribution profile of SELP-520-A solutions. While for the other polymers the temperature increase had size of the molecules, for SELP-520-A it only caused for decreased polydispersity of the molecules. If we look at the PDI values, we could observe that, as time went by, there was a tendency for a decrease in the PDI values, indicating for decreased polydispersity.

3.2.3. Monitorization of the gelling process as a function of polymer concentration and temperature

For the monitorization of the gelling process, SELP aqueous solution at different concentrations, 2.5%, 5%, 10% and 15 % (w/v) were prepared and placed in an incubator at 37 °C and 65 °C (above and below their T_t) and cured for 2 h. The process was accompanied using an image capturing device, and a time-lapse video was obtained to observe solution's macroscopical appearance changes (Figure 13; https://drive.google.com/open?id=1ltFMUNdFNTN-cYUd2Ya7PLTLMJq3TnwE gels cured at 37 °C and https://drive.google.com/open?id=1KzX4ggbJkGm0teXDKdTdBYqWA9q-yHxu gels cured at 65 °C). Below the thermal events temperatures (at 37 °C), SELP-59-A and SELP-520-A solutions were clear and transparent, meanwhile SELP-1020-A solutions were already opaque in the beginning of the experiment. After 2 h, SELP-59-A solutions turned opaque and SELP-1020-A solutions were opaquer than in the beginning, but with no noticeable changes in SELP-520-A aspect. We also performed an inversion test to observe the gelation degree for these samples.

SELP-1020-A was the only SELP that showed the formation of a non-flowing hydrogel after 2 h of curing at 37 °C for all concentrations tested. SELP-59-A showed this gelation behaviour at concentrations above 10% (w/v). No hydrogel formation was observed for SELP-520-A at any concentrations, even though a clear increase in viscosity, in function of polymer concentration, was observed. Gel formation is a process that depends on polymer structure, molecular weight and concentration (Cappello *et al.*, 1998). However, since the SELP copolymers analysed in this study were designed to have the similar molecular weight, differences in the gelation process can only be attributed to their differences in composition and concentration. It was previously reported that at the same concentrations SELPs which presented more

silk-like units per block would gel faster and therefore the same would happen with increasing concentrations (Cappello *et al.*, 1998; Haider *et al.*, 2005). And, as was expected, SELP-1020-A presented gel formation at all concentrations tested, since it had the more silk-like units when compared to the other polymers. SELP-59-A was only able to form non-flowing hydrogels at superior concentrations, since it had less silk-like units per repeat, thus increasing the amount of polymer needed to form a fully crosslinked network. It was no surprise that SELP-520-A failed to produce a non-flowing hydrogel, even though it has the same number of silk units per repeat as SELP-59-A. This polymer it has a lower silk to elastin ratio, meaning that either the concentration or cure time needed to be further raised to obtain the same results as for the other polymers (Figure 14).

Dandu and co-workers (2009) also tested the effect of differences in compositions between the SELP analogues SELP-47-K, SELP-815-K and SELP-415-K. With the same curing time (4 h), SELP-47-K and SELP-815-K were found to form stable hydrogels in the concentrations range of 4-12 wt%. As for SELP-415K, gelation was only observed at a minimum concentration of 12 wt%. These differences were thought to be due related to the lower S:E ratio of SELP-415K when compared to the other copolymers, resulting in less hydrogen bonding sites (silk units) and thus requiring a higher polymer concentration in order to from robust, non-flowing hydrogels. These results indicated that SELP copolymers are capable of forming non-flowing hydrogels at physiological conditions (37 °C), showing the dependence of the gelling process on the cure time and concentration rather than the temperature. Even so, it was proved that increasing the temperature also increased gelling rates (Cappello *et al.*, 1998; Dandu *et al.*, 2009).

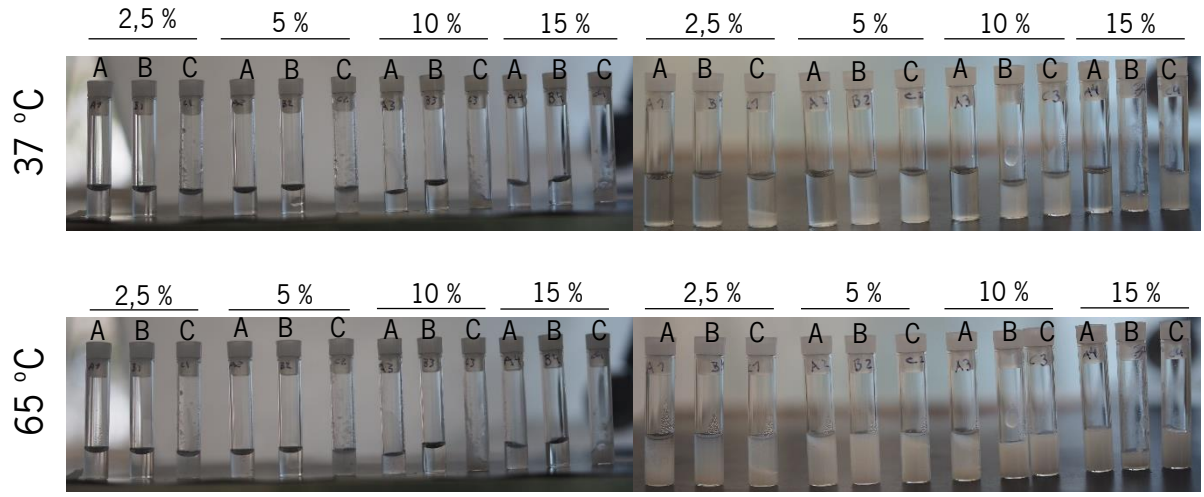

Figure 13 - Gelation process of SELP solutions prepared at various concentrations (w/v) and cured at 37 °C (upper figure) and at 65 °C (lower figure) for two hours. Photos taken in the beginning (left, t= 0h) and in the end (right, t = 2h) of the experiment).

At 65 °C, SELP solutions had very different behaviours. At time zero, SELP-59-A solutions, at all concentrations were transparent, as for SELP-520-A and SELP-1020-A solutions at 2.5% (w/v), the remaining solutions presented a opaquer appearance. As time went by, all solutions became opaquer and stiffer. This change was noticeable right in the beginning of the experiment, first for SELP-1020-A, then SELP-520-A while SELP-59-A solutions needed more time to obtain a clear change in appearance. A concentration-dependent behaviour was observed, since the solution of 2.5% (w/v) was the first to turn opaque, followed by the 5%, 10% and lastly 15%. Since the inversion test was not performed at this temperature, analysis of hydrogel formation in this study was done merely by macroscopical observation (a completely opaque solution was considered as a hydrogel). We noted that all SELP copolymers were able to form a hydrogel at concentrations as low as 5% (w/v), being that for SELP-1020-A solutions the same was observed lower temperature (37 °C). Once again, the obtained results corroborate the previous experiments and the literature, where was found that an increase in temperature caused higher gelling rates (Cappello *et al.*, 1998).

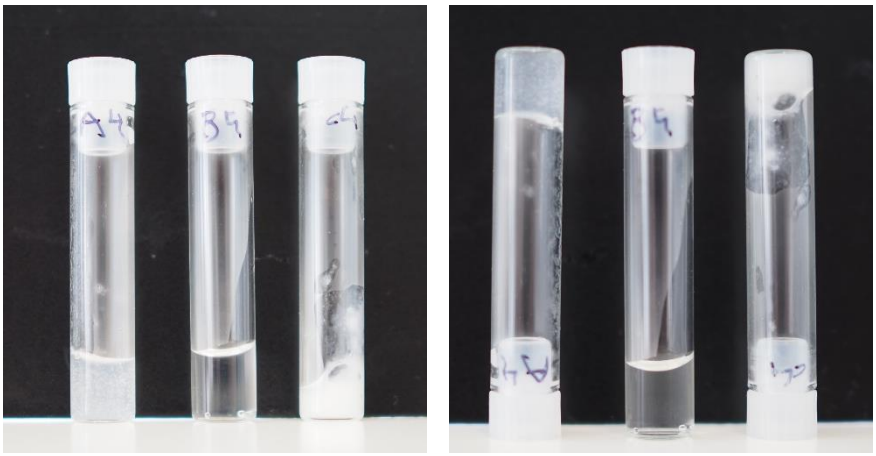

Figure 14 - Inversion test performed on (from left to right) SELP-59-A, SELP-520-A and SELP-1020-A solutions at 15% (w/v), cured at 37 °C for two hours. Left picture shows non-inverted tubes and right picture shows the inverted tubes, with exception of the non-gelled sampled

Effect of temperature on gelling characteristics was first studied by Cappello and co-workers (1998). In viscometry experiments of SELP-816 and SELP-47K it was noticed that higher temperature would result in faster gelling rates. It is noteworthy that SELP composition had impacted the experiments, as in this study, the analogue SELP-816, which have higher silk content per repeat, showed higher gelling rates than SELP-47K, at all temperatures tested. Effect of cure time on hydrogel formation was also assessed in a different study (Haider *et al.*, 2005). SELP-415K-8mer and SELP-47K hydrogels were prepared at different concentrations (6, 9 and 12 wt%) and with different curing times (4, 24 or 48 h). SELP-

47K was able to form firm hydrogels after 4 h of cure time at 6 ,9 and 12 wt%. Meanwhile, at 4 h of curing time only polymer solutions at 12 wt% of SELP-415K-8mer polymer gelled. When the cure time was extended to 24 and 48 h, hydrogel formation was observed for SELP-47K at all concentrations, whereas for SELP-415K-8mer, gelation only occurred in solutions with 9 and 12 wt%. With increasing curing time, silk-like units are more likely to encounter one another, align and thereby allowing for the formation of more and/or stronger crosslinks and resulting in denser networks (Dandu *et al.*, 2009; Hwang *et al.*, 2009). More recently, a similar study was performed in order to determine the critical gelation concentration (CGC) of SELP-415K and SELP-47K solutions, defined as the concentration above which the crosslinks in the hydrogel are physically robust to form a non-flowing gel phase (Dandu *et* al., 2009). SELP copolymers with higher silk-to-elastin ratio presented the lowest CGC (4-12 wt%) while the polymer with lower silk-to-elastin ratio was only able to form non-flowing hydrogels at 12 wt%. In the latter case, has the lower S:E ratio shows less hydrogen bonding sites (silk-units) when compared to the other polymers, thus requiring an increment of polymer chains or a higher CGC to self-assemble and form firm hydrogels (Haider *et al.*, 2005).

Making a parallelism with our results, we observed that the gelling process, is not only dependent on polymer composition (S:E ratio) and concentration, but also temperature. Meaning that an increase in temperature resulted in hydrogels formation, for all SELP copolymers, at least in the higher concentrations. These same samples were flash frozen, freeze-dried and a structure analysis was performed on the obtained aerogels using Scanning Electron Microscopy (SEM) and Fourier-transform infrared spectroscopy with attenuated total reflectance (FTIR-ATR).

3.2.4. Morphological and structural analysis of SELP aerogels.

SELP hydrogels at 5% (w/v), 10% (w/v) and 15% (w/v) were cured below and above their transition temperature (T_t), 37 °C and 65 °C, respectively, for 2 hours. The temperatures used in this assay were chosen accordingly to the DSC and spectrophotometry results. They were then freeze-dried and the morphological evaluation in function of polymer concentration and temperature was performed utilizing scanning electron microscopy (SEM) (For SEM images of all gels evaluated see Annex II, Figures 24,25 and 26).

At 37 °C, all polymers showed higher-order and more defined structures as concentration increased (Figure 15 and Annex II, Figures 24, 25 and 26). A well-defined porous structure was observed at concentrations of 10% (w/v) for SELP-520-A and of 15% (w/v) for SELP-59-A, but no defined network formation was observed for SELP-1020-A at this temperature (Figure 15). When comparing the pore size of both polymers networks, we observed that, for both concentrations, SELP-520-A presented a smaller mean pore size (7 ±2 nm at 10% (w/v) and 148 ± 53 nm at 15% (w/v)) relatively to SELP-59-A (420 ± 162 nm at 15% (w/v)) (Table 8). At 37 °C, no pore formation was observed in SELP-1020-A gels, even though a clear reorganization of structure is taking place as temperature increases. Interestingly, at 5% (w/v) and 10% (w/v) we observed fibrillar-like structures for this analogue. Another type of structure was also observed, particle formation was observed in SELP-520-A and SELP-1020-A gels at lower concentrations (5% (w/v) and 10% (w/v)).

The effect of polymer concentration in the pore-like structures was only observed for SELP-520-A gels, where an increase of the concentration from 10% to 15% (w/v) resulted in an increase in the mean pore size, from 7 ± 2 nm to 148 ± 53 nm (Table 8). This increase can be due to a higher number of crosslink-forming chains present at the higher concentration gels, and since this polymer presents low silk-to-elastin ration coupled with long flexible elastin units, it is explicable why an increase in concentration rendered a looser network.

Table 8 - Mean pore size (nm) of SELP hydrogels which presented a defined porous network. Pore sizes were measured using ImageJ software (Schneider *et al.*, 2012).

	SELP-59A		**SELP-520-A**				**SELP-1020-A**	
	37 °C	65 °C	37 °C		65°C		65 °C	
	15%	15%	10%	15 %	10%	15%	10 %	15%
Mean size (nm)	420	142	7	148	82	9 070	113	108
Standard deviation	62	44	2	53	024	2 042	132	25

When the temperature was risen to 65 °C (above the T_t) a clear difference is observed in the overall morphology and formed structures in the hydrogel (Annex II Figure 24, 25 and 26). The observed structures have a denser and more organized network for all polymers, and the level of organization increases as the polymer concentration rises. Similar to the results obtained at 37 °C, a well-defined porous structure was observed at concentrations starting as low as 10% (w/v) for SELP-520-A and at 15% (w/v) for SELP-59-A. At this temperature, it was also possible to observe a defined porous network in 10%

and 15% (w/v) SELP-1020-A gels (Figure 15). SELP-59-A gels at 15% (w/v) showed a mean pore size of 142 ± 44 nm while SELP-520-A gels presented mean pore size of 82 ± 24 nm and 9070 ± 2042 nm, for 10% (w/v) and 15% (w/v), respectively. SELP-1020-A gels had a mean pore size of 113 ± 132 nm at 10% (w/v) and 108 ± 25 nm at 15% (w/v) (Table 9). Although SELP-1020-A gels did not present a well-defined porous structure at lower concentrations, it was possible to observe laminar-like structures. The size of these same structures appears to decrease as concentration is increased from 5% (w/v) to 10% (w/v), but when the concentration is further increased, there's an obvious shift from the laminar structures to a porous structure. Furthermore, particle-like structures were observed in SELP-520-A and SELP-1020-A 5% (w/v) gels and in SELP-59-A gels, at all concentrations tested (Figure 16).

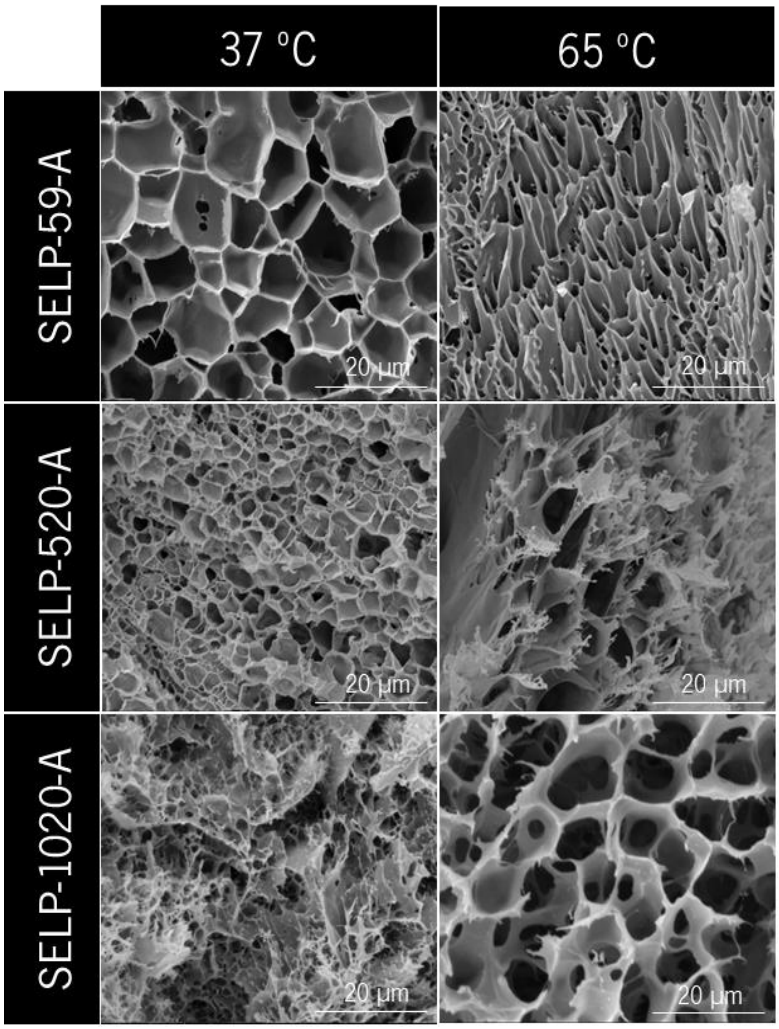

Figure 15 - SEM micrographs showing the porous structure formed in freeze-dried 15% (w/v) SELP hydrogels cured for 2 hours below (37 °C) and above (65 °C) the transition temperature (T_t) .

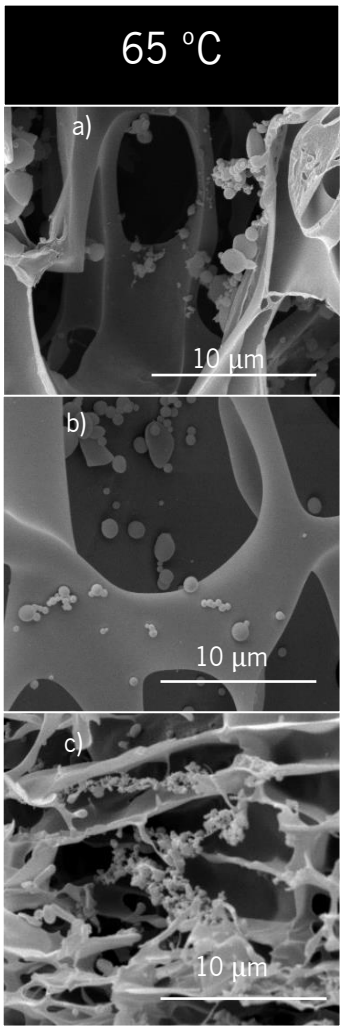

Figure 16 – SEM micrographs showing particle formation in hydrogels of a) SELP-59-A, b) SELP-520-A and c) SELP-1020-A at low polymer concentration (5% (w/v)).

Concentration effect was evaluated on pore formation only in SELP-520-A and SELP1020-A gels (10% and 15% (w/v)), since for SELP-59-A gels these structures were only observed at the highest concentration (15% (w/v)). SELP-520-A showed a high increase (almost tenfold) in the mean pore size when the concentration increased, whereas for SELP-1020-A the concentration effect was barely noticeable, since no significant changes in pore size were observed. This tendency had already been demonstrated in SELP-520-A gels cured at 37 °C. The difference in the concentration effect on pore morphology is related to the increased silk content of SELP-1020-A when compared to SELP-520-A. As SELP-1020-A has more silk-like blocks (higher S:E ratio) lead to an easier/stronger crosslink formation, even at lower concentrations. SELP-520-A presents less crosslink forming units, so it demonstrates a higher dependence on concentration than SELP-1020-A.

The temperature increase had different effects on the copolymers tested: in SELP-1020-A resulted in pore formation; in the case of SELP-59-A and SELP-520-A it resulted in changes in the mean pore size. Interestingly, these SELPs presented the opposite behaviour when subjected to the same stimulus (at the same concentration) - the temperature increase resulted in an increase in pore size for SELP-520-A but a decrease for SELP-59-A. The cause of this opposition may be attributed to differences the length of the elastin-like blocks. Due to the smaller interrupting elastin units in SELP-59-A, it is easier for the silk units to find one another and establish connections, thus decreasing the size of the pores when compared to SELP-520-A, with longer interrupting blocks between the crosslink forming units, thereby giving rise to a more "loose" network.

The presence of small particles was also observed, at this temperature, in all copolymers, even though at different concentrations and temperatures (Figure 16 and Table 9).

Table 9 - Mean particle size (nm) of SELP hydrogels where formation of particles occurred. Particle area was measured using ImageJ software (Schneider *et al.*, 2012).

	SELP-59A		**SELP-520-A**		**SELP-1020-A**	
	65 °C		37 °C	65°C	37 °C	65 °C
	5%	10%	5 %	5%	5 %	5%
Mean Particle size (nm)	41	61	69	43	3	25
Standard deviation	24	25	28	14	1	8

All polymers showed the presence of particles at lower concentrations (5% (w/v)) and at both temperatures tested, apart from SELP-59-A, where particle formation was observed only at 65 °C. In fact, SELP-59-A was the only polymer to show particle formation at higher concentrations (10% (w/v)) (Table 9). We also observed in SELP-59-A, that the mean particle size increased with concentration, from 41 ± 24 nm at 5% (w/v) to 61 ± 25 nm at 10% (w/v), even though it is not a significant number and with a smaller number of particles observed. SELP-1020-A showed an increment of particles size influenced by temperature - 3 ± 1 nm at 37 °C to 25 ± 8 nm at 65 °C. As for SELP-520, the opposite happened, where particle size decreased when the temperature increased - 69 ± 28 nm at 37 °C and 43 ± 14 nm at 65 °C. The presence of particles was not entirely surprising since previous reports stated that SELPs are able to form micelle-like particles at low concentrations, due to the hydrophobic nature of the polymers. Our results are consistent with previous findings, where the presence of particles was observed only in lower concentrations (5% and 10% (w/v)). Particle formation in both SELP-1020-A and SELP-520-A showed to be independent of temperature, since particles were observed in both temperatures tested, at low concentrations (5% (w/v)). On the other hand, for SELP-59-A, only at 65 °C particles were observed, though at higher concentrations (5% and 10 % (w/v)), showing dependence on temperature. This dependence demonstrated by SELP-59-A can be attributed to the combination of decreased length of the elastin-like blocks and the silk-like blocks, when compared to SELP-520-A and SELP-1020-A, meaning that an increase in the temperature is needed to observe this hydrophobically-driven behaviour.

The particle sizes obtained by SEM were slightly larger than the ones observed in the DLS assays, this difference can be attributed to several different parameters, such as increased polymer concentration (2.5%-15% compared to 0.5% (w/v) in DLS) and increased cure temperature (2 h compared to 20 min in DLS).

Changes in secondary structure of freeze-dried SELP hydrogels were also evaluated by ATR-FT-IR spectroscopy. The most used spectral region for this type of analysis is the amide I band (1600-1700 cm^{-1}), since it mainly arises from C = O stretch vibrations (>80 %), providing information on the secondary structure of the protein backbone (Hu *et al.*, 2010; Machado *et al.*, 2015). Generally, an amide I peak in the region from 1600 to 1640 cm^{-1} is assigned to a β-sheet conformation, which increases during silk crystallization. Random coils and α-helices are associated with the region between 1640 and 1660 cm^{-1}, and the remaining part of the spectra from 1660 to 1690 cm^{-1} is related to β-turn structures (Hu *et al.*, 2006, 2009). Changes in FT-IR spectra were evaluated in function of polymer concentration and curing temperature, both below and above the calculated polymers' transition temperatures (37 °C and 65 °C, respectively).

SELP solutions, at four different concentrations (2,5%, 5%, 10% and 15% (w/v)), were prepared, cured for 2 h at two predetermined temperatures and finally freeze-dried and analysed using FTIR-ATR (Figure 17) (See Annex II – Figure 27 for complete FTIR spectra). No changes in the secondary structure were found in the different concentrations analysed, whereas an increase on the absorbance was found. This is mainly due to the higher number of polymer chains that were able to establish physical contact during cure time, at higher concentrations (Iglesias *et al.*, 1995). When the curing temperature was evaluated, significant changes in the spectra were observed. Both SELP-520-A and SELP-1020 (Figure 17 b) and c), respectively) demonstrated a decrease in peak width with temperature increase, surprisingly the same was not seen in SELP-59-A (Figure 17 a)), but the opposite behaviour instead. Below the T_t, SELP-59-A hydrogels presented a peak at roughly 1630 cm^{-1}, indicative of presence of β-sheet conformation, when the temperature is increased to above the T_t, there's and unexpected peak change to higher wavenumbers, around 1645 cm^{-1} and an increase in peak width. The increase in the peak width along with the peak shift, are indicative of both β-sheet and random coils conformations. This spectrum suggests that at lower temperatures the polymer chains are already able to form stable crosslinks and adopt β-sheet conformations, and as the temperate increases, the β-sheet content is accompanied by an increase in random coil This might be a result of the small sizes of both the elastin- and the silk-like blocks, which may hinder β-sheet formation.

As for SELP-520-A and SELP-1020-A the results were as expected, since temperature increase resulted in less breadth peaks and at lower wavenumbers. The temperature effect was quite evident for both polymers, even though at lower temperatures, the peaks for SELP-1020-A spectrum were less broad that the ones found in SELP-520-A spectrum - meaning a higher content of β-sheet conformations in SELP-1020-A gels when compared to the ones of SELP-520-A. The SELP-1020-A gels presented broad peaks, seemingly two peaks together, one around 1630 cm^{-1} and another around 1650 cm^{-1}, suggesting a combination of both β-sheet and random coil conformations. When the temperature was increased, there was a clear reduction in the peak width and removal of the peak at 1650 cm^{-1} giving place to one sole peak at around 1630 cm^{-1}. In SELP-520-A spectrum, changes were observed only in terms of its width, which decreased when the curing temperature was increased. These results suggest that both copolymers present a combination of β-sheet and random coil conformations at lower temperatures that are substituted by β-sheet structures when the temperature is increased. The increased evidence of random coil conformations SELP-1020-A is probably due to the long elastin-like blocks, which are known to adopt random coil conformations below their T_t.

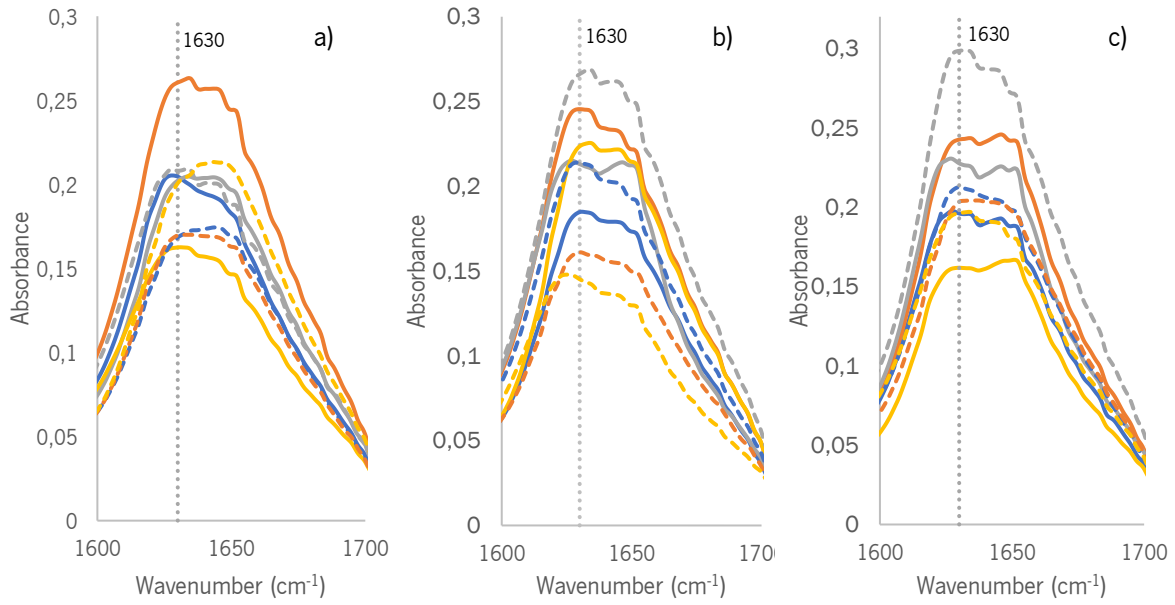

Figure 17 - FTIR-ATR spectra of the amide I region (1700 – 1600 cm^{-1}) of freeze-dried SELP hydrogels at different concentrations, 2,5 % (blue); 5 % (orange), 10 % (grey) and 15 % (w/v) (yellow), and cure temperatures of 37 °C (full lines) and 65 °C (dashed lines). a) SELP-59-A; b) SELP-520-A; c) SELP-1020-A.

Most of the studies found regarding secondary structural changes on SELP materials focused in fibbers (Machado, *et al.*, 2013b; Qiu *et al.*, 2011, 2010; Roberts *et al.*, 2018) and films (Fernandes *et al.*, 2018; Machado *et al.*, 2015; Pereira *et al.*, 2017; Sun *et al.*, 2013) usually accompanied with material post-treatments, such as methanol treatment (Chen *et* al., 2017; Machado, *et al.*, 2013; Machado *et al.*, 2015; Roberts *et al.*, 2018; Teng *et al.*, 2009; Zhu *et al.*, 2016) as the variable. The methanol pre-treatments are known to lead to higher crystalline content in the obtained hydrogels when compared to the controls. In the study developed by Machado and colleagues (2015), the author demonstrated that exposure of the fabricated films to a methanol saturated environment increased the β-sheet content in 50 to 60% when compared to non-treated films (Machado *et al.*, 2015). Still, to our knowledge, no studies were found regarding temperature effect on SELPs secondary structure that can be used to make a direct comparison with the work done in this dissertation. Even so, we conclude that SELP copolymer crystallization is influenced by temperature changes. Also due to differences between the copolymers secondary structure, one can also affirm that the SELP composition affects this parameter, mainly the length and number of the silk units. SELP-1020-A displayed the biggest changes in the FTIR spectra and is the one with longer silk-like units.

3.2.5. Characterization of SELP mechanical/rheological properties

Mechanical performance of several SELP solutions was performed by rheological methods. Both polymer composition and cure temperature control the cross-linking density, that in turn, is largely responsible for the hydrogel's mechanical properties (Dandu *et al*, 2009). The monitorization of shear storage modulus, G', loss modulus, G'', and loss factor, tan δ are of critical importance to study the hydrogels' properties. Essentially, the elastic modulus G' represents the solid-like behaviour (stiffness), whereas G'' represents the liquid component (flow) of a viscoelastic hydrogel. If the obtained G' value is much higher than the G'', the sample behaves as an elastic solid and if G''> G', the sample behaves more like a viscous liquid (Chow *et al.*, 2008; Yan & Pochan, 2010).

The present study aims to determine the gel point and evaluate the difference between the initial and final moduli values (G' and G''), when samples are subjected to a temperature ramp from 4 °C to 65 °C and determine its gel point. Gel point is defined as the instant at which the weight-average molecular weight reaches infinity, were the polymer is in a transition state between a liquid and a solid (Boey & Qiang, 2000). Gelation point can be determined accordingly to different criteria such as using the maximum peak of tan δ, the crossover between the G' and G'' curves or the real dynamic viscosity (Laza *et al.*, 1999). For this study the tan δ peak maximum was chosen to determine gel point due to easier interpretation and simpler data presentation.

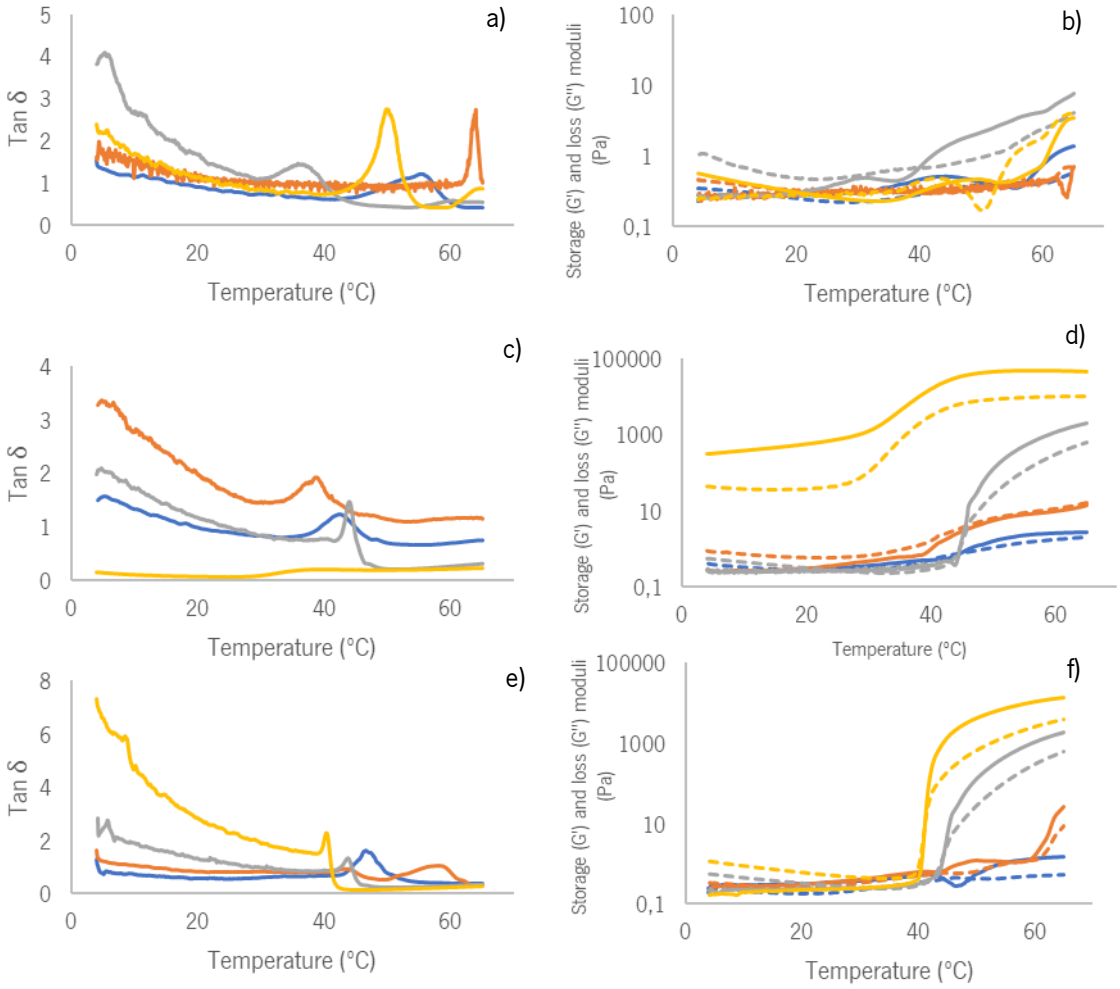

Figure 18 - Response curves of SELP solutions in function of temperature and tan δ (left), and temperature vs G' (solid line) and G'' (dashed line) (right). Aqueous solutions of (a, b) SELP-59-A, (c, d) SELP-520-A, and (e, f) SELP-1020-A with concentrations of 2.5% (blue), 5% (orange), 10% (grey) and 15% (yellow) were submitted to a constant strain of 1% and frequency of 1 Hz.

All polymers presented gel point temperature intervals (Figure 18 a), c) and e)) that were in accordance to the previously determined T_t by DSC and UV-Vis spectrophotometry. SELP-59-A displays the highest temperature variability, having a gel point between 50 °C and 60 °C. This result is not entirely surprising since this interval covers both transition temperatures of this polymer (53 °C and 61 °C). The same phenomenon was observed for SELP-1020-A solutions, where the gel point ranged from 40 °C to 47 °C. In this case, the gel point temperatures only covered the first transition temperature (42-47 °C) and not the second (53 °C). The wide gel point intervals presented by both SELP-59-A and SELP-1020-A could be due to the fact that these two polymers present a two-step thermal assembly process, on the other hand, SELP-520-A which only has one T_t (41-45 °C), presented a narrower temperature interval for gel point, ranging from 40 °C to 47 °C. It is noteworthy that no gel point was observed for SELP-520-A solutions at 15% (w/v), probably due to solution polymerization prior to the experience, in fact the solution

was already opaque when the experiment was performed. The concentration effect in this study was only noticeable for SELP-1020-A solutions, where an increase in polymer concentration led to a decrease in the gel point temperature.

Shear modulus (G') and loss modulus (G'') monitorization in function of temperature was used to determine the mechanical strength of the SELP hydrogels (Figure 18 b), d) and f)). The storage modulus is related to the stiffness of the material and the loss modulus is related to the dampening and energy dissipation of the material due to its viscous properties. The values of both moduli were evaluated in the beginning (prior to gelation) and in the end of the experiment (after gelation occurred) (Table 10). As it was expected, all polymers demonstrated a rise in both moduli as the experience was carried out. The concentration effect was quite noticeable for all copolymers, where an increase in polymer concentration lead to an increased in the measured moduli. This was expected since the crosslinking density is related to polymer concentration, which in turn governs the mechanical properties. This phenomenon has also already been previously described in SELP hydrogels (Cresce *et al.*, 2008), where Dynamic Mechanical Analysis was used to perform mechanical properties evaluation on SELP47-K hydrogels at concentrations of 4. 8 and 12 wt%, cured for the same time. The storage modulus for SELP-47-K hydrogels at 4 wt% was 75.4 kPa while for the 12 wt% hydrogel was 1600 kPa. The concentration effect is due to a higher density of crosslink-forming silk-like units at higher concentrations, leading to more dense networks and thus increased mechanical strength (Gustafson *et al.*, 2010).

Table 10 – SELP rheology studies: Initial and final storage (G') and loss (G'') moduli

	Storage (G') and Loss (G'') moduli (Pa)	**SELP-59-A**		**SELP-520-A**		**SELP-1020-A**	
		Initial	**Final**	**Initial**	**Final**	**Initial**	**Final**
2.5 %	G'	0.2	1.4	0.2	2.9	0.2	1.5
	G''	0.4	0.6	0.4	2.1	0.2	0.5
5%	G'	0.3	0.7	0.3	14.5	0.2	25.9
	G''	0.5	0.7	0.9	16.5	0.3	9
10 %	G'	0.3	7.8	0.3	2000	0.5	2000
	G''	1	4.2	0.6	621	0.2	598
15%	G'	0.2	4.1	316	46000	0.2	14000
	G''	0.6	3.4	45	9000	1.2	4000

All copolymers tested presented final G' > G'' values (Table 10), which means that the samples displayed a more liquid-like behaviour at the end of the experience (Yan & Pochan, 2010). From all copolymers tested, SELP-59-A presented the lowest shear modulus value at the end of the experiment, at all concentrations tested (1-8 Pa). The G' values obtained for SELP-520-A and SELP-1020-A solutions, were very similar at lower concentrations (from 2.5% (w/v) to 10% (w/v)), only at higher concentrations the polymer composition effect was noticeable. Surprisingly, at 15% (w/v) concentration, SELP-520-A solution presented a higher G' value, of 45 838 Pa, than the one presented by SELP-1020-A at the same concentration, 13 915 Pa. This was not as expected since longer silk units coupled with smaller elastin-like blocks would tend to form more crosslinks with more frequency and so, based on this theory, SELP-1020-A would present the highest G' values, followed by SELP-59-A and finally SELP-520-A. A reasonable explanation is that the shear modulus values are influenced not mainly by the silk content, but by elastin content. Another explanation relates to their thermal transition properties. The duration of this experiment was only dependent on the time required by the rheometer to reach the desired temperature, at it is known that these mechanical properties are also influenced by cure time (Haider *et al.*, 2005). The reduced "cure time" of this experiment coupled with large differences in the transition temperature of these polymers may be the reason behind the obtained results, since it is known that SELP self-assembly occurs mainly after the T_t has been reached (Xia *et al.*, 2011). Since SELP-520-A is the only copolymer which presents only one T_t, between 41 °C and 45 °C, that is below both the T_t of the other two copolymers tested, showed a longer curing time than the rest of the samples, due to a faster reach of the known transition temperature. Even though SELP-1020-A and SELP-59-A have two thermal transition temperatures, both T_t of SELP-59-A are much higher (53 °C and 61 °C) than the ones for SELP-1020-A (42-47 °C and 53 °C), thus decreasing even more the cure time above the respective T_t, and so, leading to a lower crosslinking degree and G' values.

4.Conclusions and final perspectives

4. Conclusion and final perspectives

The physical-chemical properties of SELP hydrogels, in function of polymer composition and concentration, as well as cure temperatures, were evaluated in this dissertation. In order to define the above relations several parameters have been measured, and are described in the following sections. For easiness of reading, the following conclusions were summarized in a bullet point-like structure.

4.1. Thermal transition properties

- Two step self-assembly process: this property has only been demonstrated by two SELP copolymers, namely SELP-1020-A and SELP-59-A. We believe this two-step transition is due to the isolated role of the elastin- and the silk-like blocks. SELP-520-A, which presented a lower S:E ratio when compared to the other polymers tested (1:4 vs. 1:2), only had one T_t. The presence of longer elastin blocks coupled with smaller silk units lead to only one transition temperature. We believe the length of the elastin blocks ended up masking the individual role of the silk in the self-assembly process.

- Transition temperature: thermal transition temperatures were found to be highly dependent on composition and varied in values as it follows: SELP-520-A < SELP-1020-A < SELP-59-A. A lower silk-to-elastin ratio seems to be the primary reason for a decreased T_t, followed by a higher content of elastin-like blocks. Since SELP self-assembly is temperature driven, SELPs with higher elastin content show lower T_t (Table 11). This is mainly due to the conformational changes in the elastin blocks above the T_t.

- Reversibility of the process: reversibility was observed in SELP-520-A and SELP-1020-A copolymers at all concentrations tested, SELP-59-A only presented reversibility in the highest concentrations (20% (w/v)). This was attributed to the length of the elastin units, since it is known that elastin-units are responsible for the reversibility of this process. SELP copolymers which presented longer silk units coupled with smaller silk units lead to a stability in the thermal event until lower temperatures (Table 11).

- Hysteresis behaviour: This property was attributed to the presence of the segment VPAVG in the copolymers used. All copolymers presented this behaviour at all concentrations tested.

The exception was SELP-59-A, where it was only seen at higher polymer concentrations. The later fact is due to the presence of smaller elastin-like blocks is this polymer when compared to the others (9 blocks in -59 vs 20 blocks in -520 and -1020).

- Size distribution profiles: All copolymers where subjected to temperatures either below the T_t or above the their T_t.SELP-520-A and SELP-59-A showed an increase in the average particle size when the temperature was increased above their respective T_t, whereas SELP-1020-A presented the opposite behaviour. These differences were attributed to the hydrophobicity differences between the silk- and the elastin-like blocks. SELP-1020-A, because it has the double amount of silk blocks (10 when compared to 5 of -59 and -520), was more prone to form smaller size aggregates when compared to SELP-59-A and SELP-520-A, with smaller hydrophobic regions.

Table 11 - Transition (T_t) and resolubilisation (T_r) temperatures for the SELP copolymers.

	T_t	T_r
SELP-59-A	53 °C; 61 °C	27 °C
SELP-520-A	41 °C	31 °C
SELP-1020-A	43 °C; 53 °C	38 °C

4.2. Gelation process

- Formation of a non-flowing gel (Table 12):

    - Temperature: All SELP copolymer solutions (2.5% - 15% (w/v)) formed stable non-flowing hydrogels when subjected to 2 h of curing time at a temperature above their T_t (65 °C).

    - Polymer composition and concentration: composition effect was only noticeable bellow the T_t (37 °C). SELPs with longer crosslink forming units or with smaller interrupting elastin blocks, namely SELP-1020-A and SELP-59-A, respectively, formed non-flowing hydrogels at all concentrations -in the case of the SELP-1020-A - and

above 10% (w/v) - for SELP-59-A solutions. Even though SELP-520-A solutions demonstrated an increase in viscosity as the concentration increased no gel-like formation was found. Differences in terms of concentrations to form a non-flowing hydrogel are due to requirement of a higher polymer concentration, for SELPs with less crosslink forming silk units (SELP-59-A) when compared with copolymers with longer silk units (SELP-1020-A).

Table 12 - Effect of concentration and cure temperature on the ability to form a non-flowing hydrogel for all SELP copolymers.

	37 ºC				**65 ºC**			
	2.5%	**5%**	**10%**	**15%**	**2.5%**	**5%**	**10%**	**15%**
SELP-59-A	-	-	✓	✓	✓	✓	✓	✓
SELP-520-A	-	-	-	-	✓	✓	✓	✓
SELP-1020-A	✓	✓	✓	✓	✓	✓	✓	✓

4.3. Morphology of the freeze-dried SELP hydrogels:

- Temperature: As temperature was increased above the copolymers defined T_t, all SELPs demonstrated a denser and more organized network, even though temperature increase had different effects on different copolymers. For SELP-1020-A an increase in the temperature resulted in the formation of a well-defined porous formation. Whereas, for SELP-59-A and SELP-520-A, which had presented this structure at 37 °C, an increase in temperature only provoked changes in the pore average size.

- Polymer concentration and composition:

  - Morphology: Polymer solution concentration was found to influence the morphology of the hydrogels. As polymer solution concentration was increased, the images showed higher-ordered pore-like structures. Also, at lower concentrations (5% and 10% (w/v), depending on the copolymer) particle formation was observed for all SELP copolymers, even though the increased temperature induced changes in the average particle size.

  - Defined pore and particle formation: a defined porous network was observed for hydrogels at concentrations as low as 10% (w/v) for SELP-520-A and SELP-1020-A, and as 15% (w/v) for SELP-59-A. For SELP-520-A and SELP-59-A, this pore formation seemed to be dependent mainly on polymer concentration, whereas for SELP-1020-A, it was also dependent on temperature increase. The concentration effect is probably due to the silk-to-elastin ratio. Polymers with longer silk units will tend to form more crosslinks, thus leading to a more tight network, less-pore like. On the other hand, polymers with smaller silk units with larger interrupting elastin-like blocks will lead to more flexible hydrogels, with "looser" networks (Table 13).

    Particle formation was seemed to be dependent on polymer concentration, since it was only observed in 5% (w/v) solutions for both SELP-520-A and SELP-1020-A and in 5% and 10% (w/v) SELP-59-A solutions. Lower polymer concentrations mean an increased difficulty for molecules to find one another to form long polymeric chains, leading to a tendency to form small and more stable particles (Table 14).

Table 13 - Effect of concentration and temperature on formation of a well-defined porous network of the SELP copolymers

	37 ºC		65 ºC	
	10 %	**15 %**	**10 %**	**15 %**
SELP-59-A	-	✓	-	✓
SELP-520-A	✓	✓	✓	✓
SELP-1020-A	-	-	✓	✓

Table 14 - Effect of concentration and temperature on formation of particles of SELP copolymers.

	37 ºC		65 ºC	
	5 %	**10 %**	**5 %**	**10 %**
SELP-59-A	-	-	✓	✓
SELP-520-A	✓	-	✓	-
SELP-1020-A	✓	-	✓	-

4.4. Secondary structure

- Temperature: Temperature increase provoked an increase in the β-sheet content for SELP-520-A and SELP-1020-A, while for SELP-59-A an increase in the random coil content was observed. These differences might be due to the small silk- and elastin-like units of SELP-59-A, when compared to the other two polymers, that, in some way, may hinder β-formation.

- Polymer concentration and composition: Polymeric solutions concentration was not found to influence the secondary structure of the hydrogels. On the other hand, the composition effect was quite evident, where SELPs with longer crosslink forming silk units, coupled with longer elastin units, demonstrated higher β-sheet structure.

4.5. Mechanical properties

- Gel point: This parameter was found to be mainly dependent on polymer composition. Gel point temperatures were found to be in the following order SELP-520-A < SELP-1020-A < SELP-59. SELP copolymers which presented smaller silk units with longer interrupting elastin blocks had the lowest gel point. This effect was attributed to the fact that the SELP assembly process is temperature driven and influenced by the presence of the elastin-like blocks, and so it was expected that polymers with higher elastin content would present a lower gel point.

The present dissertation was a thorough study on the physical-chemical properties of hydrogels fabricated using one particular set of SELP copolymers, based on the elastin-like pentapeptide VPAVG. The versatility of this family had already been studied before, and once again, they have proven to exhibit the same remarkable properties. The simple usage of this pentapeptide as opposed to the regularly used (VPGVG), render the copolymers an acute hysteresis behaviour. This means that after polymerization/gelation had occurred, the materials will remain insoluble for a longer range of temperatures. Effect of temperature as well as polymer structure and composition, have also been well established during this dissertation. With such detailed work, one can only imagine the possible applications of the hydrogels produced. By simply shifting concentration, cure temperature or polymer selected, hydrogels with the most varied morphologies and mechanical properties can be achieved. One of the major uses for these material will be in the biomedical area, due to the already known biocompatibility and ability to form gels whithout the need for aditives. For example, if these polymers should follow the trend left by other "old guard" SELPs and gelate under physiological conditions (37 °C), they can be aplicable as injectable materials, for drug delivery, for example. If this low temperature gelation is not possible, the SELP solution may be allowed to gelificate at higher temperatures and later on be implanted on the host. Due to theirparticle formation ability, substance entrapment is also a possibility, simply by using lowering polymer concentrations. Diffusion rates can be altered by changing curing temperature or polymer concentration, to obtain denser (for lower diffusion rate) or "looser" (for higher diffusion rate) networks. Another area where these hydrogels have potential application is in the regenerative medicine field or as scaffolds for cell growth. For hydrogels with better mechanical performance, stiffer and more resistant, SELPs with longer silk-like units should be chosen, coupled with a higher polymer concentration. On the other hand, if a soft and pliable hydrogel is needed one should go with a polymer with longer elastin-units. Assessment

of cell viability, material injectability, drug loading capacity as well as release rates (among others) should be a target of study, if these copolymers are to be used in the biomedical field. Still, due to the extensive characterization done in this dissertation, it seems easier to find a determined application and then work backwards, i.e., by choosing the adequate polymer, as well as the adequate concentration and cure temperatures in order to achieve the desired characteristics for the intended application.

5.References

5. References

Abascal, N. C., & Regan, L. (2018). The Past, Present and Future of protein-based materials. *Open Biology*, *8*(180113), 1–8. https://doi.org/10.1098/rsob.180113

Ahad, E. (1974). Differential scanning calorimetry of aqueous polymer solutions and gels. *Journal of Applied Polymer Science*, *18*(6), 1587–1602. https://doi.org/10.1002/app.1974.070180601

Ahmed, E. M. (2015). Hydrogel: Preparation, characterization, and applications: A review. *Journal of Advanced Research*, *6*(2), 105–121. https://doi.org/10.1016/j.jare.2013.07.006

Altunbas, A., & Pochan, D. J. (2012). Peptide-Based and Polypeptide-Based Hydrogels for Drug Delivery and Tissue Engineering. *Topics in Current Chemistry*, *310*, 135–168. https://doi.org/10.1007/128_2011_206

Anderson, J. P., Cappello, J., & Martin, D. C. (1994). Morphology and primary crystal structure of a silk-like protein polymer synthesized by genetically engineered Escherichia coli bacteria. *Biopolymers*, *34*(8), 1049–1058. https://doi.org/10.1002/bip.360340808

Arzensek, D. (2010). *Dynamic light scattering and application to proteins in solutions*. Seminar - 4th Year, University of Ljubljana - Faculty of Mathematics and Physics. http://www-f1.ijs.si/~rudi/sola/Dynamic_light_scattering_and_application_to_proteins_in_solutions.pdf

Badruddoza, A. Z. M., Godfrin, P. D., Myerson, A. S., Trout, B. L., & Doyle, P. S. (2016). Core–Shell Composite Hydrogels for Controlled Nanocrystal Formation and Release of Hydrophobic Active Pharmaceutical Ingredients. *Advanced Healthcare Materials*, *5*(15), 1960–1968. https://doi.org/10.1002/adhm.201600266

Barroca, M., Rodrigues, P., Sobral, R., Costa, M. M. R., Chaves, S. R., MacHado, R., Casal, M., & Collins, T. (2016). Antibiotic free selection for the high level biosynthesis of a silk-elastin-like protein. *Scientific Reports*, *6*(December), 1–11. https://doi.org/10.1038/srep39329

Bassas-Galia, M., Follonier, S., Pusnik, M., & Zinn, M. (2017). Natural polymers: A source of inspiration. In *Bioresorbable Polymers for Biomedical Applications: From Fundamentals to Translational Medicine*. Elsevier Ltd. https://doi.org/10.1016/B978-0-08-100262-9.00002-1

Bemmelen, J. M. V. (1894). Der Hydrogel und das kristallinische Hydrat des Kupferoxydes. *Zeitschrift Für Anorganische Und Allgemeine Chemie*, *5*(466).

Boey, F. Y. C., & Qiang, W. (2000). Determining the gel point of an epoxy-hexaanhydro-4-methylphthalic anhydride (MHHPA) system. *Journal of Applied Polymer Science*, *76*(8), 1248–1256. https://doi.org/10.1002/(SICI)1097-4628(20000523)76:8<1248::AID-APP5>3.0.CO;2-0

Cappello, J., Crissman, J., Dorman, M., Mikolajczak, M., Textor, G., Marquet, M., & Ferrari, F. (1990). Genetic Engineering of Structural Protein Polymers. *Biotechnology Progress*, *6*(3), 198–202. https://doi.org/10.1021/bp00003a006

Cappello, J., Crissman, J. W., Crissman, M., Ferrari, F. A., Textor, G., Wallis, O., Whitledge, J. R., Zhou, X., Burman, D., Aukerman, L., & Stedronsky, E. R. (1998). In-situ self-assembling protein polymer gel systems for administration, delivery, and release of drugs. *Journal of Controlled Release*, *53*(1–3), 105–117. https://doi.org/10.1016/S0168-3659(97)00243-5

Casal, M., Cunha, A. M., & Machado, R. (2014). Future Trends for Recombinant Protein-Based Polymers: The Case Study of Development and Application of Silk-Elastin-Like Polymers. *Bio-Based Plastics: Materials and Applications*, 311–329. https://doi.org/10.1002/9781118676646.ch12

Castillo, J. J., Shanbhag, B. K., & He, L. (2017). Comparison of Natural Extraction and Recombinant Mussel Adhesive Proteins Approaches. In *Food Bioactives* (pp. 111–135). Springer. https://doi.org/10.1007/978-3-319-51639-4

Chai, Q., Jiao, Y., & Yu, X. (2017). Hydrogels for Biomedical Applications: Their Characteristics and the Mechanisms behind Them. *Gels*, *3*(1), 6. https://doi.org/10.3390/gels3010006

Chen, L., Zhou, M. L., Qian, Z. G., Kaplan, D. L., & Xia, X. X. (2017). Fabrication of Protein Films from

Genetically Engineered Silk-Elastin-Like Proteins by Controlled Cross-Linking. *ACS Biomaterials Science and Engineering*, *3*(3), 335–341. https://doi.org/10.1021/acsbiomaterials.6b00794

Chow, D., Nunalee, M. L., Lim, D. W., Simnick, A. J., & Chilkoti, A. (2008). Peptide-based biopolymers in biomedicine and biotechnology. *Materials Science and Engineering R: Reports*, *62*(4), 125–155. https://doi.org/10.1016/j.mser.2008.04.004

Collins, T., Azevedo-Silva, J., da Costa, A., Branca, F., Machado, R., & Casal, M. (2013). Batch production of a silk-elastin-like protein in E. coli BL21(DE3): Key parameters for optimisation. *Microbial Cell Factories*, *12*(1), 1–16. https://doi.org/10.1186/1475-2859-12-21

Cox, M. M. J. (2012). Recombinant protein vaccines produced in insect cells. *Vaccine*, *30*(10), 1759–1766. https://doi.org/10.1016/j.vaccine.2012.01.016

Cresce, A. W., Dandu, R., Burger, A., Cappello, J., & Ghandehari, H. (2008). Characterization and real-time imaging of gene expression of adenovirus embedded silk-elastinlike protein polymer hydrogels. *Molecular Pharmaceutics*, *5*(5), 891–897. https://doi.org/10.1021/mp800054w

Dandu, R., Cresce, A. Von, Briber, R., Dowell, P., Cappello, J., & Ghandehari, H. (2009). Silk-elastinlike protein polymer hydrogels: Influence of monomer sequence on physicochemical properties. *Polymer*, *50*(2), 366–374. https://doi.org/10.1016/j.polymer.2008.11.047

Devi, L., & Gaba, P. (2019). Hydrogel: An updated primer. *Journal of Critical Reviews*, *6*(4). https://doi.org/10.22159/jcr.2019v6i4.33266

Dinerman, A. A., Cappello, J., Ghandehari, H., & Hoag, S. W. (2002). Solute diffusion in genetically engineered silk-elastinlike protein polymer hydrogels. *Journal of Controlled Release*, *82*(2–3), 277–287. https://doi.org/10.1016/S0168-3659(02)00134-7

Feksa, L. R., Troian, E. A., Muller, C. D., Viegas, F., Machado, A. B., & Rech, V. C. (2018). Hydrogels for biomedical applications. In *Nanostructures for the Engineering of Cells, Tissues and Organs* (pp. 403–438). https://doi.org/10.1016/B978-0-12-813665-2.00011-9

Fernandes, M. M., Correia, D. M., da Costa, A., Ribeiro, S., Casal, M., Lanceros-Méndez, S., & Machado, R. (2018). Multifunctional magnetically responsive biocomposites based on genetically engineered silk-elastin-like protein. *Composites Part B: Engineering*, *153*, 413–419. https://doi.org/10.1016/j.compositesb.2018.09.019

Frandsen, J. L., & Ghandehari, H. (2012). Recombinant protein-based polymers for advanced drug delivery. *Chemical Society Reviews*, *41*(7), 2696–2706. https://doi.org/10.1039/c2cs15303c

Gomes, S., Leonor, I. B., Mano, J. F., Reis, R. L., & Kaplan, D. L. (2012). Natural and genetically engineered proteins for tissue engineering. *Progress in Polymer Science (Oxford)*, *37*(1), 1–17. https://doi.org/10.1016/j.progpolymsci.2011.07.003

Greish, K., Araki, K., Li, D., O'Malley, B. W., Dandu, R., Frandsen, J., Cappello, J., & Ghandehari, H. (2009). Silk-Elastinlike Protein Polymer Hydrogels for Localized Adenoviral Gene Therapy of Head and Neck Tumors. *Biomacromolecules*, *10*(8), 1–13. https://doi.org/10.1038/jid.2014.371

Guilherme, M. R., Aouada, F. A., Fajardo, A. R., Martins, A. F., Paulino, A. T., Davi, M. F. T., Rubira, A. F., & Muniz, E. C. (2015). Superabsorbent hydrogels based on polysaccharides for application in agriculture as soil conditioner and nutrient carrier: A review. *European Polymer Journal*, *72*, 365–385. https://doi.org/10.1016/j.eurpolymj.2015.04.017

Gupta, P., & Nayak, K. K. (2015). Characteristics of Protein-Based Biopolymer and Its Application. *Polymer Engineering and Science*, 485–498. https://doi.org/10.1002/pen.23298

Gustafson, J. A., & Ghandehari, H. (2010). Silk-elastinlike protein polymers for matrix-mediated cancer gene therapy. *Advanced Drug Delivery Reviews*, *62*(15), 1509–1523. https://doi.org/10.1016/j.addr.2010.04.006

Gustafson, J. A., Greish, K., Frandsen, J. L., Cappello, J., & Ghandehari, H. (2009). Silk-elastinlike recombinant polymers for gene therapy of head and neck cancer: from molecular definition to controlled gene expression. *Journal of Controlled Release*, *140*(3), 256–261.

https://doi.org/10.1016/j.jconrel.2009.05.022
Gustafson, J. A., Price, R. A., Greish, K., Cappello, J., & Ghandehari, H. (2010). Silk-Elastinlike Hydrogel Improves the Safety of Adenovirus-Mediated Gene-Directed Enzyme Prodrug Therapy. *Molecular Pharmaceutics*, *7*(4), 1050–1056. https://doi.org/10.1021/mp100161u
Hacker, D. L., & Balasubramanian, S. (2016). Recombinant protein production from stable mammalian cell lines and pools. *Current Opinion in Structural Biology*, *38*(Figure 1), 129–136. https://doi.org/10.1016/j.sbi.2016.06.005
Haider, M., Cappello, J., Ghandehari, H., & Leong, K. W. (2008). In vitro chondrogenesis of mesenchymal stem cells in recombinant silk-elastinlike hydrogels. *Pharmaceutical Research*, *25*(3), 692–699. https://doi.org/10.1007/s11095-007-9282-8
Haider, M., Leung, V., Ferrari, F., Crissman, J., Powell, J., Cappello, J., & Ghandehari, H. (2005). Molecular engineering of silk-elastinlike polymers for matrix-mediated gene delivery: Biosynthesis and characterization. *Molecular Pharmaceutics*, *2*(2), 139–150. https://doi.org/10.1021/mp049906s
Halley, P. J., & Dorgan, J. R. (2011). Next-generation biopolymers: Advanced functionality and improved sustainability. *MRS Bulletin*, *36*(9), 687–691. https://doi.org/10.1557/mrs.2011.180
Hao, Q., Chen, T., Wang, R., Feng, J., Chen, D., & Yao, W. (2018). A separation-free polyacrylamide/bentonite/graphitic carbon nitride hydrogel with excellent performance in water treatment. *Journal of Cleaner Production*, *197*, 1222–1230. https://doi.org/10.1016/j.jclepro.2018.06.289
Hart, D. S., & Gehrke, S. H. (2006). Thermally Associating Polypeptides Designed for Drug Delivery Produced by Genetically Engineered Cells. *Journal of Pharmaceutical Sciences*, *9*(3), 484–516. https://doi.org/10.1002/jps
Herrero-Vanrell, R., Rincón, A. C., Alonso, M., Reboto, V., Molina-Martinez, I. T., & Rodríguez-Cabello, J. C. (2005). Self-assembled particles of an elastin-like polymer as vehicles for controlled drug release. *Journal of Controlled Release*, *102*(1), 113–122. https://doi.org/10.1016/j.jconrel.2004.10.001
Hoffman, A. S. (2012). Hydrogels for biomedical applications. *Advanced Drug Delivery Reviews*, *64*(SUPPL.), 18–23. https://doi.org/10.1016/j.addr.2012.09.010
Hu, X., Wang, X., Rnjak, J., Weiss, A. S., & Kaplan, D. L. (2010). Biomaterials Derived from Silk-Tropoelastin Protein Systems. *Biomaterials*, *31*(32), 8121–8131. https://doi.org/10.1016/j.biomaterials.2010.07.044. Biomaterials
Hu, Xiao, Kaplan, D., & Cebe, P. (2006). Determining beta-sheet crystallinity in fibrous proteins by thermal analysis and infrared spectroscopy. *Macromolecules*, *39*(18), 6161–6170. https://doi.org/10.1021/ma0610109
Hu, Xiao, Kaplan, D., & Cebe, P. (2007). Effect of water on the thermal properties of silk fibroin. *Thermochimica Acta*, *461*(1–2), 137–144. https://doi.org/10.1016/j.tca.2006.12.011
Hu, Xiao, Lu, Q., Kaplan, D. L., & Cebe, P. (2009). Microphase separation controlled β-sheet crystallization kinetics in fibrous proteins. *Macromolecules*, *42*(6), 2079–2087. https://doi.org/10.1021/ma802481p
Huang, W., Rollett, A., & Kaplan, D. L. (2015). Silk-elastin-like protein biomaterials for the controlled delivery of therapeutics. *Expert Opinion on Drug Delivery*, *12*(5), 779–791. https://doi.org/10.1517/17425247.2015.989830
Huang, W., Tarakanova, A., Dinjaski, N., Wang, Q., Xia, X., Chen, Y., Wong, J. Y., Buehler, M. J., & Kaplan, D. L. (2016). Design of Multistimuli Responsive Hydrogels Using Integrated Modeling and Genetically Engineered Silk–Elastin-Like Proteins. *Advanced Functional Materials*, *26*(23), 4113–4123. https://doi.org/10.1002/adfm.201600236
Hwang, D., Moolchandani, V., Dandu, R., Haider, M., Cappello, J., & Ghandehari, H. (2009). Influence of polymer structure and biodegradation on DNA release from silk-elastinlike protein polymer

hydrogels. *International Journal of Pharmaceutics*, *368*(1–2), 215–219. https://doi.org/10.1016/j.ijpharm.2008.10.021. Influence

Iglesias, M. J., Jiménez, F., Laggoun-Défarge, F., & Suárez-Ruiz, I. (1995). FTIR study of pure vitrains and associated coals. *Energy & Fuels*, *9*(3), 458–466. https://doi.org/10.1016/0140-6701(95)94946-u

Isaacson, K. J., Jensen, M. M., Watanabe, A. H., Green, B. E., Correa, M. A., Cappello, J., & Ghandehari, H. (2018). Self-Assembly of Thermoresponsive Recombinant Silk-Elastinlike Nanogels. *Macromolecular Bioscience*, *18*(1), 1–11. https://doi.org/10.1002/mabi.201700192

Jang, Y., & Champion, J. A. (2016). Self-Assembled Materials Made from Functional Recombinant Proteins. *Accounts of Chemical Research*, *49*(10), 2188–2198. https://doi.org/10.1021/acs.accounts.6b00337

Jensen, M. M., Jia, W., Isaacson, K. J., Schults, A., Cappello, J., Prestwich, G. D., Oottamasathien, S., & Ghandehari, H. (2017). Silk-elastinlike protein polymers enhance the efficacy of a therapeutic glycosaminoglycan for prophylactic treatment of radiation-induced proctitis. *Journal of Controlled Release*, *263*, 46–56. https://doi.org/10.1016/j.jconrel.2017.02.025

Jeon, O., Shin, J. Y., Marks, R., Hopkins, M., Kim, T. H., Park, H. H., & Alsberg, E. (2017). Highly elastic and tough interpenetrating polymer network-structured hybrid hydrogels for cyclic mechanical loading-enhanced tissue engineering. *Chemistry of Materials*, *29*(19), 8425–8432. https://doi.org/10.1021/acs.chemmater.7b02995

Jonker, A. M., Lo, D. W. P. M., & Hest, J. C. M. Van. (2012). *Peptide- and Protein-Based Hydrogels*.

Kapoor, S., & Kundu, S. C. (2016). Silk protein-based hydrogels: Promising advanced materials for biomedical applications. *Acta Biomaterialia*, *31*, 17–32. https://doi.org/10.1016/j.actbio.2015.11.034

Kim, W. (2013). Recombinant protein polymers in biomaterials. *Frontiers in Bioscience (Landmark Edition)*, *1*(18), 289–304.

Kim, W., & Conticello, V. P. (2007). Protein engineering methods for investigation of structure-function relationships in protein-based elastomeric materials. *Polymer Reviews*, *47*(1), 93–119. https://doi.org/10.1080/15583720601109586

Knight, A. S., Zhou, E. Y., Francis, M. B., & Zuckermann, R. N. (2015). Sequence Programmable Peptoid Polymers for Diverse Materials Applications. *Advanced Materials*, *27*(38), 5665–5691. https://doi.org/10.1002/adma.201500275

Kopecek, J. (2007). Hydrogel biomaterials: A smart future? *Biomaterials*, *28*(34), 5185–5192. https://doi.org/10.1016/j.biomaterials.2007.07.044

Kopecek, J., & Yang, J. (2007). Hydrogels as smart biomaterials. *Polym International*, *56*, 1078–1098. https://doi.org/10.1002/pi

Krishna, O. D., & Kiick, K. L. (2010). Protein- and Peptide-Modified Synthetic Polymeric Biomaterials. *Biopolymers*, *94*(1), 32–48. https://doi.org/10.1016/j.physbeh.2017.03.040

Laza, J. M., Julian, C. A., Larrauri, E., Rodriguez, M., & Leon, L. M. (1999). Thermal scanning rheometer analysis of curing kinetic of an epoxy resin: 2. An amine as curing agent. *Polymer*, *40*(1), 35–45. https://doi.org/10.1016/S0032-3861(98)00217-1

Lorber, B., Fischer, F., Bailly, M., Roy, H., & Kern, D. (2012). Protein analysis by dynamic light scattering: Methods and techniques for students. *Biochemistry and Molecular Biology Education*, *40*(6), 372–382. https://doi.org/10.1002/bmb.20644

Luan, C. -H, Harris, R. D., Prasad, K. U., & Urry, D. W. (1990). Differential scanning calorimetry studies of the inverse temperature transition of the polypentapeptide of elastin and its analogues. *Biopolymers*, *29*(14), 1699–1706. https://doi.org/10.1002/bip.360291403

Luan, C. H., & Urry, D. W. (1999). Elastic, plastic, and hydrogel-forming protein-based polymers. In *Polymer Data Handboo* (Mark JE, pp. 78–79). Oxford University Press.

Lutz, J. F. (2008). Polymerization of oligo(ethylene glycol) (meth)acrylates: Toward new generations of smart biocompatible materials. *Journal of Polymer Science, Part A: Polymer Chemistry*, *46*(11), 3459–3470. https://doi.org/10.1002/pola.22706

Lyons, R. E., Lesieur, E., Kim, M., Wong, D. C. C., Huson, M. G., Nairn, K. M., Brownlee, A. G., Pearson, R. D., & Elvin, C. M. (2007). Design and facile production of recombinant resilin-like polypeptides: Gene construction and a rapid protein purification method. *Protein Engineering, Design and Selection*, *20*(1), 25–32. https://doi.org/10.1093/protein/gzl050

Machado, R., Azevedo-Silva, J., Correia, C., Collins, T., Arias, F. J., Rodríguez-Cabello, J. C., & Casal, M. (2013). High level expression and facile purification of recombinant silk-elastin-like polymers in auto induction shake flask cultures. *AMB Express*, *3*, 1–15. https://doi.org/10.1186/2191-0855-3-11

Machado, R., Da Costa, A., Sencadas, V., Garcia-Arévalo, C., Costa, C. M., Padrão, J., Gomes, A., Lanceros-Méndez, S., Rodríguez-Cabello, J. C., & Casal, M. (2013). Electrospun silk-elastin-like fibre mats for tissue engineering applications. *Biomedical Materials (Bristol)*, *8*(6). https://doi.org/10.1088/1748-6041/8/6/065009

Machado, R., Ribeiro, A. J., Padrão, J., Silva, D., Nobre, A., Teixeira, J. A., Arias, F. J., Cunha, A. M., Rodríguez-Cabello, J. C., & Casalla, M. (2009). Exploiting the sequence of naturally occurring elastin: Construction, production and characterization of a recombinant thermoplastic proteinbased polymer. *Journal of Nano Research*, *6*, 133–145. https://doi.org/10.4028/www.scientific.net/JNanoR.6.133

Machado, Raul, Da Costa, A., Sencadas, V., Pereira, A. M., Collins, T., Rodríguez-Cabello, J. C., Lanceros-Méndez, S., & Casal, M. (2015). Exploring the Properties of Genetically Engineered Silk-Elastin-Like Protein Films. *Macromolecular Bioscience*, *15*(12), 1698–1709. https://doi.org/10.1002/mabi.201500132

Madhavan, A., Pandey, A., & Sukumaran, R. K. (2017). Expression system for heterologous protein expression in the filamentous fungus Aspergillus unguis. *Bioresource Technology*, *245*, 1334–1342. https://doi.org/10.1016/j.biortech.2017.05.140

McGill, M., Holland, G. P., & Kaplan, D. L. (2019). Experimental Methods for Characterizing the Secondary Structure and Thermal Properties of Silk Proteins. *Macromolecular Rapid Communications*, *40*(1), 1–14. https://doi.org/10.1002/marc.201800390

McMillan, R. A., Lee, T. A. T., & Conticello, V. P. (1999). Rapid assembly of synthetic genes encoding protein polymers. *Macromolecules*, *32*(11), 3643–3648. https://doi.org/10.1021/ma981660f

Megeed, Z., Cappello, J., & Ghandehari, H. (2002). Genetically engineered silk-elastinlike protein polymers for controlled drug delivery. *Advanced Drug Delivery Reviews*, *54*(8), 1075–1091. https://doi.org/10.1016/S0169-409X(02)00063-7

Megeed, Z., Haider, M., Li, D., O'Malley, B. W., Cappello, J., & Ghandehari, H. (2004). In vitro and in vivo evaluation of recombinant silk-elastinlike hydrogels for cancer gene therapy. *Journal of Controlled Release*, *94*(2–3), 433–445. https://doi.org/10.1016/j.jconrel.2003.10.027

Mi, L. (2006). *Molecular Cloning of Protein-Based Polymers*. 2099–2107.

Nagapudi, K., Brinkman, W. T., Leisen, J., Thomas, B. S., Wright, E. R., Haller, C., Wu, X., Apkarian, R. P., Conticello, V. P., & Chaikof, E. L. (2005). Protein-based thermoplastic elastomers. *Macromolecules*, *38*(2), 345–354. https://doi.org/10.1021/ma0491199

Nagarsekar, A., Crissman, J., Crissman, M., Ferrari, F., Cappello, J., & Ghandehari, H. (2002). Genetic synthesis and characterization of pH- and temperature-sensitive silk-elastinlike protein block copolymers. *Journal of Biomedical Materials Research*, *62*(2), 195–203. https://doi.org/10.1002/jbm.10272

Nagarsekar, A., Crissman, J., Crissman, M., Ferrari, F., Cappello, J., & Ghandehari, H. (2003). Genetic engineering of stimuli-sensitive silkelastin-like protein block copolymers. *Biomacromolecules*, *4*(3), 602–607. https://doi.org/10.1021/bm0201082

Nemours, E. I. P. (1936). Methacrylate Resins. *Industrial & Engineering Chemistry*, *28*, 1160–1163.

Nobbman, U. (2017). *Polydispersity - What does it mean for DLS and Chromatography*. https://www.materials-talks.com/blog/2017/10/23/polydispersity-what-does-it-mean-for-dls-and-chromatography/

Nowak, A. P., Breedveld, V., Pakstis, L., Ozbas, B., Pine, D. J., & Deming, T. J. (2002). Rapidly recovering hydrogel scaffolds from self-assembling diblock copolypeptide amphiphiles. *Nature*, *417*(6887), 424–428. https://doi.org/10.1038/417424a

Numata, K., Subramanian, B., Currie, H. A., & Kaplan, D. L. (2009). Bioengineered silk protein-based gene delivery systems. *Biomaterials*, *30*(29), 5775–5784. https://doi.org/10.1016/j.biomaterials.2009.06.028

Nuutila, K., Laukkanen, A., Lindford, A., Juteau, S., Nuopponen, M., Vuola, J., & Kankuri, E. (2018). Inhibition of Skin Wound Contraction by Nanofibrillar Cellulose Hydrogel. *Plastic and Reconstructive Surgery*, *141*(3), 357e-366e. https://doi.org/10.1097/PRS.0000000000004168

Ozaki, C., Somamoto, S., Kawabata, S., & Tabata, Y. (2014). Effect of an artificial silk elastin-like protein on the migration and collagen production of mouse fibroblasts. *Journal of Biomaterials Science, Polymer Edition*, *25*(12), 1266–1277. https://doi.org/10.1080/09205063.2014.926580

Peppas, N. A., Bures, P., Leobandung, W., & Ichikawa, H. (2000). Hydrogels in pharmaceutical formulations. *European Journal of Pharmaceutics and Biopharmaceutics*, *50*(1), 27–46. https://doi.org/10.1016/S0939-6411(00)00090-4

Pereira, A. M., Machado, R., da Costa, A., Ribeiro, A., Collins, T., Gomes, A. C., Leonor, I. B., Kaplan, D. L., Reis, R. L., & Casal, M. (2017). Silk-based biomaterials functionalized with fibronectin type II promotes cell adhesion. *Acta Biomaterialia*, *47*, 50–59. https://doi.org/10.1016/j.actbio.2016.10.002

Pieters, B. J. G. E., Van Eldijk, M. B., Nolte, R. J. M., & Mecinović, J. (2016). Natural supramolecular protein assemblies. *Chemical Society Reviews*, *45*(1), 24–39. https://doi.org/10.1039/c5cs00157a

Qiu, W., Cappello, J., & Wu, X. (2011). Autoclaving as a chemical-free process to stabilize recombinant silk-elastinlike protein polymer nanofibers. *Applied Physics Letters*, *98*(26), 2012–2015. https://doi.org/10.1063/1.3604786

Qiu, W., Huang, Y., Teng, W., Cohn, C. M., Cappello, J., & Wu, X. (2010). Complete recombinant silk-elastinlike protein-based tissue scaffold. *Biomacromolecules*, *11*(12), 3219–3227. https://doi.org/10.1021/bm100469w

Rath, A., Glibowicka, M., Nadeau, V. G., Chen, G., & Deber, C. M. (2009). Detergent binding explains anomalous SDS-PAGE migration of membrane proteins. *Proceedings of the National Academy of Sciences of the United States of America*, *106*(6), 1760–1765. https://doi.org/10.1073/pnas.0813167106

Reguera, J., Lagarón, J. M., Alonso, M., Reboto, V., Calvo, B., & Rodriguez-Cabello, J. C. (2003). Thermal behavior and kinetic analysis of the chain unfolding and refolding and of the concomitant nonpolar solvation and desolvation of two Elastin-like polymers. *Macromolecules*, *36*(22), 8470–8476. https://doi.org/10.1021/ma034572q

Reuter, L. J., Bailey, M. J., Joensuu, J. J., & Ritala, A. (2014). Scale-up of hydrophobin-assisted recombinant protein production in tobacco BY-2 suspension cells. *Plant Biotechnology Journal*, *12*(4), 402–410. https://doi.org/10.1111/pbi.12147

Roberts, E. G., Rim, N. G., Huang, W., Tarakanova, A., Yeo, J., Buehler, M. J., Kaplan, D. L., & Wong, J. Y. (2018). Fabrication and Characterization of Recombinant Silk-Elastin-Like-Protein (SELP) Fiber. *Macromolecular Bioscience*, *18*(12), 1–10. https://doi.org/10.1002/mabi.201800265

Rodríguez-Cabello, J. C., Alonso, M., Díez, M. I., Caballero, M. I., & Herguedas, M. M. (1999). Structural investigation of the poly(pentapeptide) of elastin, poly(GVGVP), in the solid state. *Macromolecular*

Chemistry and Physics, *200*(8), 1831–1838. https://doi.org/10.1002/(SICI)1521-3935(19990801)200:8<1831::AID-MACP1831>3.0.CO;2-V

Rodríguez-Cabello, J. C., Martín, L., Alonso, M., Arias, F. J., & Testera, A. M. (2009). "Recombinamers" as advanced materials for the post-oil age. *Polymer*, *50*(22), 5159–5169. https://doi.org/10.1016/j.polymer.2009.08.032

Sambrook, S., & Russel, D. W. (2006). *The Condensed Protocols from Molecular Cloning: A Laboratory Manual* (1st editio). Cold SprinngHarbor Laboratory Press.

Scheller, J., & Conrad, U. (2001). Production of Spider Silk Proteins in Transgenic Tobacco and Potato. *Molecular Farming: Plant-Made Pharmaceuticals and Technical Proteins*, *19*(June), 171–181. https://doi.org/10.1002/3527603638.ch11

Schneider, C. A., Rasband, W. S., & Eliceiri, K. W. (2012). NIH Image to ImageJ: 25 years of image analysis. *Nature Methods*, *9*(7), 671–675.

Sengupta, D., & Heilshorn, S. C. (2010). Protein-engineered biomaterials: Highly tunable tissue engineering scaffolds. *Tissue Engineering - Part B: Reviews*, *16*(3), 285–293. https://doi.org/10.1089/ten.teb.2009.0591

Shirai, A., Matsuyama, A., Yashiroda, Y., Hashimoto, A., Kawamura, Y., Arai, R., Komatsu, Y., Horinouchi, S., & Yoshida, M. (2008). Global analysis of gel mobility of proteins and its use in target identification. *Journal of Biological Chemistry*, *283*(16), 10745–10752. https://doi.org/10.1074/jbc.M709211200

Silva, N. H. C. S., Vilela, C., Marrucho, I. M., Freire, C. S. R., Pascoal Neto, C., & Silvestre, A. J. D. (2014). Protein-based materials: From sources to innovative sustainable materials for biomedical applications. *Journal of Materials Chemistry B*, *2*(24), 3715–3740. https://doi.org/10.1039/c4tb00168k

Sivashanmugam, A., Murray, V., Cui, C., Zhang, Y., Wang, J., & Li, Q. (2009). Practical protocols for production of very high yields of recombinant proteins using Escherichia coli. *Protein Science*, *18*(5), 936–948. https://doi.org/10.1002/pro.102

Soni, R. (2017). Yeast as a Versatile System for Heterologous Protein Expression; Genetically Modified Yeast Strain to Express Human Drug Metabolism Enzymes. *Journal of Bacteriology & Mycology: Open Access*, *5*(1), 1–2. https://doi.org/10.15406/jbmoa.2017.05.00122

Su, R. S. C., Kim, Y., & Liu, J. C. (2014). Resilin: Protein-based elastomeric biomaterials. *Acta Biomaterialia*, *10*(4), 1601–1611. https://doi.org/10.1016/j.actbio.2013.06.038

Sun, Z., Qin, G., Xia, X., Cronin-Golomb, M., Omenetto, F., & D., K. (2013). Photoresponsive retinal-modified silk-elastin copolymer. *Journal of American -Chemical Society*, *135*(9), 3675–3679. https://doi.org/10.1021/ja312647n

Teng, W., Cappello, J., & Wu, X. (2009). Recombinant silk-elastinlike protein polymer displays elasticity comparable to elastin. *Biomacromolecules*, *10*(11), 3028–3036. https://doi.org/10.1021/bm900651g

Thakur, S., Thakur, V. K., & Arotiba, O. A. (2018). Hydrogels: Recent Advances. In *Hydrogels* (pp. 29–50). Springer Singapore. https://doi.org/10.1007/978-981-10-6077-9

Trabbic-Carlson, K., Meyer, D. E., Liu, L., Piervincenzi, R., Nath, N., LaBean, T., & Chilkoti, A. (2004). Effect of protein fusion on the transition temperature of an environmentally responsive elastin-like polypeptide: A role for surface hydrophobicity? *Protein Engineering, Design and Selection*, *17*(1), 57–66. https://doi.org/10.1093/protein/gzh006

Urry, D. W., Luan, C. H., Peng, S. Q., Parker, T. M., & Gowda, D. C. (1992). Hierarchical and Modulable Hydrophobic Folding and Self-assembly in Elastic Protein-base Polymers: Implications for Signal Transduction. *Japanese Society of Biofeedback Research*, *255*, 411–421. https://doi.org/10.1557/PROC-255-411

Van Vlierberghe, S., Dubruel, P., & Schacht, E. (2011). Biopolymer-based hydrogels as scaffolds for tissue

engineering applications: A review. *Biomacromolecules*, *12*(5), 1387–1408. https://doi.org/10.1021/bm200083n

Wang, H., Paul, A., Nguyen, D., Enejder, A., & Heilshorn, S. C. (2018). Tunable Control of Hydrogel Microstructure by Kinetic Competition between Self-Assembly and Crosslinking of Elastin-like Proteins [Research-article]. *ACS Applied Materials and Interfaces*, *10*(26), 21808–21815. https://doi.org/10.1021/acsami.8b02461

Wang, Q., Xia, X., Huang, W., Lin, Y., Xu, Q., & Kaplan, D. L. (2014). High throughput screening of dynamic silk-elastin-like protein biomaterials. *Advanced Functional Materials*, *24*(27), 4303–4310. https://doi.org/10.1002/adfm.201304106

Wichterle, O., & Lím, D. (1960). Hydrophilic Gels for Biological Use. *Nature*, *185*(4706), 117–118. https://doi.org/10.1038/185117a0

Winkler, S., Wilson, D., & Kaplan, D. L. (2000). Controlling β-sheet assembly in genetically engineered silk by enzymatic phosphorylation/dephosphorylation. *Biochemistry*, *39*(41), 12739–12746. https://doi.org/10.1021/bi001335w

Wold, F. (1981). In Vivo Chemical modification of proteinsv(Post-Translational Modification). *Annual Review of Biochemistry*, *50*(1), 783–814.

Worldwide, M. . I. (2011). *Dynamic Light Scattering Common Terms Defined*. Inform -White Paper. http://www.biophysics.bioc.cam.ac.uk/wp-content/uploads/2011/02/DLS_Terms_defined_Malvern.pdf

Wu, H., Liu, S., Xiao, L., Dong, X., Lu, Q., & Kaplan, D. L. (2016). Injectable and pH-Responsive Silk Nanofiber Hydrogels for Sustained Anticancer Drug Delivery. *ACS Applied Materials and Interfaces*, *8*(27), 17118–17126. https://doi.org/10.1021/acsami.6b04424

Xia, X. X., Xu, Q., Hu, X., Qin, G., & Kaplan, D. L. (2011). Tunable self-assembly of genetically engineered silk-elastin-like protein polymers. *Biomacromolecules*, *12*(11), 3844–3850. https://doi.org/10.1021/bm201165h

Xu, C., Breedveld, V., & Kopeček, J. (2005). Reversible hydrogels from self-assembling genetically engineered protein block copolymers. *Biomacromolecules*, *6*(3), 1739–1749. https://doi.org/10.1021/bm050017f

Yahia, Lh. (2015). History and Applications of Hydrogels. *Journal of Biomedical Sciencies*, *04*(02), 1–23. https://doi.org/10.4172/2254-609x.100013

Yamaoka, T., Tamura, T., Seto, Y., Tada, T., Kunugi, S., & Tirrell, D. A. (2003). Mechanism for the phase transition of a genetically engineered elastin model peptide (VPGIG)40 in aqueous solution. *Biomacromolecules*, *4*(6), 1680–1685. https://doi.org/10.1021/bm034120l

Yan, C., & Pochan, D. J. (2010). Rheological properties of peptide-based hydrogels for biomedical and other applications. *Chemical Society Reviews*, *39*(9), 3528–3540. https://doi.org/10.1039/b919449p

Yang, Y. J., Holmberg, A. L., & Olsen, B. D. (2017). Artificially Engineered Protein Polymers. *Annual Review of Chemical and Biomolecular Engineering*, *8*(1), 549–575. https://doi.org/10.1146/annurev-chembioeng-060816-101620

Yang, Z., & Zhang, Z. (2018). Engineering strategies for enhanced production of protein and bio-products in Pichia pastoris: A review. *Biotechnology Advances*, *36*(1), 182–195. https://doi.org/10.1016/j.biotechadv.2017.11.002

Yeo, J., Huang, W., Tarakanova, A., Zhang, Y. W., Kaplan, D. L., & Buehler, M. J. (2018). Unraveling the molecular mechanisms of thermo-responsive properties of silk-elastin-like proteins by integrating multiscale modeling and experiment. *Journal of Materials Chemistry B*, *6*(22), 3727–3734. https://doi.org/10.1039/c8tb00819a

Zhu, J., & Marchant, R. E. (2011). Design properties of hydrogel tissue-engineering scaffolds Junmin. *Expert Review of Medical Devices*, *8*(5), 607–626. https://doi.org/10.1586/erd.11.27.Design

Zhu, Jingxin, Huang, W., Zhang, Q., Ling, S., Chen, Y., & Kaplan, D. L. (2016). Aqueous-based coaxial electrospinning of genetically engineered silk elastin core-shell nanofibers. *Materials*, *9*(4), 0–13. https://doi.org/10.3390/ma9040221

6.Annex

6. Annex

I. Materials and Methods

a. Bacterial strain and culture media

- *E. coli* BL21(DE3) was used for protein production. Information about the strain used: [F- *omp*T *gal* dcm lon *hsd*S_B(r_B- m_B-) λ(DE3) (*lac*I *lac*UV5-T7 gene 1 *ind*1 *Sam*7 *nin*5)]

- Lysogeny Broth (LB) (purchased from Grisp (Lot: 7E01122C) or tryptone 1%(w/v), yeast extract 0.5% (w/v), sodium chloride (NaCl) 0.5% (w/v));

- Terrific Broth (TB) (purchased form Grispr (Lot: 7E0803G) or tryptone 1.2% (w/v), yeast extract 2.4% (w/v), glycerol 0.5% (w/v), KH_2PO_4 2.3% (w/v), K_2HPO_4 16% (w/v).

b. Solutions

- **TE Buffer -** Tris base 0.5 M, EDTA 0.01 M
- **SDS-PAGE Sample Loading Buffer 5x** - 0.25 M Tris-Hcl, pH 6.8, 0.01 M DTT; 4.1 M Glycerol, 0.3 M SDS, 0.15 mM bromophenol blue, β-mercaptoethanol 0.14 M
- ***1x* SDS-PAGE running buffer** - Tris base 0.25 M, glycine 1.9 M, SDS 0.03 M
- **Tris pH 8.8 -** Tris-HCl 0.75 M
- **Tris pH 6.8** - Tric-HCl 0.25 M

Table 15 - "Recipe" for making 1 polyacrylamide gel being 1mm thick, used in the SDS-PAGE runs.

	Resolving gel (10 %)	**Stacking gel (10 %)**
Acrylamide/ bis-acrylamide	1.6 mL	415 µL
Tris pH 8.8	1.9 mL	-
Tris pH 6.8	-	630 µL
Deionized H_2O	1.1 mL	1.4 mL
SDS (10% (w/v))	47 µL	25 µL
APS (10% (w/v))	35 µL	15 µL
TEMED	6 µL	5 µL

Tris base was purchased from Sigma (Lot SLBS0616V), glycine, Acrylamide/ bis-Acrylamine (37.5:1 solution) (Batch 18021) and Sodium Dodecyl Sulphate (SDS) solution (20% (w/v)(Batch: 17121) were purchased from enzytech, deionized water was obtained using the MILI-Q system, Ammonium Persulfate (APS) was purchased from Sigma-Aldrich (Lot #BCBL6887V), TEMED was purchased from PanReac AppliChem (Lot: 8G011733).

II. Results

a. Differential Scanning Calorimetry

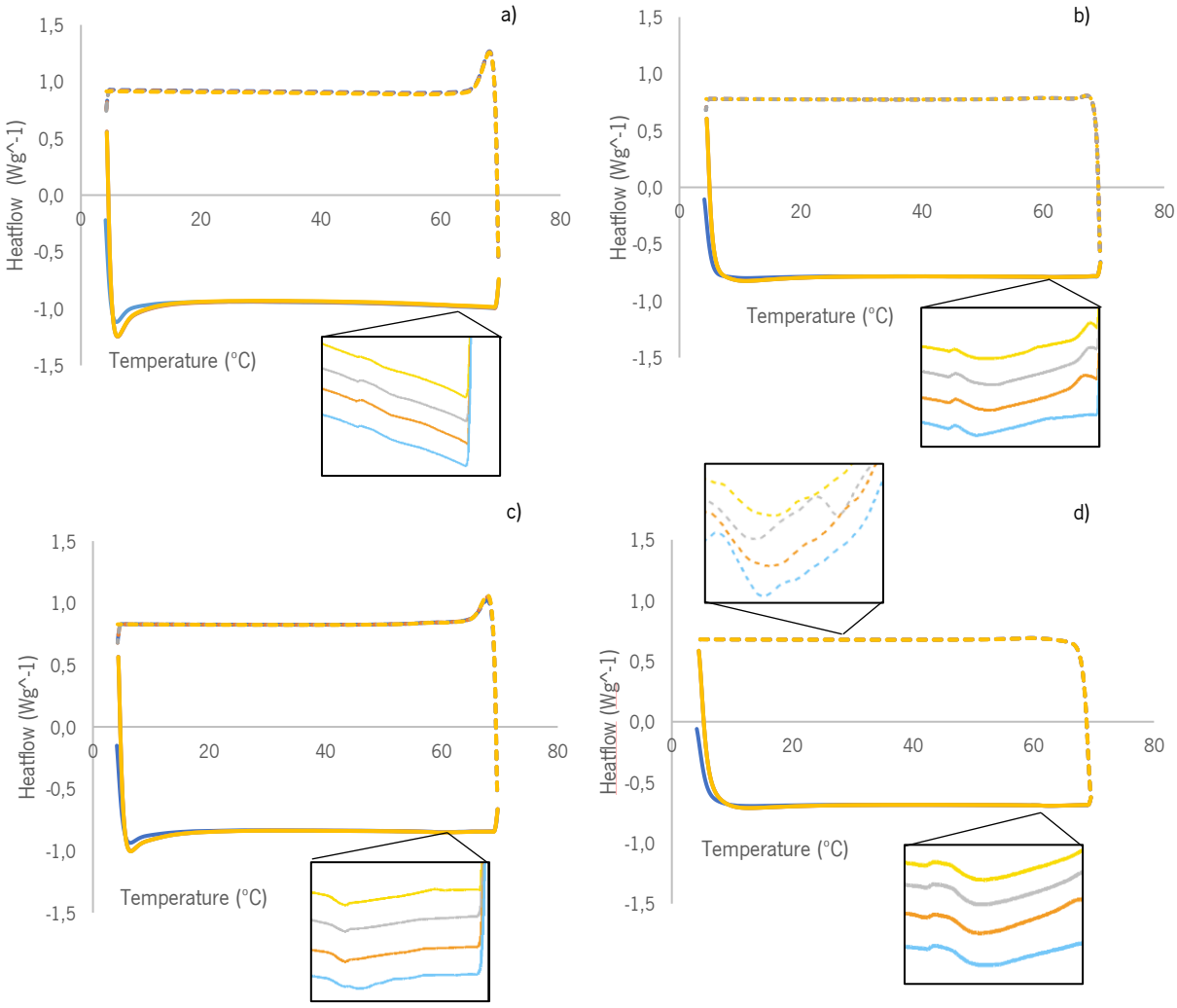

Figure 159 - DSC runs of SELP-59-A solutions prepared at different concentrations: 5% (a), 10% (b), 15% (c) and 20% (d) (w/v), subjected to four heating (solid lines) and cooling (dashed lines) cycles (1- blue; 2 – orange; 3 -grey; 4 -yellow. The transitions are n ot very evident is these type of graphics, only by using the StarE software (Mettler Toledo) to zoom in on the graphics and find the exothermic and endothermic peaks, and so, their respective enthalpy values and the temperatures at the onset and peak are described in table 14.

Table 16 - Temperatures at which the peak, onset and endset of the exo-/ endothermal reaction occurred, as well as it's corresponding enthalpy value (ΔH) for SELP-59-A solutions. Values determined using StarE software (Mettler Toledo).

		Heating				Cooling			
	Cycle	Cycle 1	Cycle 2	Cycle 3	Cycle 4	Cycle 1	Cycle 2	Cycle 3	Cycle 4
5%	Integral (mJ)	-1.8	-1.5	-1,1	-0.9	-	-	-	-
	Onset (°C)	59.8	60.5	59.6	59.9	-	-	-	-
	Peak (°C)	62.2	63.0	62.9	62.9	-	-	-	-
	Endset (°C)	673	68.1	67.7	68.6	-	-	-	-
10%	Integral (mJ)	-0.85	-2.9	-2.9	-2.3	-	-	-	-
	Onset (°C)	59.5	59.6	59.7	59.6	-	-	-	-
	Peak (°C)	61.3	63.9	62.6	62.3	-	-	-	-
	Endset (°C)	64.1	66.1	68.3	67.3	-	-	-	-
15%	Integral (mJ)	-0.43	-2.4	-2.2	-2.1	-	-	-	-
	Onset (°C)	64.1	59.7	59.6	59.6	-	-	-	-
	Peak (°C)	65.0	62.2	62.2	61.7	-	-	-	-
	Endset (°C)	66.7	67.0	66.1	65.8	-	-	-	-
20%	Integral (mJ)	-2.4	-2.3	-3.2	-3.6	0.8	0.8	0.7	0.7
	Onset (°C)	58.9	58.8	58.8	58.6	30.7	29.9	29.3	29.3
	Peak (°C)	62.0	61.5	61.8	61.7	26.6	25.6	25.3	25.3
	Endset (°C)	66.5	66.6	68.1	67.9	21.0	19.6	15.9	15.9

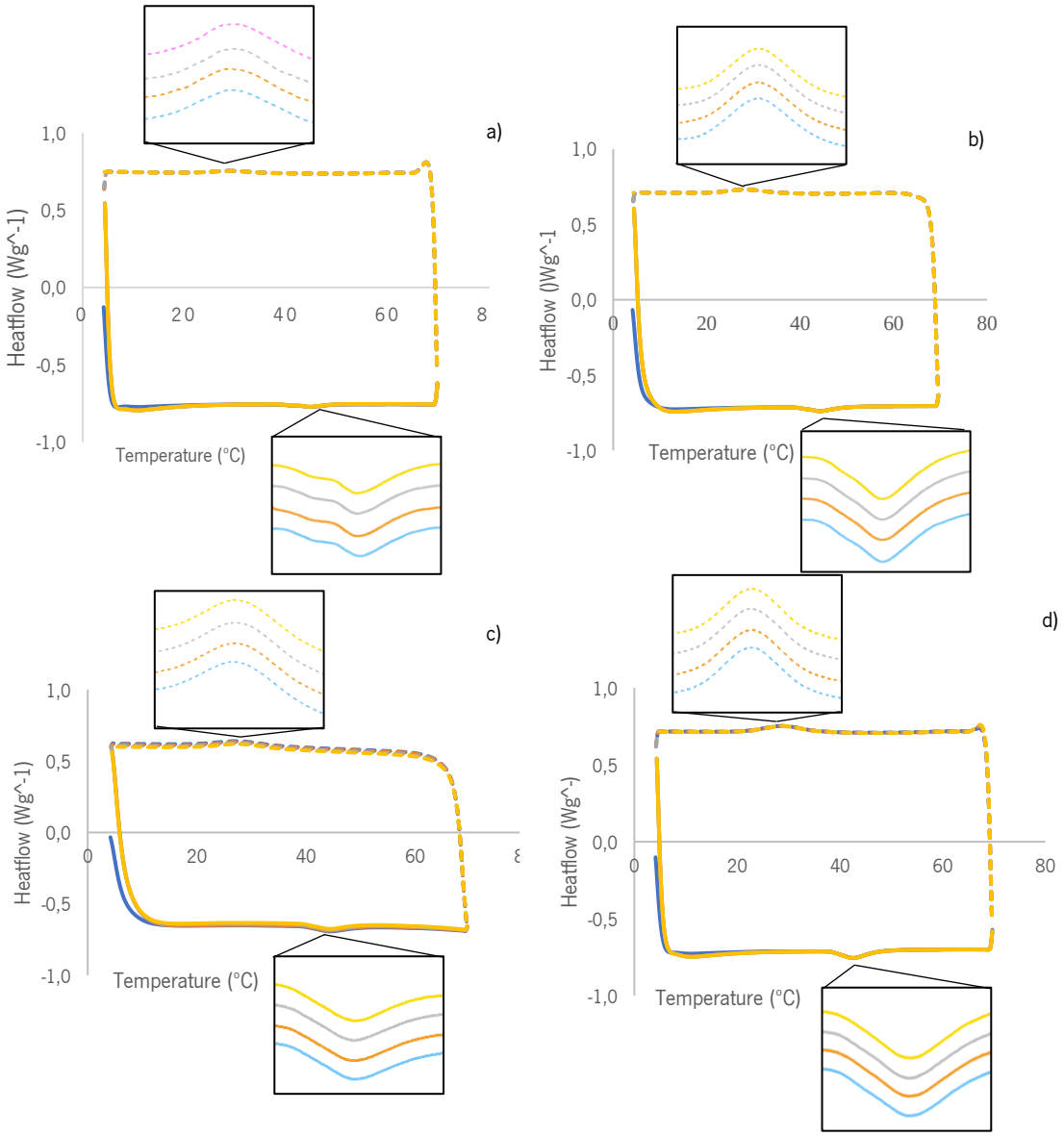

Figure 20 - DSC runs of SELP-520-A solutions prepared at different concentrations: 5% (a), 10% (b), 15% (c) and 20% (d) (w/v), subjected to four heating (solid lines) and cooling (dashed lines) cycles (1- blue; 2 – orange; 3 -grey; 4 -yellow). Their respective enthalpy values and the temperatures at the onset and peak are described in table 15

Table 17 - Temperatures at which the peak, onset and endset of the exo-/ endothermal reaction occurred, as well as it's corresponding enthalpy value (ΔH) for SELP-520-A solutions. Values determined using StarE software (Mettler Toledo).

		Heating				Cooling			
	Cycle	**Cycle 1**	**Cycle 2**	**Cycle 3**	**Cycle 4**	**Cycle 1**	**Cycle 2**	**Cycle 3**	**Cycle 4**
5%	Integral (mJ)	-8.5	-8.9	-8.7	-8.7	10.8	9.7	10.3	11.7
	Onset (°C)	41.0	41.1	41.1	41.1	36.7	35.7	35.3	36.7
	Peak (°C)	44.8	44.6	44.5	44.5	28.8	28.5	29.5	29.2
	Endset (°C)	49.1	48.9	49.0	49.1	22.2	22.9	23.3	23.4
10%	Integral (mJ)	-19.1	-18.0	-19.7	-18.5	24.3	25.9	25.3	24.8
	Onset (°C)	39.6	39.7	39.6	39.9	36.0	36.2	36.0	36.0
	Peak (°C)	44.4	44.3	44.3	44.3	28.4	28.4	28.4	28.5
	Endset (°C)	49.6	49.5	49.7	49.5	21.2	21.2	21.2	21.3
15%	Integral (mJ)	-25.9	-25.0	-25.1	-25.0	36.5	36.2	38.4	36.3
	Onset (°C)	39.5	39.5	39.5	39.4	35.5	35.3	35.7	35.6
	Peak (°C)	44.3	44.3	44.3	44.3	27.7	27.5	27.8	27.7
	Endset (°C)	50.2	50.0	50.0	49.6	19.7	19.6	20.0	20.0
20%	Integral (mJ)	-26.1	-26.8	-25.9	-26.1	32.5	9.7	36.6	35.8
	Onset (°C)	35.9	35.7	36.3	36.1	35.9	36.4	36.3	36.1
	Peak (°C)	28.8	28.5	28.7	29.0	28.8	28.8	28.7	29.0
	Endset (°C)	21.8	22.9	21.5	21.6	21.8	21.5	21.5	21.6

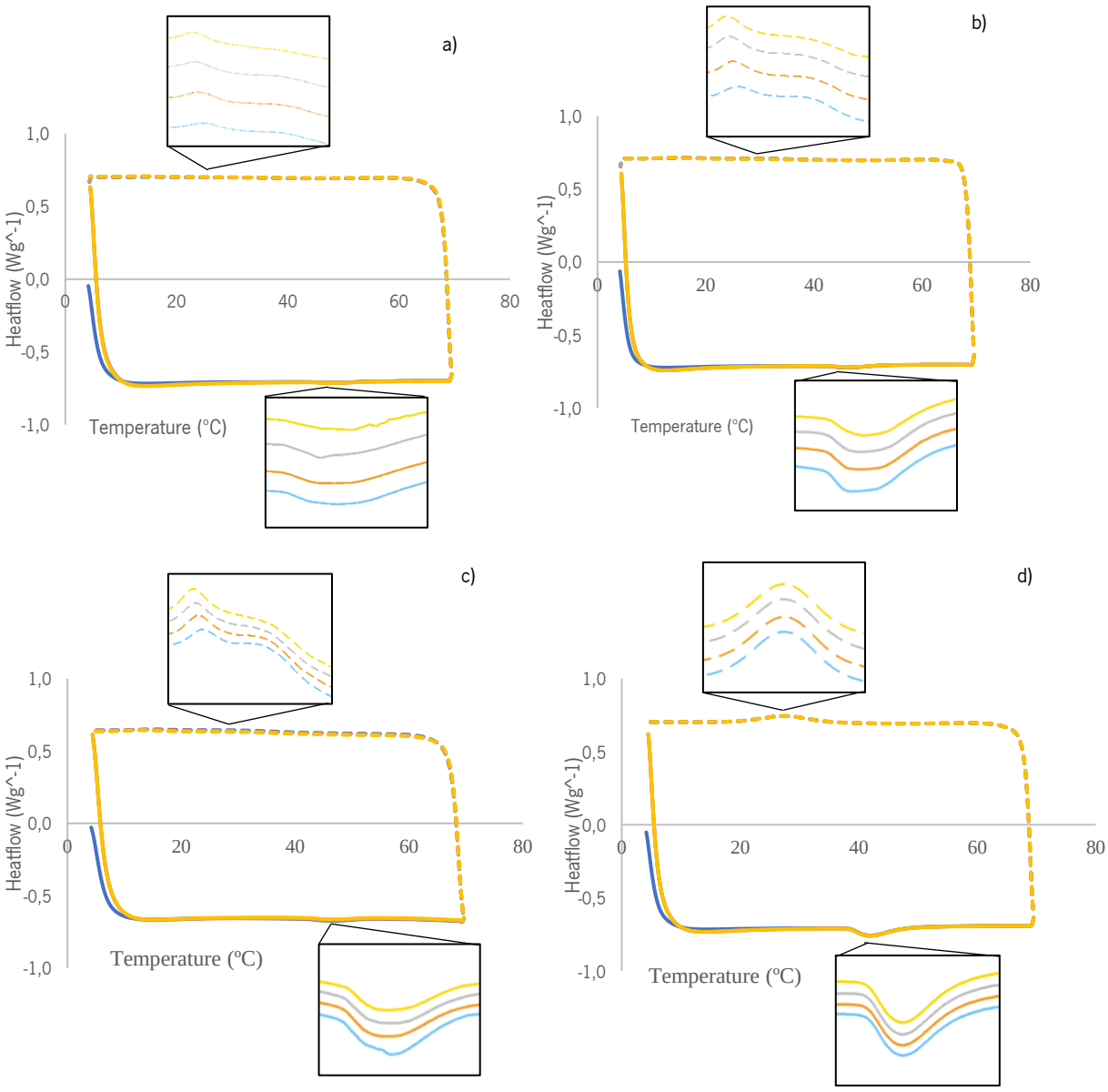

Figure 21 - DSC runs of SELP-520-A solutions prepared at different concentrations: 5% (a), 10% (b), 15% (c) and 20% (d) (w/v), subjected to four heating (solid lines) and cooling (dashed lines) cycles (1- blue; 2 – orange; 3 -grey; 4 -yellow). Their respective enthalpy values and the temperatures at the onset and peak are described in table 16 and table 17.

Table 18 - Temperatures at which the peak, onset and endset of the endothermal reaction occurred, as well as it's corresponding enthalpy value (ΔH) for SELP-1020-A solutions, during the heating runs. Values determined using StarE software (Mettler Toledo).

	Cycle	**Cycle 1**	**Cycle 2**	**Cycle 3**	**Cycle 4**
5%	Integral (mJ)	-5.2	-3.8	-4.0	-5.0
	Onset (°C)	44.8	44.9	44.8	44.2
	Peak (°C)	49.2	49.2	47.2	49.2
	Endset (°C)	54.2	53.4	53.5	53.5
10%	Integral (mJ)	-6.9	-5.4	-5.3	-5.7
	Onset (°C)	43.1	43.3	43.2	43.2
	Peak (°C)	47.5	47.5	47.1	47.3
	Endset (°C)	52.2	52.1	51.9	52.5
15%	Integral (mJ)	-8.5	-7.2	-6.1	-5.7
	Onset (°C)	42.3	42.5	42.9	42.9
	Peak (°C)	46.8	46.8	46.7	46.4
	Endset (°C)	52.2	52.2	52.3	52.5
20%	Integral (mJ)	-45.6	-44.7	-44.5	-44.9
	Onset (°C)	38.5	38.5	38.4	38.4
	Peak (°C)	42.2	42.0	42.0	42.0
	Endset (°C)	47.9	47.9	47.9	47.8

Table 19 -Temperatures at which the peak, onset and endset of the exothermal reactions occurred, as well as it's corresponding enthalpy value (ΔH) for SELP-1020-A solutions, during the cooling runs. Values determined using StarE software (Mettler Toledo).

		Cycle 1		**Cycle 2**		**Cycle 3**		**Cycle 4**	
5%	Integral (mJ)	2.1	1.3	3.0	2.4	2.9	1.7	2.9	1.0
	Onset (°C)	20.7	39.4	20.3	39.8	19.4	39.9	18.8	42.0
	Peak (°C)	16.2	32.3	15.4	32.6	14.4	31.3	13.9	31.3
	Endset (°C)	11.0	27.0	10.1	23.9	9.6	25.4	9.8	26.2
10%	Integral (mJ)	3.0	2.6	3.3	3.4	4.0	1.9	4.8	2.2
	Onset (°C)	21.6	38.3	20.2	40.5	19.5	39.2	19.2	36.7
	Peak (°C)	16.1	32.5	15.3	32.0	14.5	31.3	13.6	32.3
	Endset (°C)	10.8	26.0	10.5	23.0	9.7	25.4	9.0	23.9
15%	Integral (mJ)	3.8	5.9	5.2	4.0	4.7	4.3	5.1	3.1
	Onset (°C)	20.6	39.2	20.0	38.9	18.9	39.3	18.5	39.5
	Peak (°C)	14.9	30.8	14.1	30.5	13.4	31.1	13.3	31.6
	Endset (°C)	9.6	22.4	8.8	23.6	8.3	22.1	8.0	23.8
20%	Integral (mJ)	58.8		63.5		64.0		63.2	
	Onset (°C)	35.0		35.2		35.4		35.4	
	Peak (°C)	27.4		27.6		27.4		27.6	
	Endset (°C)	19.5		19.3		19.3		19.2	

b. UV-Vis

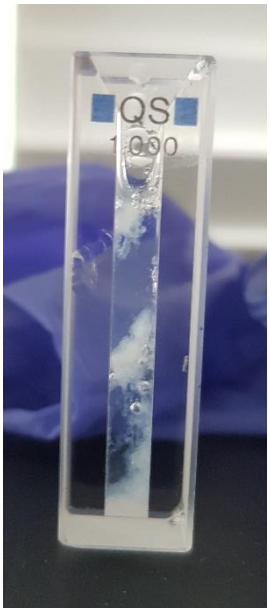

Figure 22 - Image of precipitation of SELP-59-A aggregates, in a 2.5 % (w/v) solution upon heating from 20 °C to 70 °C.

c. Dynamic Light Scattering

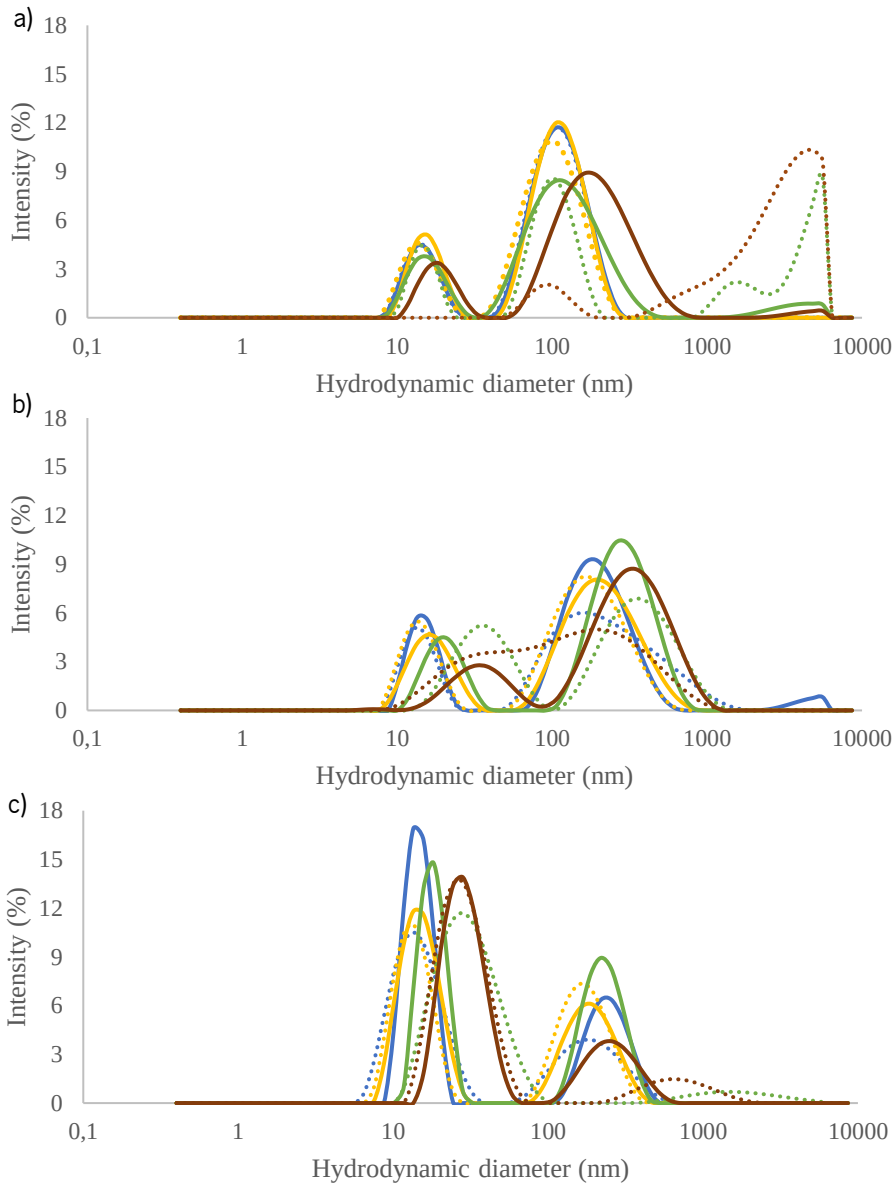

Figure 2316 - - Size distribution profiles at measurement 1 (t1= 4 min)(full lines) and measurement 2 (t2 = 20 min) (dashed lines) of 0,5% (w/v) aqueous solutions of SELP-59-A (a), SELP-520-A (b) and SELP-1020-A (c) at 25 °C (blue), 37 °C (yellow), 50 °C (green) and 65 °C (brown)

Table 20 - Size distribution profiles of the SELP-59-A aqueous solutions at the different temperatures tested, at measurement 1 (t1 = 4 min) and measurement 6 (t2= 20 min), represented by the number and size of populations present, as well as their corresponding percentage of the total intensity of the scattered light.

		Measurement 1			Measurement 6		
	Peak	**Size (d.nm)**	**% Intensity**	**PDI**	**Size (d.nm)**	**% Intensity**	**PDI**
25 ºC	1	117.4 (± 43.4)	80.4	0.622	115.1 (± 42.5)	80.2	0.603
	2	14.8 (± 3.5)	19.6		14.6 (± 3.4)	19.8	
	3	-	-		-	-	
37 ºC	1	117.5 (± 41.4)	78.2	0.554	107.4 (± 42.3)	78.9	0.543
	2	15.7 (± 3.5)	21.8		14.4 (± 3.6)	21.1	
	3	-	-		-	-	
50 ºC	1	134.6 (± 68.6)	76.4	0.563	105.2 (± 30.8)	45.2	0.732
	2	15.8 (± 4.1)	18.1		4532 (± 910.5)	27.2	
	3	3737	5.5		14,9 (± 2.7)	15.1	
65 ºC	1	210.4 (± 112.8)	82.9	0.604	1731 (± 561.7)	45.4	1
	2	18.8 (±4.6)	15.3		4061 (± 993.6)	40.4	
	3	4326 (±956)	1.7		113.6 (±45)	10.6	

Table 21 - Size distribution profiles of the SELP-520-A aqueous solutions at the different temperatures tested, at measurement 1 (t1 = 4 min) and measurement 6 (t2=20 min), represented by the number and size of populations present, as well as their corresponding percentage of the total intensity of the scattered light.

		Measurement 1			Measurement 6		
	Peak	**Size (d.nm)**	**% Intensity**	**PDI**	**Size (d.nm)**	**% Intensity**	**PDI**
25 ºC	1	210.3 (± 93.7)	73.7	1	289.9 (± 235.2)	78	1
	2	15 (± 3.2)	23.3		14.1 (± 3.3)	22	
	3	4438 (± 906.3)	3.1		-	-	
37 ºC	1	233.8 (± 122.4)	74.1	0.697	195.3 (± 98.9)	74.3	0.638
	2	17.1 (± 5.1)	25.9		14.4 (± 3.6)	25.7	
	3	-	-		-	-	
50 ºC	1	307.8 (± 125.1)	77.8	0.771	410.6 (± 204.8)	62	0.588
	2	20.6 (± 5.5)	22.2		38.1 (± 15.1)	38	
	3	-	-		-	-	
65 ºC	1	369.1 (± 184.2)	79.5	0.608	179.3 (± 180.9)	100	0.544
	2	36.5 (± 15.3)	20		-	-	
	3	7.3 (± 1.2)	0.2		-	-	

Table 22 - Size distribution profiles of the SELP-1020-A aqueous solutions at the different temperatures tested, at measurement 1 (t1= 4 min) and measurement 6 (t2= 20 min), represented by the number and size of populations present, as well as their corresponding percentage of the total intensity of the scattered light.

		Measurement 1			Measurement 6		
	Peak	**Size (d.nm)**	**% Intensity**	**PDI**	**Size (d.nm)**	**% Intensity**	**PDI**
25 °C	1	14.74 (± 2.8)	64.3	0.505	14.9 (± 5.3)	66.9	0.435
	2	249.7 (± 73.8)	35.7		205.9 (± 97)	33.1	
	3	-	-		-	-	
37 °C	1	15.2 (± 4.2)	60.6	0.470	13.7 (± 3.6)	53.3	0.527
	2	195.9 (± 68.3)	39.4		178.3 (± 61.5)	46.7	
	3	-	-		-	-	
50 °C	1	18.2 (± 3.5)	53	0.537	32 (± 11.5)	92.4	0.235
	2	233.8 (± 66.2)	47		1854 (± 114)	7.6	
	3	-	-		-	-	
65 °C	1	29.2 (± 8.6)	47.3	0.363	29.1 (±10.3)	87.2	0.272
	2	268.8 (± 98.5)	25.7		746.9 (± 359.7)	12.8	
	3	-	-		-	-	

d. Scanning Electron Microscopy

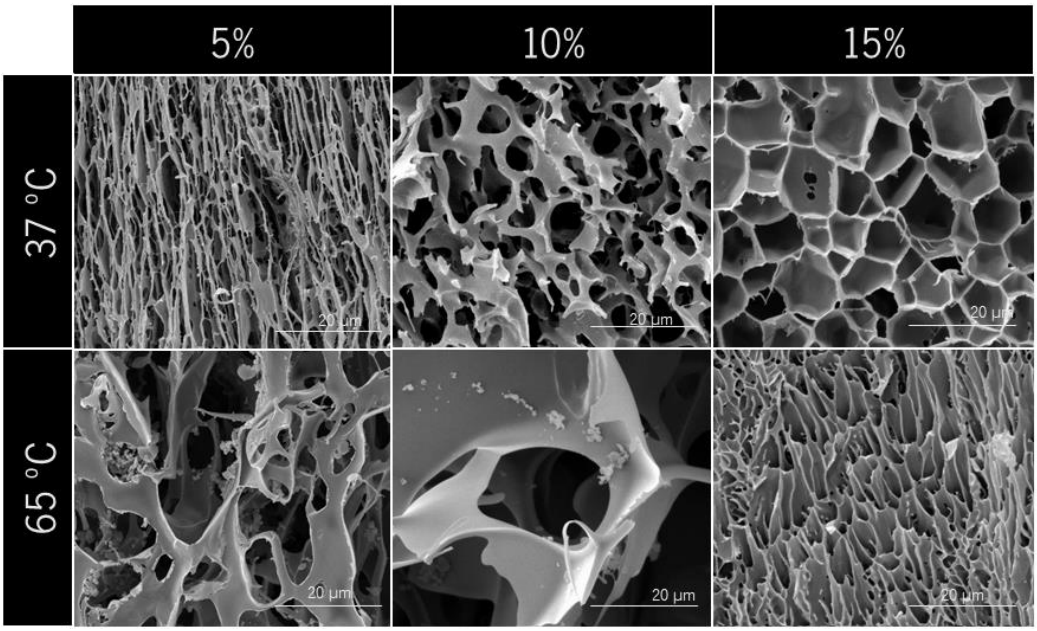

Figure 24 - SEM micrographs (x5000) of SELP-59-A gels, at different concentrations, cured below (37 °C) and above (65 °C) the Tt.

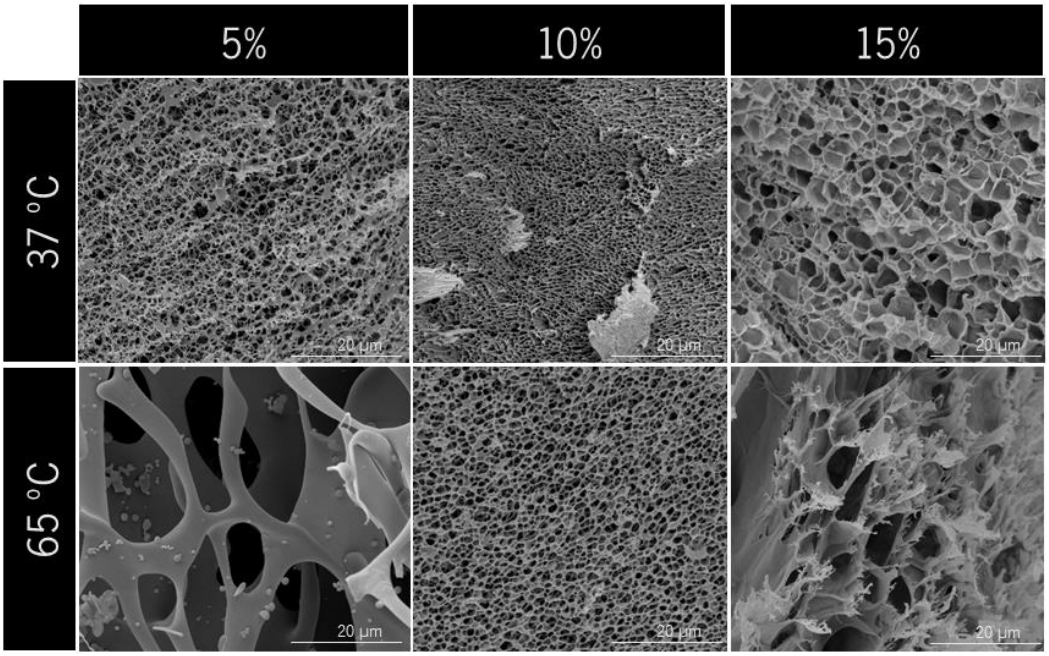

Figure 25 - SEM micrographs (x5000) of SELP-520-A gels, at different concentrations, cured below (37 °C) and above (65 °C) the T_t.

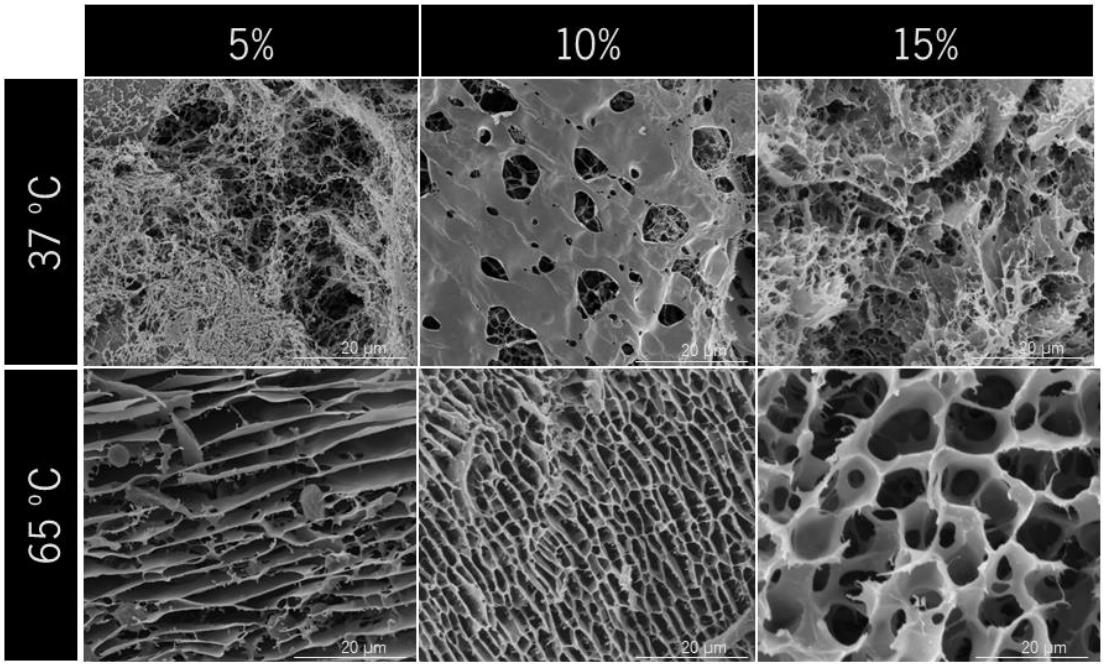

Figure 26 - SEM micrographs (x5000) of SELP-1020-A gels, at different concentrations, cured below (37 °C) and above (65 °C) the T_t.

e. ATR-FT-IR

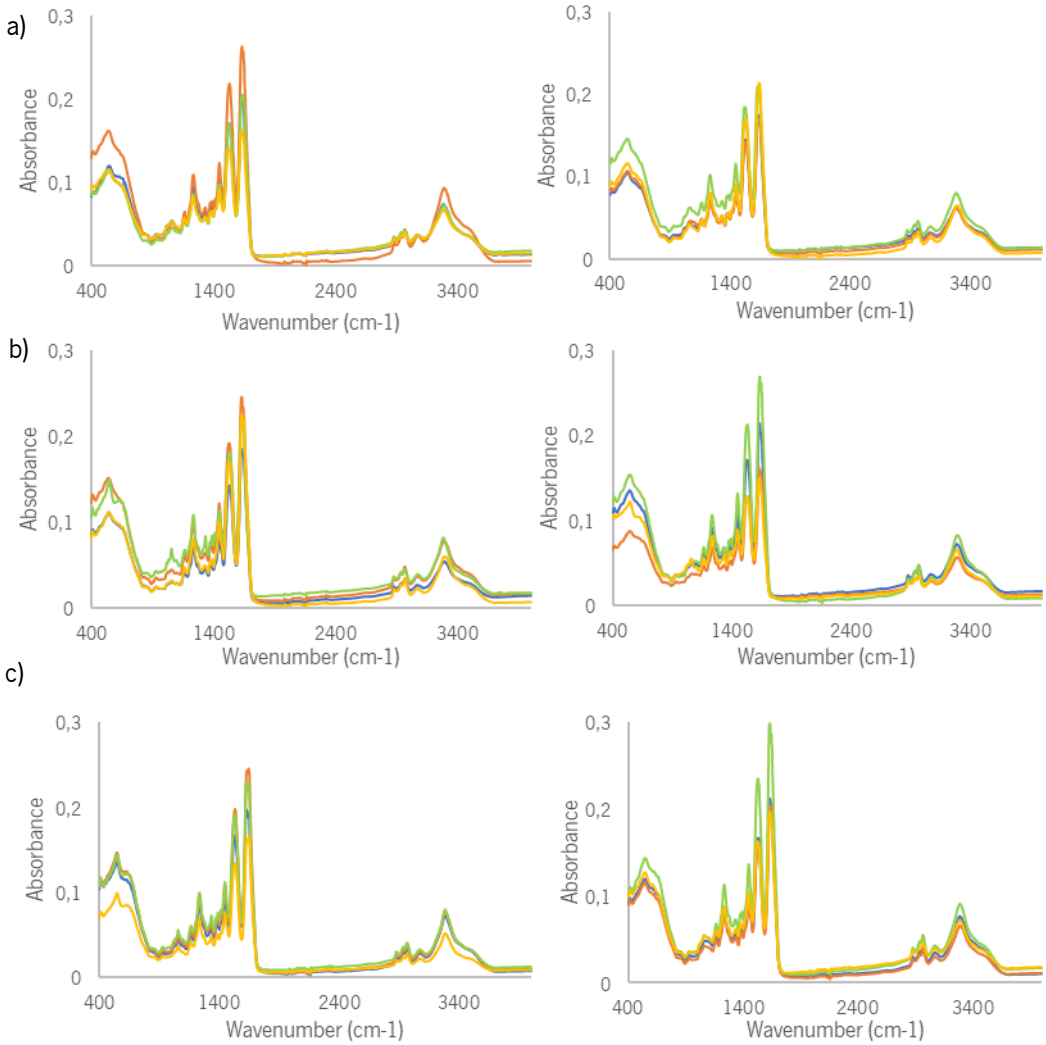

Figure 27 – ATR-FT-IR spectra of SELP freeze-dried hydrogels, prepared at different concentrations, 2,5% (blue); 5% (orange), 10% (green) and 15% (w/v) (yellow) and cure temperatures, 37 °C (left) and 65 °C (right). a) SELP-59-A; b) SELP-520-A; c) SELP-1020-A.